Bio-geo-optical properties and remote sensing of CDOM in optically complex inland waters

María Encina Aulló Maestro

September 2019

A Thesis submitted for the degree of
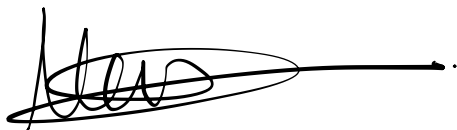**Doctor of Philosophy**
Biological and Environmental Sciences, Faculty of Natural Sciences
University of Stirling

Declaration of authorship

I, María Encina Aulló Maestro, declare that this thesis has been composed by me and it embodies the results of my own research.

Where appropriate I have acknowledged the nature and extent of work carried out in collaboration with others.

………………………….

María Encina Aulló Maestro

27th September 2019

A mis muy queridos y admirados padres

Thesis abstract

A substantial number of studies demonstrate the sensitivity of lakes to climate change and show that physical, chemical, and biological lake properties respond rapidly to climate-related changes. The indicators include variables such as temperature, dissolved organic carbon (DOC) or plankton composition.

DOC is also known to play a primary role in protecting freshwater organisms from exposure to UV radiation and a big fraction of it is typically represented by dissolved organic matter (DOM). Moreover, the conservative properties between the coloured fraction of DOM (CDOM) and DOC, and the possibility of remotely estimating CDOM from space given its optical properties, makes it often used as a proxy for DOC.

The development and validation of remote-sensing-based approaches for the retrieval of CDOM concentrations requires a comprehensive understanding of the sources and magnitude of variability in the optical properties of dissolved material within lakes.

The present study aims to contribute with the knowledge of remote sensing of CDOM in inland water bodies with the specific objectives of characterising the link between CDOM absorption and DOC content in inland waters, investigating how changes in CDOM absorption can be used to infer information on its concentration, sources and decomposition and finally, to present an extensive CDOM algorithm validation exercise.

The results of this Thesis indicate that the relationship between CDOM and DOC can vary remarkably. Strongest relationships have been found in waters with low anthropogenic influence, whereas waters more influenced by human activity present less clear linkages between the two parameters. As aromaticity increases in more productive waters we can then infer low CDOM to DOC relationships to them.

Remote-sensing models for DOC estimation based on the relationship between CDOM and DOC should therefore consider local variability and optical complexity, considering at least groups of water types according to their absorption features.

In-lake spatial and seasonal variability in the quantity and quality of CDOM should also be taken into account. Photobleaching has been found to be a major factor controlling the in-lake transformation and degradation of CDOM, and a key process influencing the spatial structure CDOM throughout the system. These results also provide an insight on the potential contribution of wetlands to DOM and CDOM in lakes, not only in terms of the concentration of CDOM, but also in terms of its seasonality.

All this leads to understand that CDOM content in complex inland waters usually present a wide range given their surrounding terrestrial characteristics and seasonal differences. The complexity of inland water bodies is currently a challenge to current remote sensing algorithms used to estimate parameters such as CDOM absorption (a_{CDOM}).

The accuracy of remote sensing-based retrievals of a_{CDOM} at 440 nm (a_{CDOM} (440)) can improve, mostly by targeting specific OWTs in algorithm development. For hypereutrophic waters with cyanobacterial blooms and abundant vegetation Blue-Green ratio based algorithms. For moderately productive waters with cyanobacteria presence, a double Blue-Green ratio based empirical algorithm is recommended. A double Blue-Green ratio and a Red-Green ratio for application in clear waters, turbid waters with high organic content, high productive waters with high cyanobacteria abundance and high reflectance at red/near-infrared spectral region. For waters high in CDOM, cyanobacteria presence and high absorption by NAP (Non-Algal Particles), a Green-Red ratio based algorithm. And finally, a semi analytic algorithm worked best for waters with high Rrs at short wavelengths.

ACKNOWLEDGEMENTS

I would like to thank all my supervisors for supporting me throughout my PhD, specially to Dr. Peter Hunter, I wish one day I manage to be a professional as you are. I will carry your name as my PhD supervisor with pride.

I would also like to thank all the technicians and colleagues of the Division of Biology and Environmental Sciences at the University of Stirling who welcomed me with warmth. The Fletcher's family, Kathleen, Stephen… Apart from my PhD, I can say I am bringing new friends for life home.

To the Spanish clan (Moha, Paloma, Almu, Patri…), it could not have been funnier and would not have been possible without your support and encouragement.

Many thanks to all those who have contributed in one way or another to this PhD: ACRE Surveying Solutions, Indra Sistemas, thank you for believing in me; my goat herd (Cristi, Mari, Qke); the foresters (Gonzalo, Natalia, Henar, Ana), you have always been there and I hope you will always be; the Earth Observation department of Indra (specially my colleagues Elena, César, Carmelo, Fran), you have taught me so much in so little; my new friends (Violeta, Goyo, Gael); my old friends (Antonio, Maribel, Luis, Rosa, Ceci, Javi, Moni, Alex…).

I will always be grateful to my scientific parents Dr. Silvia Merino de Miguel and Dr. Ignacio Garcia-Amorena. I am where I am because I was lucky to find you on my way.

To my uncles and aunts, you have always been proud of me, and this have pushed me to try and deserve so.

Thank you "*abuelos*" (Guti, Alfonso, Kiti and Dr. Manuel Aulló Urech), you are always with me and will always be.

Thank you, Roger. For believing in me, for letting me borrow a bit of your strength.

Pierre, my husband. Thank you for always being with me and supporting me in so many ways. Looking forward to moving on and achieving our next goals together.

Thank you, Isa, you make me feel a rock star and those are the kind of feelings that have pulled me right here. And tato Miguel, you bring the so necessaries joy and art.

To my parents, because I owe you everything. You are the best example, and nothing will ever be enough to demonstrate how grateful I am.

To Claudia Isabel because since the 1st of January 2018, you are just the reason.

TABLE OF CONTENTS

LIST OF FIGURES

16

LIST OF TABLES

1. CHAPTER 1 – INTRODUCTION

1.1. Research context

The Earth's climate is changing rapidly with impacts on terrestrial and aquatic ecosystems (Morel and Prieur, 1977; UNFCC, 1992). In this context, the sensitivity of inland waters to climate is being understood as a good indicator of global climate change (Carpenter et al., 2007; Pham et al., 2008; Williamson et al., 2008; Tranvik et al., 2009; Adrian et al., 2009).

Lakes constitute a significant component of the global carbon cycle (Tranvik et al., 2009) and can affect carbon (C) balances at regional scales (Cole et al., 2007). Moreover, they are distributed worldwide, and provide indicators directly related with response variables such as dissolved organic carbon (DOC), considered one of the most effective indicators of climate change (Adrian et al., 2009).

DOC is also one of the main attenuating substances in freshwater and coastal marine waters absorbing strongly in the UV and shorter visible wavelengths (Häder et al., 2007) and playing a primary role in protecting freshwater organisms (Schindler and Curtis, 1997). However, its full effects in aquatic ecosystems and the origin of those are still an issue to address.

There is a need of a wider spatial and temporal coverage in DOC measurements and the assessment of DOC distributions from satellite measurements of the optical properties of the coloured part of the dissolved organic matter (CDOM) can be an interesting approach.

This relationship has already worked well (Stedmon et al., 2011; Yamashita et al., 2011), even though there are exceptions generally related to lakes and lake-influenced rivers that show weaker relationships. Moreover, one of the most challenging points of

developing remote sensing algorithms for estimation of DOC lays on the fact of its high variability.

The current research focuses on the remote retrieval of CDOM concentration and it was undertaken under the auspices of the GloboLakes project.

1.2. Lakes as sentinels of climate change

1.2.1. Lakes and climate change

There is now irrefutable evidence that the Earth's climate is changing rapidly as a result of anthropogenic activity with detrimental impacts on terrestrial and aquatic ecosystems (Morel and Prieur, 1977; UNFCC, 1992). Also, the confidence that warming of lakes and rivers are occurring in many regions with effects on water quality and composition is high (IPCC, 2007). Inland waters provide many ecosystem services to both humans and wildlife such as water for drinking, bathing, recreation, and commercial and industrial use (Williamson et al., 2008); so increased temperatures will consequently affect human society and ecosystems (McCarthy, 2001) which makes it a particularly important field of study.

A substantial number of studies demonstrate the sensitivity of lakes to climate and shows that physical, chemical, and biological lake properties respond rapidly to climate-related changes (ACIA, 2004; Rosenzweig et al., 2008). Thereby, lakes could be understood as good sentinels of global climate change (Carpenter et al., 2007; Pham et al., 2008; Williamson et al., 2008; Tranvik et al., 2009; Adrian et al., 2009). They provide indicators which can measure response variables (water temperature, dissolved organic carbon [DOC], or plankton composition), they are distributed worldwide, integrate responses over time, respond directly to climate change and also incorporate the effects of climate driven changes occurring within the catchment (Adrian et al.,

2009). Moreover, inland waters are not only sentinels and integrators of terrestrial process but also of atmospheric processes (Williamson et al., 2008) and when properly interpreted can give us abundant information about the effect of climate change on water resources (Williamson et al., 2008).

1.2.2. Global budget of carbon in lakes

The force of gravity links terrestrial ecosystems with coastal oceans through the biogeochemistry of inland waters. Elements move over time from mountains to sea through the river network and during this transport, elements can be buried in sediments, assimilated into the tissues of living organisms or exported in form of gas, avoiding or delaying their downstream transport.

Carbon in the biosphere has been generally understood as distributed among three major reservoirs: land, ocean and atmosphere (Bolin, 1981; IPCC, 2001), being the role of inland waters often not taken into account and when acknowledged, only as mere conveyors of carbon (C) through the riverine pipe. However, many inland water ecosystems depend on terrestrial carbon inputs to sustain their biological energy demands, making them important players in global biogeochemical cycles as storage, exchange with the atmosphere and transport to the ocean (Cole et al., 2007b). Inland water bodies constitute a significant component of the global carbon cycle (Tranvik et al., 2009) and although their area is small, these systems can affect C balances at regional scales (Cole et al., 2007).

The largest pool of organic carbon (OC) in a lake is DOC, while particulate organic carbon (POC) is the dominant form of OC in sediments (Cole et al., 2007; Dean and Gorham, 1998).

Carbon storage rates in lakes commonly increase with lake productivity and are inversely proportional to lake size (Kortelainen et al., 2004; Mulholland and Elwood, 1982). Because they are subsidized by terrestrial inputs, aquatic systems can simultaneously be net accumulators of sedimentary organic matter and net sources of carbon dioxide (CO_2) to the atmosphere (Cole et al., 2007) (**Figure 1-1**). Fluvial and ground water exports of C may be affected by climate change-induced changes in hydrology, as well as indirectly by the anthropogenic rise in atmospheric carbon dioxide (CO_2; Cole et al., 2007).

Emissions to the atmosphere

0.75

C
(from land)   1.9   Inland waters   0.9   C
(to ocean)

0.23

Sediment storage
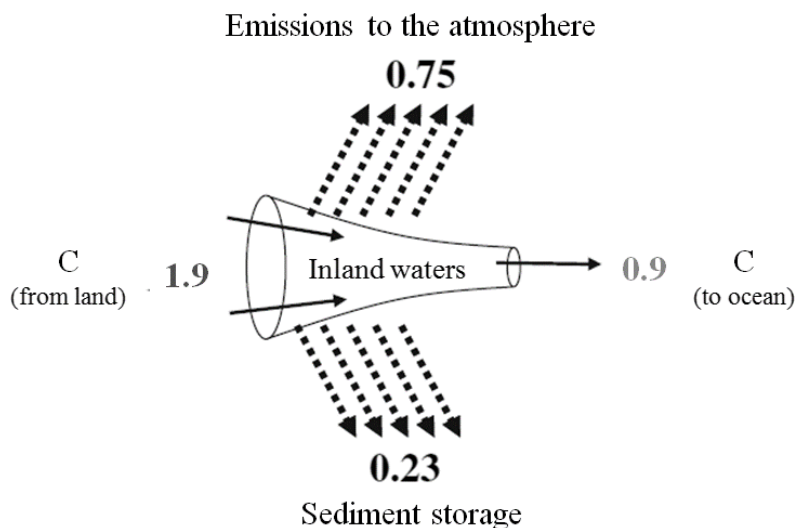
Figure 1-1 Modified from Cole et al. 2007. Inland waters are active components of the global C cycle. They store terrestrially-derived carbon in sediments and lose CO_2 in emissions to the atmosphere in addition to transporting it to the ocean.

Dissolved Inorganic Carbon (DIC) and DOC are the predominant carbon inputs to most lakes, followed by POC and particulate inorganic carbon (PIC). Given that 90–95% of the total organic carbon (TOC) in lakes consists of DOC (Wetzel, 2001), it is considered one of the most effective indicators of climate change (Adrian et al., 2009) and its concentrations may be particularly appropriate for detecting changes within the terrestrial environment (Tranvik et al., 2009).

24

To understand how terrestrial and aquatic sources of organic carbon interact to
determine fates of organic carbon in a lake, **Figure 1-2** depicts a modified version of
Hanson et al. (2004) which shows an idealized lake situated in a forested landscape.
Where (1) represents a positive net of primary production in the surrounding terrestrial
systems and implies an accumulation of biomass; (2) represents the mineralized
biomass exporting DIC in groundwater and surface water; (3) represents additional
biomass leached through surface water as DOC or translocated as POC; (4) represents a
portion of the lake POC that settles to the sediments; (5) the POC in the sediments that
slowly mineralise and release DIC to the water column; (6) the CO_2 partial pressure
gradient between the lake and the atmosphere driving net atmospheric flux of DIC and
in (7) all forms of carbon are exported from the lake through surface flow. Although
this system is rarely analysed in an integrated way, many of the fluxes and
transformations have been quantified in the bibliography.
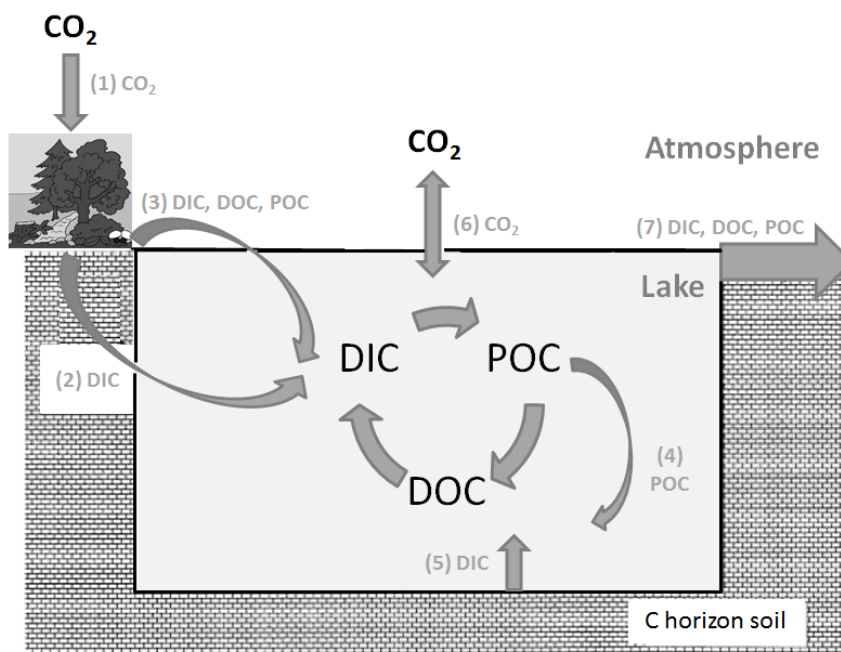
Figure 1-2 Diagram of carbon cycling through a landscape with a lake. Modified from Hanson et al.
2004.

1.2.3. Role of DOC in Carbon Cycle

Photosynthesis is the primary source of energy that supports all aquatic life in a water body and phytoplankton fixes atmospheric carbon becoming the base of the aquatic food web through the process of photosynthesis. Rates of photosynthesis are dependent on the intensity and spectral quality of light, which in an aquatic environment are closely related to the optical characteristics of the water and its depth.

Light availability is strongly influenced by the water itself, the presence of dissolved organic matter (DOM) and other attenuating substances. Consequently, a large fraction of the light incident at the water surface is attenuated and unavailable for photosynthesis

DOC and POC are the main attenuating substances in freshwater and coastal marine waters. Recent models analysing the absorption of the components show that DOC absorbs strongly in the UV and shorter visible wavelength (Häder et al., 2007) and its concentrations often show a large spatial and temporal variability.

Recent observations in lakes revealed that a gradual, long-term increase in DOC has been taking place in many freshwater systems from mid- to high latitudes of the northern hemisphere (Roulet and Moore, 2006; Clark et al., 2010) . This trend has been called "brownification" (Kritzberg and Ekström, 2011) and even though there are a large number of recent studies approaching the causes of this phenomenon, it currently remains poorly understood (Clark et al., 2010).

Increases in DOC can translate in higher respiration rates (Williamson et al., 1999) even though, primary production can diminish as a result of shading (Carpenter et al., 1998). Moreover, higher concentrations of DOC promote photo-oxidation (Lindell et al., 2000) and can, therefore, deplete oxygen (O_2) decreasing the water mixing depth in

shallow lakes (Fee et al., 1996), diminishing the supply of O2 to deeper layers and inducing significand decreases in the biological biodiversity of the ecosystem (Townsend et al., 1992) meaning a possible significant decrease of lake productivity.

Consequences of decreased productivity are a reduced sink capacity for atmospheric carbon dioxide and negative effects on species diversity, ecosystem stability, trophic interactions and ultimately global biogeochemical cycles (Häder et al., 2007).

However, the full effects of DOC variations in aquatic ecosystems and the origin of these interactions are still a complex issue to address and therefore, the understanding of the actual role of DOC in the carbon cycle is currently limited by the very few information available, with data often restricted to local-regional observations. The need of a wider spatial and temporal coverage in DOC has been usually addressed through the assessment of DOC distributions from satellite measurements of the optical properties (absorption and fluorescence) of the coloured part of the dissolved organic matter (CDOM).

The relationship between CDOM and DOC has been widely investigated (Ferrari et al., 1996; Guéguen et al., 2005; Griffin et al., 2018) and, even though strong positive correlations have been observed, it varies widely among geographic regions and seasons and such variability limits our capability to predict DOC from CDOM absorption. The characterisation of the link between CDOM absorption (a_{CDOM}) and DOC content within a wide range of inland water bodies is currently needed.

1.3. Remote sensing of inland water bodies

The remote estimation of the optical properties of water constituents has been historically based on the analysis of Chlorophyll-a (Chl-a) and CDOM (Morel and Gordon, 1980; Gordon et al., 1988). The high variability and complex interactions

between water constituents in inland waters makes its remote estimation different from open ocean waters and has historically made its remote estimation more challenging.

Nevertheless, remote sensing has now been recognised for long time as having the potential to complement conventional approaches to lake monitoring, and Palmer et al. (2015) provide with a complete review of history and progress up to 2015.

Remote sensing of inland waters is based on the optical properties of water constituents (Morel, 2001). These properties can be divided in two categories: i) properties that depend on the medium and the directional structure of the ambient light field, known as apparent optical properties (AOPs), and ii) those which depend only on the medium and are independent of the ambient light field, known as inherent optical properties (IOPs).

1.3.1. Physical principles

Optical imaging remote sensing sensors collect electromagnetic radiation with wavelengths between 400 and 1500 nm. It involves acquisition and analysis of optical data in form of electromagnetic radiation captured by the sensor after reflecting off an area of interest on ground or water. The properties of an element depend on the material it is made of and its physical and chemical state, the surface roughness as well as the angle of the incident sunlight. The way it reflects, absorbs or scatters light varies with the wavelength of the incident electromagnetic energy. The amount of reflectance form an element can be measured then as a function of this wavelength and this is called spectral reflectance of this specific element. It is a measure of how much energy an element reflects at a specific wavelength. Many elements reflect different amount of energy in different parts of the electromagnetic spectrum, these differences in reflectance mae it possible to identify different materials by analysing their spectral reflectance signatures. Different water constituents scatter and absorb differently at

different wavelengths; thus, the targets can be identified by their spectral signatures in the remotely sensed images.

The optical active water constituents (OACs), include phytoplankton (most commonly expressed as the Chl-a concentration), detritus and minerals (collected referred to as non-algal particles [NAP]), CDOM and water itself and they all have an impact on the optical signature of the water in the visible wavelengths. This makes possible to derive from optical remote sensing data, information about the characteristics of the water body and the type and concentration of its constituents.

Remote Sensing of inland water bodies studies the colour of water through the observation of water leaving radiance (L_w) spectra to describe its properties from a distance without taking water samples. The development of water remote sensing techniques has not only been based on empirical relationships between the spectral properties and the quality parameters of the water body. More complex neural network and inversion methods have also been applied to estimate inherent optical properties (IOPs) (Odermatt et al., 2012). Moreover, Hoogenboom et al. (1998) used matrix inversion methods for retrieving Chl-a and suspended matter and Arst and Kutser (1994) used a modelling approach for estimating Chl-a, CDOM and suspended matter from modelled spectra.

Water remote sensing instruments allow us to record the colour of a water body which provides information on the presence and abundance of OACs. Thus, the value of this parameter will change with changes in the IOPs and concentrations of the optically active substances in the water.

2.2.2.1. IOPs

The propagation of light within the ocean is described by a radiative transfer equation (RTE). The most common form of RTE describes the change of radiance with depth, which is caused by scattering and absorption of light by seawater. In addition to the OACs, the water-leaving radiative signal can also be influenced by gas bubbles, foam and white caps and other organisms such as zooplankton. IOPs (Figure 1-3) describe water and the substances in it, independent of sunlight and other ambient sources.

IOPs depend only on the water and other substances that are dissolved or suspended in it (as distinguished from AOPs). The two fundamental IOPs are:

- Absorption (a)
- Scattering (b)

Others commonly derived from these include:

- Total scattering coefficient (b)
- Backscattering coefficient (b_b)
- Beam attenuation coefficient ($c = a + b$)

Fluorescence may be considered an IOP although it is usually treated separately from the previous ones.
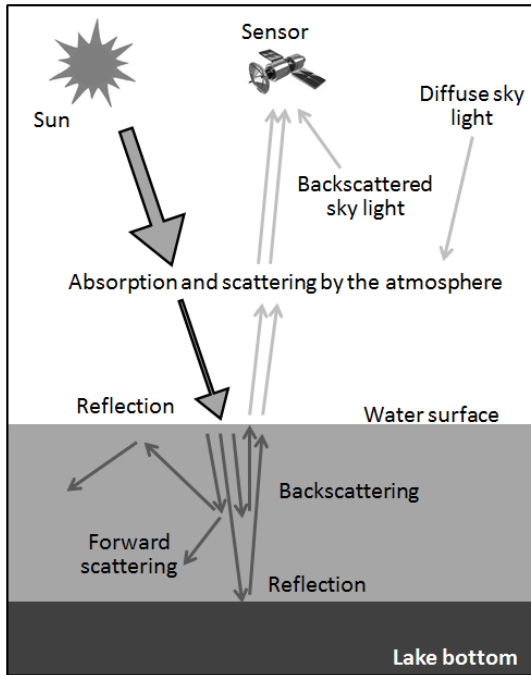
Figure 1-3 Scheme of how Inherent Optical Properties (IOP's) affect to signals received by remote sensing sensors

Instruments for IOP measurement provide their own carefully controlled illumination and are designed to reject the effects of ambient light. In contrast, AOPs are typically derived from measurements of ambient light.

2.2.2.2. AOPs

AOPs are those that depend both on IOPs and on the light field in which they are measured. The most widely-used AOP is water remote sensing reflectance (R_{rs}). R_{rs} is defined as the ratio of water leaving radiance (L_w) to downwelling radiance (E_d) expressed per steradian (sr^{-1}).

However, R_{rs} is also influenced by the solar zenith angle and viewing direction and in order to compare measurements at different times and/or locations, these effects should be removed. The normalized water-leaving reflectance ($[\rho_w]_N$, equation **(1-1)**) is an AOP

that reduces these effects while retaining a strong dependence on the water IOPs.

$$[\rho_w]_N = {(L_w * \pi)}/{E_d} \tag{1-1}$$

2.2.2.3. *The radiative transfer equation*

The radiative transfer theory provides the connection between the IOPs and the AOPs. The physical environment and the radiative transfer equation (RTE, equation **(1-2)** connect the optical properties of the water body and the light within the water thereby providing the theoretical framework for all oceanography and ocean colour remote sensing.

$$cos\theta \cdot \frac{dL(\theta, \emptyset)}{cdz}$$

$$= -L(\theta, \emptyset) + w_0 \cdot \int_{4\pi} \tilde{\beta}(\theta', \emptyset' \to \theta, \emptyset) \cdot L(\theta', \emptyset') \cdot d\Omega(\theta', \emptyset') + S(\theta, \emptyset) \tag{1-2}$$

where a is the absorption coefficient, β is the volume scattering function, b_b is the backscattering coefficient, b is the total scattering coefficient, c is the beam attenuation coefficient, w_0 the single scattering albedo and $\tilde{\beta}$ is the scattering phase function.

2.2.2.4. *The composition of the absorption spectra*

When light penetrates a water body, photons can be absorbed (the radiation energy converts into excitation energy of the molecules) or scattered (the energy is redistributed of the incident beam to all directions).

Because IOPs are conservative properties, the magnitude of the absorption coefficient varies linearly with the concentration of the absorbing material. The absorption coefficient can be expressed as the sum of the different absorption coefficients (**equation 1-3**) that makes up the water body and, even though, it is not possible to

measure the absorption properties of every individual absorbing component of a water body, the individual components can be grouped into similarly absorbing constituents based on similarity in their optical properties.

Absorption by pure water (**Figure 1-4**) is weak in the blue and strong in the red parts of the spectrum and varies with temperature and salinity. Absorption by particles is separated into phytoplankton (PHY) and NAP. Phytoplankton absorption presents the bigger spectral variations of any of the components but in general exhibits peaks in the blue and red regions of the spectrum. NAP absorption is strongest in the blue, decreasing approximately exponentially to the red given its composition of living zooplankton and bacteria, as well as the non-pigmented parts of phytoplankton and detrital material. CDOM absorption (a_{CDOM}) spectra is very similar to that of NAP due in part to the similarity in composition, but generally exhibits a steeper exponential slope.

$$a(\lambda) = a_w + a_{PHY}[a_{NAP}(\lambda) + a_{CDOM}(\lambda)] \qquad \text{1-3}$$

- Absorption spectrum for pure water (data from Pope and Frye 1992)
- Generic phytoplankton absorption spectrum for mixed algal composition (modified from Roesler et al. 1989)
- Generic non-algal particle absorption spectrum for mixed composition
- Generic coloured dissolved organic matter (CDOM) absorption spectrum for mixed composition
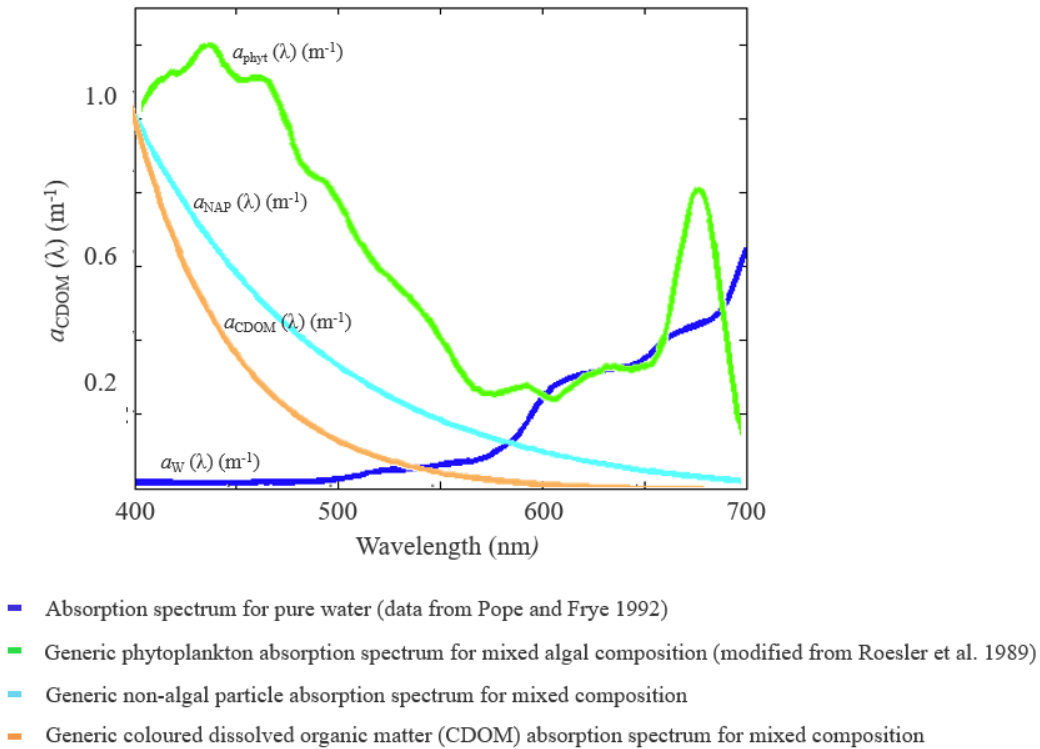
Figure 1-4 Absorbing components of a water body

For oligotrophic environments with very low concentrations of suspended and dissolved material, the absorption coefficient is dominated by water (**Figure 1-5a**) and the wavelength of minimum absorption is in the blue, hence the blue colour of the seawater. For eutrophic environments with high concentrations of suspended and dissolved material (**Figure 1-5b**), the absorption coefficient is dominated by that material and the wavelength of minimal absorption shifts to the green, lending green colour to that environment.

- ■ Total absorption
- ■ Absorption spectrum for pure water (data from Pope and Frye 1992)
- ■ Generic phytoplankton absorption spectrum for mixed algal composition (modified from Roesler et al. 1989)
- ■ Generic non-algal particle absorption spectrum for mixed composition
- ■ Generic coloured dissolved organic matter (CDOM) absorption spectrum for mixed composition
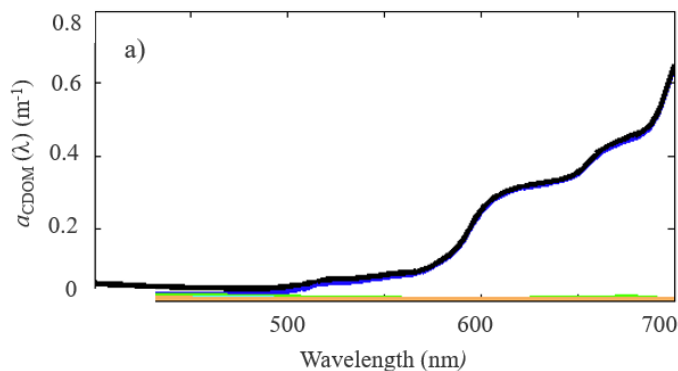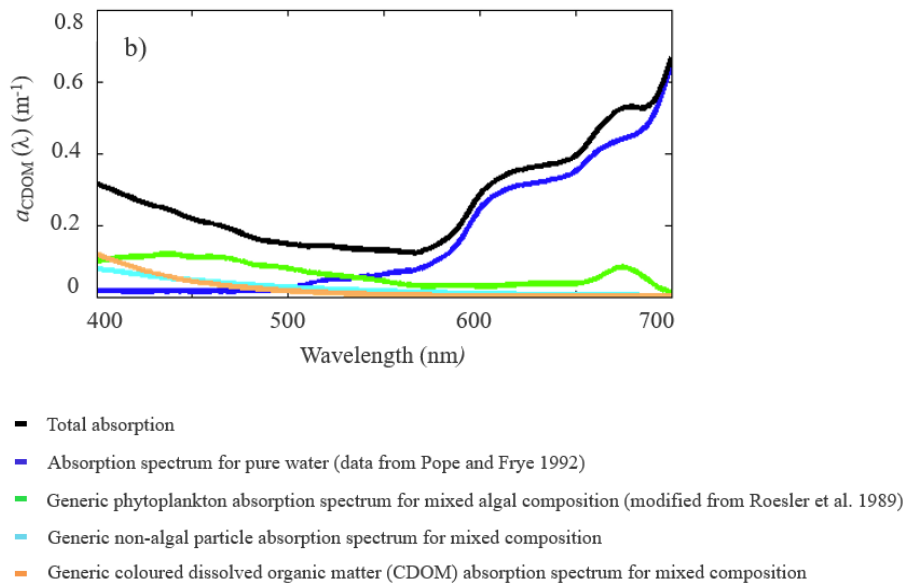
Figure 1-5 Component and total absorption spectra in **a)** clear open ocean waters where water dominates the absorption and **b)** eutrophic coastal waters where particulate and dissolved organic matter dominate the blue and green portions of the spectrum.

1.3.2. Optical water types

The optical water classification system introduced by (Morel and Prieur, 1977) distinguishes between optical Case 1 and 2 waters. The Case 1 and 2 classification system is used to classify waters for modelling purposes.

Case 1 waters have optical properties dominated by phytoplankton and, their co-varying degradation products; chlorophyll concentration is high relative to the scattering coefficient (ß). As the pigment concentration increases, the R_{rs} values in the blue-violet region (380-495nm) decrease progressively and a minimum is formed around 440nm, which corresponds to the maximum absorption of chlorophyll. The maxima shift toward 565-570nm, which is the wavelength where simultaneously the absorption due to pigments is at its minimum. The irregularity near 480nm may be attributed to carotenoids.

The second maximum of absorption by Chl-a creates a minimum near 665 nm and at 685nm a second maximum appears. The enhancement of scattering and of back-

scattering on the long wavelength side of the absorption peak could explain the existence of the R_{rs} maximum at 685nm.

Case 2 waters have optical properties dominated by other in-water constituents, such as total suspended matter (TSM) or CDOM. Waters higher in inorganic particles than in phytoplankton. As the turbidity increases the following modifications appear: The R_{rs} values are generally higher than for case 1 throughout the spectrum and of a different shape. There is no longer, a minimum at 440 nm, on the contrary, the curves become convex between 400 and 560nm. The maximum is flatter than in case 1, but located at the same wavelength, 560 nm. The increase in back-scattering (b_b) is not compensated by a proportional increase in absorption, since R_{rs} values become higher as turbidity increases.
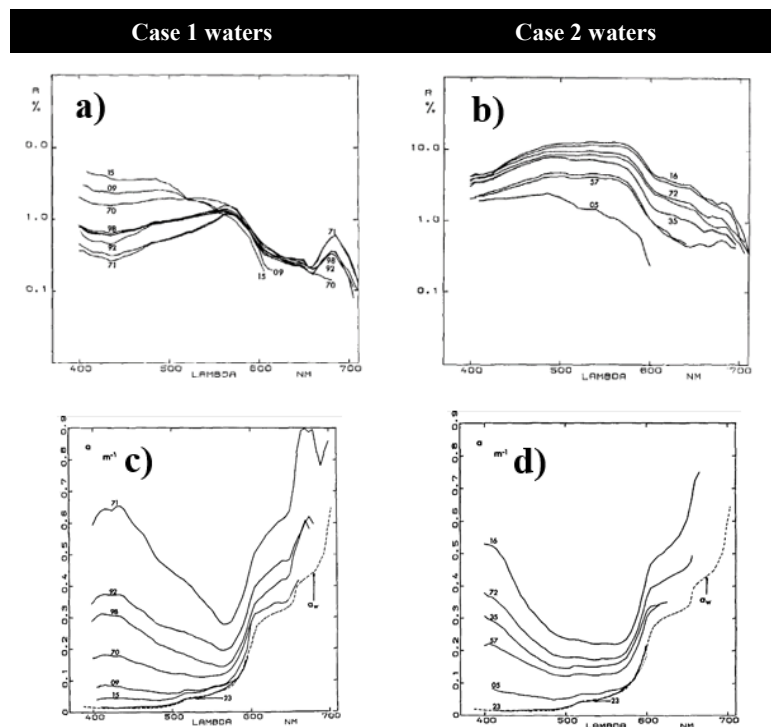
Figure 1-6 Attenuation (k_d), scattering (b_w) and absorption (a_w) coefficients for pure water. a) Experimental R_{rs} curves for different stations listed in inset. b) Experimental R_{rs} curves illustrating case 2 waters. c) Spectral values of absorption coefficient, ex

The Case 1-2 scheme is commonly used as a way to classify waters for modelling purposes. Thus bio-optical models have been developed for the prediction of inherent optical properties (IOPs, namely the absorption, scattering, and backscattering coefficients) in Case 1 waters (Mobley et al., 2004).

Although Case 1 waters cover a larger proportion of the Earth's surface, there is far more variability within Case 2 waters and in an attempt to described this variability more accurately, there have been recent new approaches. Moore et al. (2014) proposed a method to classify waters into seven optical water types (OWTs; **Figure 1-7**) and Spyrakos et al. (2018) identified 13 OWTs (**Figure 1-8**) for inland waters based on comprehensive data from more than 250 aquatic systems. This last approach has been considered the most suitable for its accuracy and applicability and, therefore, will be the approach followed along the development of this Thesis.
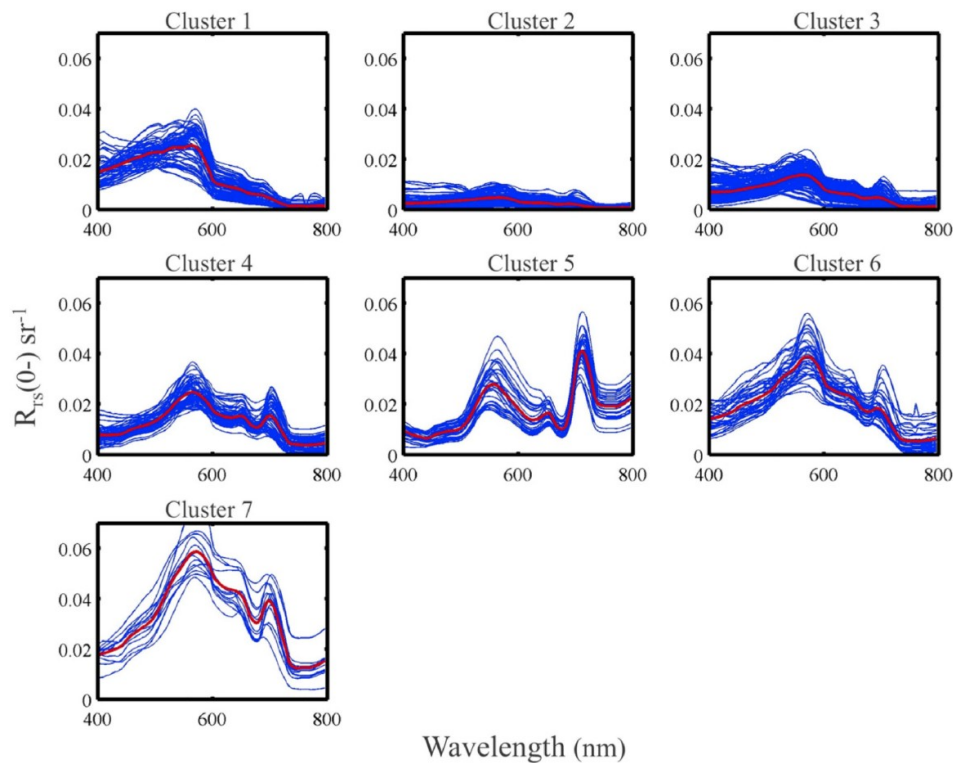
Figure 1-7 Reflectance data sorted into seven clusters from Moore et al. (2014). Blue lines are individual in-situ reflectance and red lines mean values.
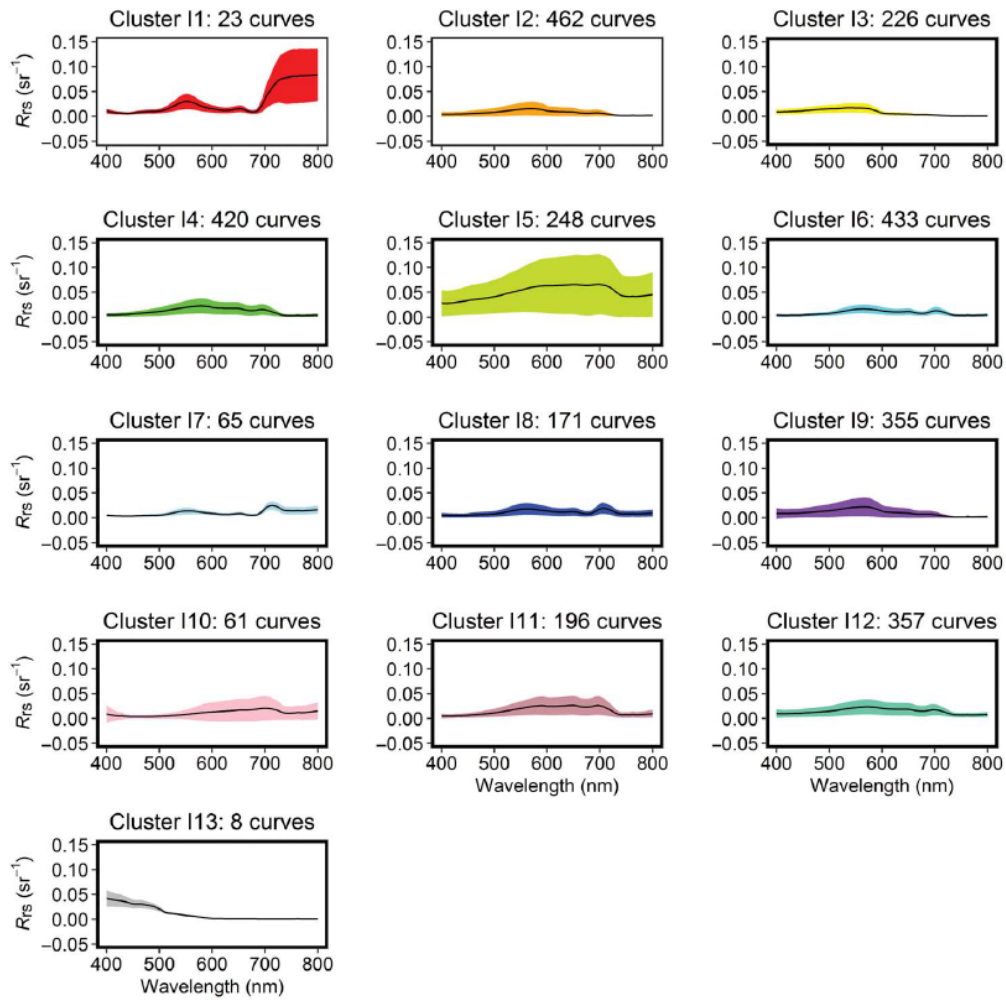
Figure 1-8 Mean remote sensing reflectance (R_{rs}) and standard deviation (shaded area) obtained in inland water s by Spyrakos et al. (2018).

1.3.3. Remote sensing of water quality

In-situ data collections are only able to represent point estimations of the quality of water conditions in time and space, and obtaining spatial and temporal variations of quality indices in large waterbodies is almost impossible (Ritchie et al., 2003). To overcome these limitations, the use of remote sensing in water quality assessment has demonstrated being a useful tool, both to understand different and simultaneous processes occurring in lakes as well as to obtain information regarding spatial and temporal variability processes, especially when combined with additional local information (Nouchi et al., 2019).

1.4. Remote sensing of CDOM

As it has been previously stated, DOC pool comprises most of the organic carbon in lakes and CDOM has widely been used to describe a fraction of the DOC pool which has historically been called *gelbstoff* or "yellow substance".

In many systems, estimation of DOC through remote sensing of CDOM works well (Stedmon et al., 2011; Yamashita et al., 2011), even though there are exceptions generally related to lakes and lake-influenced rivers that show weaker relationships linked with low-colour autochthonous CDOM from phytoplankton and macrophytes (Spencer et al., 2012). It has also been demonstrated that low-colour DOM from wastewater or agricultural origin may shift the CDOM-DOC relationship.

One of the most challenging points of developing remote sensing algorithms for estimation of DOC relates to the fact that the relationship between CDOM and DOC is very variable, being even negative or poorly defined in some occasions (Zhao and Song, 2018). Moreover, the relationships can vary between regions and/or seasons (Brezonik et al., 2015). Given this and taking into account the fact that CDOM

absorption is the only proxy for remote estimation of DOC, further research is considered needed for the retrieval of DOC in lakes from space.

Both DOC and CDOM can be of autochthonous (derived from in-situ primary and bacterial production) or allochthonous (terrigenous) origin and composed of low molecular weight (LMW) or high molecular weight (HMW) substances (Sempéré and Cauwet, 1995; Del Vecchio, 2004; Aurin et al., 2010; Martínez–Pérez et al., 2019). Most near-shore CDOM is usually of terrigenous origin composed by HMW substances and it is degraded over time both by microbial activity, photooxidation and other abiotic processes.

CDOM tends to dominate the blue and UV part of the spectrum and it is the most important factor controlling UV and blue light penetration. Its presence reduces the photosynthetically active radiation available for phytoplankton and macrophyte growth and generates heat in the surface layers of the water column, thus affecting mixing (Pegau, 2002). In the UV, CDOM also causes surface heating, but acts protecting aquatic organisms by the reduction of high frequency radiation harmful for cell structures.

The absorption of light by CDOM initiates a variety of processes that lead to multiple reactions ending up with the loss of CDOM absorption (Kouassi et al., 1990; Reche et al., 1999; Twardowski and Donaghay, 2001; Del Vecchio and Blough, 2002) and acting as a sink of CDOM. These "photobleaching" reactions can increase transparency of surface waters with important consequences (Williamson et al., 1996). It is therefore to understand the dynamics of CDOM and the significance of photobleaching as sink in inland water bodies.

1.4.1. Compilation of algorithmic approaches

Many approaches have been proposed to retrieve CDOM from remote sensing imagery. Some are empirical models (based on band ratios) but also semi/quasi-analytical models, matrix inversion methods (MIM), artificial neural networks (ANN) and optimisation methods.

The development of reliable methods for estimating CDOM across optically different inland waters needs to deal with several issues. Between others, CDOM levels vary seasonally in a water body (Lars J. Tranvik et al., 2009; K. Toming et al., 2016; Zhu et al., 2018; Chen et al., 2019; Massi et al., 2020). Moreover, spectral properties of CDOM vary spatially and over time in a given water body (Babin et al., 2003; Keith et al., 2002; Kutser et al., 2009b). Finally, the relationship between measured CDOM absorptivity at 440 nm (a_{CDOM} (440))and DOC as mg per litre is not constant (Vodacek et al., 1997; K. Toming et al., 2016; Hestir et al., 2015; C.G. Griffin et al., 2018; Chen et al., 2019).

On top of that, to retrieve CDOM values from spectral reflectance data is difficult for several reasons; sometimes, it has been described as the most difficult parameter to measure accurately in inland waters. First of all, CDOM absorbs but does not scatter or reflect light, therefore, the upwelling water-leaving radiance is very small in CDOM rich waters. CDOM absorbance does not present any peak; instead, its absorption follows a simple quasi-exponential decrease with increasing wavelength. This means that its effects on reflectance are higher in the blue region of the electromagnetic spectrum, just where atmospheric correction is more difficult (Kutser et al., 2005). Finally, the measurement of low levels of CDOM in optically complex waters (those containing mineral suspended solids, algae and associated organic particles) is especially difficult given the light scattering induce by these particles.

First attempts to retrieve water quality information remotely were made for the application of Landsat satellites and knowledge about the radiative transfer process in optically complex waters has developed enormously since then. Large number of algorithms for the retrieval of biogeochemical parameters have been developed for inland waters, but its applicability and associated uncertainties for its application on the full range of optical water types needs to be further developed (Palmer et al., 2015b). Sources, magnitude and variability in the IOPs of the water as well as specific properties in highly turbid waters also need to be tackled.

1.4.2. Algorithm selection, decision process

The first empirical algorithm found in the literature to retrieve CDOM remotely is based on a blue-green band ratio, generally more suitable for oceanic environments (Tassan, 1994). Since then, some of the most used algorithms for CDOM retrieval are based on green-red band ratios (Kutser et al., 2005b, 2015; Kaire Toming et al., 2016; Ligi et al., 2017).

The problem of empirical algorithms, even though they are the ones of simplest application given that do not require a big knowledge about IOPs and AOPs of the water, is that they are usually developed under specific site characteristics and therefore very sensitive to changes in the specific composition of water constituents when the conditions change (IOCCG, 2000).

Semi-analytical methods retrieve total absorption and scattering from Rrs at a reference wavelength and then infer individual contributions from classes of optically active constituents by application of semi-empirical models (Lee et al., 2009).

Matrix inversion methods also require knowledge about site specific IOPs and are, therefore, generally not applicable across different environments without the support of

field measurements. And finally, artificial neural network (ANN) approaches such as Doerffer and Schiller (2007) have also been successfully developed and applied.

However and even though there are several algorithms of each category developed and successfully applied in different coastal or open sea environments, few studies have looked at their utility on inland water bodies and when done, it has been based on specific environments (Zhu et al., 2014a).

Several studies have recently been published looking at the comparison in performance of existing bio-optical models, mainly for the estimation of Chl-a concentration in inland waters (i.e. Gurlin et al., 2011; Augusto-Silva et al., 2014; Beck et al., 2016) and TSM (i.e. Petus, 2013).

Most algorithms to determine Chl-a concentration are based on measurements of 675 and 700 nm wavelengths. Neil et al. (2019) investigated the accuracy of several algorithms to retrieve Chl-a concentrations, concluding that empirical three-band ratio algorithms perform generally poorly when compared to two band empirical algorithms. Moreover, they state that the blue-green ratio algorithms are more sensitive to changes in Chl-a concentration at low reflectance levels, whilst semi-analytical models are better at dealing with optical complexity. They finally show that accuracy in the retrieval can be improved by targeting specific OWTs in algorithm development.

Remote sensing algorithms have also been widely used to estimate TSM providing spatial and temporal variations. Ritchie (1976) showed that the most useful range of spectrum for the determination of suspended particles in surface waters was between 700 and 800 nm. The use of single band based algorithms can provide a robust approach when the band is chosen appropriately (Nechad et al., 2009). Curran et al. (1987) and Novo et al. (1989) demonstrated that single band algorithms may be applied

in those cases where TSM increases with increasing reflectance. However, the complex composition of inland waters can cause variation in colours and therefore in reflectance, and thus, different spectral bands have been proposed for TSM retrievals (Doxaran et al., 2002; Nechad et al., 2009; Feng et al., 2014). CDOM estimation models have also been reviewed by Odermatt et al. (2012) and Zhu et al. (2014).

The majority of these algorithms have been tried on individual or small groups of water bodies with generally limited variability on their optical water types, only Neil et al. (2019) applies an optical water type tuning approach, testing the original algorithms on a set of 2807 samples collected from 185 global inland water bodies and considering 13 different optical water types.

1.5. Conclusions

While CDOM is widely accepted as a good estimator of DOC in inland water bodies a great diversity of spectral characteristics and relatively weak relationships between CDOM and DOC have also been found. Moreover, the composition of DOM also presents seasonal variations that can influence its dynamics.

Most of the studies found, looking at the origin, distribution and degradation of DOM and how this influences its optical properties, have been undertaken in coastal waters or in high latitude lakes. Few studies have focused on large shallow temperate lakes. Even though in these systems the DOC pool is typically smaller than at higher latitudes it still plays a significant role in regulating light availability and therefore lake metabolism, while the influence of processes such as photobleaching is also likely to be more pronounced.

1.6. Thesis objectives

The general aim of this Thesis is to contribute with the knowledge of remote sensing of CDOM in inland water bodies. For this, it approaches the following research lines addressed by the subsequent Thesis chapters:

1. To look at the regional variability in CDOM optical properties aiming to characterise the link between CDOM absorption and DOC content in inland waters.

2. To explore spatial and seasonal variability in optical properties of CDOM and its degradation. Investigating how changes in its absorption can be used to infer information on the concentration, sources and decomposition of CDOM.

3. To present an extensive CDOM algorithm validation exercise.

1.7. Thesis structure

The Thesis is structured to guide the reader through the research questions previously outlined.

First of all, a literature review (CHAPTER 1 –) gives an overview of previous works carried out in this area and provides with background information on subjects relevant to this study.

Following there are three data chapters. Chapter 2 looks at the relationship between CDOM absorption and DOC in UK and other European lakes in order to characterise the link between CDOM absorption and DOC content within a wide range of inland water bodies. It defines a_{CDOM}-DOC relationships in these inland waters, tests different parameters for describing the variation in the a_{CDOM}-DOC ratio and determine the general conditions for which CDOM may be used as a proxy of DOC. Chapter 3 delves into the spatio-seasonal variability of CDOM absorption deepening into the

photobleaching phenomena and Chapter 4 evaluates the accuracy of a_{CDOM} algorithm performance over a wide range of optical water types (OWTs) examining the influence that specific parameters such as Chl-a and other optically active constituents have on the estimation performance.

The concluding chapter (Chapter 5) summarises the findings of the preceding three chapters and makes recommendations for further investigations based on these conclusions.

2. CHAPTER 2 – THE RELATIONSHIP BETWEEN COLOURED DISSOLVED ORGANIC MATTER ABSORPTION AND DISSOLVED ORGANIC CARBON IN UK AND EUROPEAN LAKES

2.1. Introduction

Dissolved organic carbon (DOC) represents the biggest reservoir of organic carbon in inland water ecosystems (Hedges, 2002; Chen and Borges, 2009), playing a major role in the global carbon cycle (Tranvik et al., 2009; Yang et al., 2015). Carbon in lakes originates from a variety of sources that can be either of allochthonous or autochthonous origin. Allochthonous carbon is of terrestrial origin and arrives through the export of organic carbon from ecosystems that enters directly as plant and litter detritus (particulate and dissolved). The second pathway (autochthonous carbon) can be the product of the *in situ* fixation of atmospheric carbon dioxide (CO_2) by photoautotrophs in the water column.

Lakes have been described as indicators and regulators of climate change (Tranvik et al., 2009; Williamson et al., 2009a), however, our understanding of the DOC stock in lakes and its rates are still limited, even though essential in order to be able to assess its role. Quantification of DOC concentration is relatively easy through field observations and laboratory analysis, but remote and inaccessible lakes are out of reach for this estimation (Brezonik et al., 2015).

Remote sensing can contribute with the possible assessment of DOC distribution from in-situ or satellite measurements of the optical properties of coloured dissolved organic matter (CDOM). Light absorption by CDOM at 440 nm (a_{CDOM} (440)) often correlates strongly with DOC concentrations (Kutser et al., 2005a; Osburn and Stedmon, 2011; Spencer et al., 2012; Griffin et al., 2018) and has been widely used in order to estimate

the composition and quantity of DOC in aquatic systems (Helms et al., 2008;

Massicotte et al., 2017). However, the correlation between a_{CDOM} (440) and DOC will

just work when the chromophoric fraction of DOM represents most of the DOC pool,

and when that chromophoric fraction has homogeneous molecular weight and

composition.

Estimated CDOM values could be converted into the DOC concentrations by using

regression models (Bieroza et al., 2009), being an univariate linear regression the most

popular approach to using optical methods for DOC estimation. CDOM optical

properties (absorption at 440nm) is the basis of the bio-optical model to derive DOC.

However, the CDOM optical properties and the CDOM-DOC relationship generally

present high seasonal and spatial discrepancies.

Allochthonous organic matter from agricultural or urban sources usually lacks

aromatic, light absorbing compounds (Tsui and Finlay, 2011). Historic landscape

modification has also led to eutrophication and, therefore, an increase in the production

of low colour DOM of autochthonous origin (Y. Zhang et al., 2009). CDOM

concentration can be measured by its absorption coefficient (a_{CDOM}) at 440 nm and its

structure and composition can be inferred from the spectral slope parameter (S_{CDOM})

calculated between two reference wavelengths (Cédric G. Fichot and Benner, 2012;

Helms et al., 2008).

For more than a decade, studies have demonstrated that satellite remote sensing can be

effectively used to trace CDOM in freshwaters (Del Castillo and Miller, 2008; Zhu et

al., 2014a; Fichot et al., 2016; Chen et al., 2017; Spyrakos et al., 2018a), assuming a

conservative relationship between CDOM absorption and DOC concentration (Spencer

et al., 2012; Tehrani et al., 2013; Chen et al., 2017). However, low colour lakes with

higher contributions of in-lake or allochthonous origin CDOM, have shown a greater

48

diversity of spectral characteristics and relatively weak relationships between CDOM and DOC (Griffin et al., 2018).

DOC concentrations in arctic rivers (e.g. Kolyma River), are higher during the spring, being lower and more stable during the autumn (Holmes et al., 2012) and the DOM to CDOM composition changes rapidly in storms and spring freshets, being the DOC concentration during the spring freshet and summer discharge higher and lower in autumn (Spencer et al., 2010). Hestir et al. (2015) looked at six reservoirs in Australia along a temperate to tropical gradient not finding a good correlation between the CDOM and DOC.

There are several studies looking at CDOM-DOC relationship for coastal waters (Fichot and Benner, 2011; Fichot et al., 2013), for inland systems literature is limited however is lately growing (Kutser et al., 2005; Spencer et al., 2012; Yunlin Zhang et al., 2007a).

The present study examines regional variability in CDOM optical properties from a multi-year dataset of samples from contrasting lakes across Europe. It specifically aims at characterising the link between CDOM absorption and DOC content within a wide range of inland water bodies. Moreover, we define a_{CDOM}-DOC relationships in these inland waters, test S_{CDOM} for describing the variation in the a_{CDOM}-DOC ratio and determine the general conditions for which CDOM may be used as a reliable proxy of DOC.

2.2. Material and methods

2.2.1. Study sites

The dataset is composed of samples from 11 European water bodies including 8 lakes in the United Kingdom (UK): Loch Leven, Loch Lomond, Loch Ness, Bassenthwaite,

Coniston, Derwent Water, Windermere and Ullswater; and three large European lakes: Lake Vänern (Sweden), Lake Geneva (Switzerland) and Lake Balaton, (Hungary). Collectively, these lakes encompass a large range of Chlorophyll-a (Chl-a), particulate organic carbon (POC), DOC and CDOM concentrations. It constitutes a diverse set of lakes climatically, tropically (eutrophic to oligotrophic), in size of lake (4.9 to 5,650 Km^2) and catchment (62.5 to 47,000 Km^2) and depth (3.3 to 310 m).

The lakes were sampled in one or more occasions between May 2013 and June 2015 and the characteristics of the sampling campaigns carried out are shown in **Table 2-1**.

Table 2-1 Record of DOC, POC, Chl-a and a_{CDOM} (440) samples, sampling sites and sampling dates

Sampling site	Sampling dates		Number of samples			
	Year	Month	DOC	POC	Chl-a	$a_{CDOM\ (440)}$
Loch Lomond	2013	May	--	--	4	6
		June	12	12	12	12
		July	6	6	6	6
		September	4	7	4	7
	2014	May	5	5	5	5
		June	6	6	3	6
	2015	June	--	4	3	--
		Total	**33**	**36**	**37**	**36**
Loch Leven	2013	May	4	4	4	4
		June	5	3	5	5
		September	8	8	8	8
	2014	August	5	5	5	4
		Total	**22**	**20**	**22**	**21**
Loch Ness	2014	July	7	7	6	7
Windermere	2013	July	7	7	7	7
	2014	August	--	5	4	5
		Total	**7**	**12**	**11**	**12**
Derwent Water	2013	July	5	5	5	5
	2014	August	5	4	5	5
		Total	**10**	**9**	**10**	**10**
Bassenthwaite	2013	July	5	5	5	5
	2014	August	5	4	5	5
		Total	**10**	**9**	**10**	**10**
Ullswater	2014	August	5	5	6	6
Coniston	2014	August	--	4	5	5
Lake Geneva	2014	June	--	--	6	6
Lake Vanern	2015	August	15	10	15	15
		September	15	7	15	15
		Total	**30**	**17**	**30**	**30**
Lake Balaton	2013	August	--	--	11	19
	2014	July	55	--	5	18
		Total	**55**	**--**	**16**	**37**

Regarding the three lakes in Scotland (UK, **Figure 2-1b**), Loch Lomond is the largest

lake in Great Britain and its trophic status ranges from mesotrophic in the shallow south

basin to oligotrophic in its deeper north basin (Habib et al., 1997; **Table 2-2**). It has

been recorded as the second richest lake in term of phytoplankton biodiversity and

fourth in terms of phytoplankton species richness (Habib et al., 1997). Loch Leven is

the largest shallow lake in Great Britain (**Table 2-2**) and has been intensively

monitored since the late 1960s; it has been strongly affected by external pressures including diffuse nutrient inputs. Nevertheless, recent efforts have improved Loch Leven water quality, cyanobacterial blooms (Brook, 1965) have reduced in frequency and spring water quality has increased (Carvalho et al., 2012) since the reduction of phosphorous (P) sources. However, dense cyanobacterial blooms still occur during hot summers.

Table 2-2 Physical characteristics of sampling sites (catchment area, mean catchment altitude, trophic status, latitude, longitude, lake length, area, volume, maximum depth and mean depth.

Lake	Catchment area (km^2)	Mean catchment altitude (m)	Trophic status	Lat/Lon	Lake length (km)	Area (km^2)	Volume (Mm^3)	Max. depth (m)	Mean depth (m)
Loch Lomond	766	8	Mesotrophic Oligotrophic	56.1114° N, 4.6289° W	39	71	2698	190	37
Loch Leven	145	107	Eutrophic	56.1966° N, 3.3764° W	6	13.3	52.4	25.5	3.9
Loch Ness	1775	15.8	Oligotrophic	57.3229° N, 4.4244° W	39	56.4	7400	230	132
Bassenthwaite	360	333	Mesotrophic Eutrophic	54.6794° N, 3.1941° W	6.2	5.3	27.9	19.0	5.3
Coniston	62.5	227	Mesotrophic	54.3432° N, 3.0716° W	8.7	4.9	113.3	56.1	24.1
Derwent Water	85.4	354	Mesotrophic	54.5769° N, 3.1468° W	4.6	5.4	29.0	22.0	5.5
Ullswater	147	393	Mesotrophic Oligotrophic	54.5762° N, 2.8860° W	11.8	8.9	223.0	63.0	25.3
Windermere	425	231	Mesotrophic Eutrophic	54.3807° N, 2.9068° W	16.8	14.8	314.5	64.0	25.1
Lake Geneva	46.800	372	Mesotrophic	42.5917° N, 88.4334° W	73	580	8900	310	154.4
Lake Vanern	47.000	44	Oligotrophic	59.0320° N, 13.6255° E	140	5.650	153.000	106	27
Lake Balaton	5.174	105	Eutrophic Mesotrophic	46.8303° N, 17.7340° E	78	592	1.9	12.2	3.3

Loch Ness is a large and deep oligotrophic lake in northern Scotland and holds the largest volume of water in the Great Britain (**Table 2-2**). Given its very low phytoplankton production (Jones et al., 1997), there is a very high dependence of the food web on allochthonous organic matter inputs from the catchment.
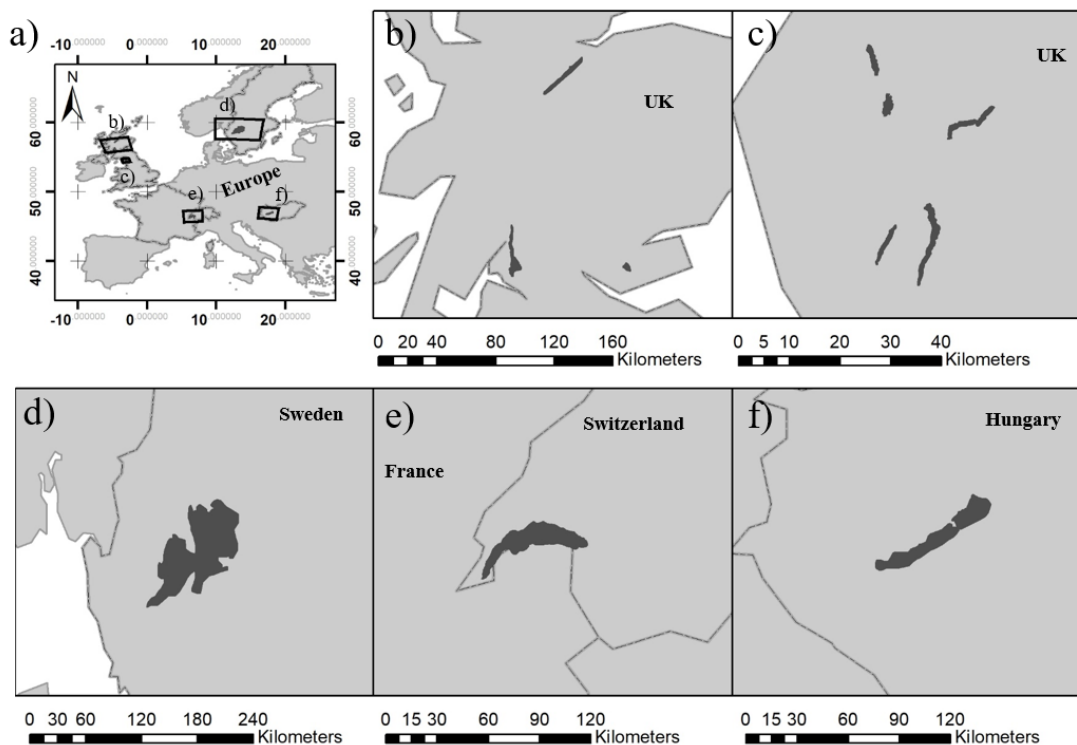
Figure 2-1 Sampling sites locations. **a)** Location of the 11 sampling sites within Europe and zooms of different areas. **b)** From top to bottom right, Loch Ness, Loch Lomond and Loch Leven, **c)** from top to bottom right, Bassenthwaite, Derwent Water, Ullswater, Coniston

Five more lakes are located within the English Lake District, Bassenthwaite Lake, Coniston, Derwent Water, Ulls Water and Windermere (**Figure 2-1c**). The lakes range from the less productive Coniston, Derwent Water and Ullswater to the more productive Windermere and Bassenthwaite (Maberly et al., 2006; **Table 2-2**). The English Lake District is one of the most popular touristic regions in the UK and has been subject of an increased use of fertilisers which has increased the ecological pressure on the lakes.

Finally, three European lakes, Lake Geneva, Lake Vanern and Lake Balaton (**Figure 2-1d, e and f; Table 2-2**). Lake Geneva is the largest freshwater body in western Europe and has been in recovery from eutrophication since the 1980s. Currently, after an intensive restoration effort, the lake has returned to its previous mesotrophic state. Lake Vänern is the third largest lake in Europe and the largest Swedish inland water (Willen, 1984). Its total biomass corresponds to that of oligotrophic lakes (Willén, 2001) and it usually presents a phytoplankton bloom in spring (between May and early June) and another one in summer (generally in August). It has some eutrophic regions particularly in shallow embayments in the southern part of the lake. Lake Balaton is one of the largest shallow lakes in Eastern Europe, situated in the mid-western part of Hungary. The site is an historical popular holiday resort and after a period of anthropogenic eutrophication from the late 1960s until the mid-1990s, restoration measures aimed at reducing the nutrient load reaching the lake led to gradual re-oligotrophication. The nutrient loading to Lake Balaton from River Zala (Szilágyi et al., 1990) induces a pronounced eutrophic (>20 mg m^{-3} Chl-a) to mesotrophic (2.6-20 mg m^{-3} Chl-a) gradient from west to east.

2.2.2. Sampling methods and analysis

- *DOC measurements*

Water samples for DOC analysis were collected using acid-rinsed polypropylene bottles at 0.3 m depth below the surface. The samples were immediately stored on ice and in the dark until they were transferred to the laboratory for filtration. The samples were filtered through 0.7 μm pre-combusted 47 mm glass-fibre membranes (Whatman GF/F) and stored cold (4 °C) and in the dark until measurement. They were after analysed for DOC concentration by thermal catalysis at 950ºC in an Elementar High

TOC instrument (Elementar Analysensysteme GmbH Germany) equipped with a platinum catalyst cartridge using synthetic air as the carrier gas.

- ### *Chl-a concentrations*

Water samples for Chlorophyll-a (Chl-a) analysis were filtered in triplicate through GF/F filter papers and stored at -80ºC in the dark until analysis. Chl-a was determined spectrophotometrically after extraction for 24 hours in 96% hot ethanol on a dual-beam Cary 100 Varian spectrophotometer.

- ### *POC*

Particulate organic carbon (POC) content was determined from lake water samples (100-200 mL) filtered through pre-combusted 47 mm diameter Whatman GF/F filters (cut to 9 mm) and stored at -80ºC. The filters were dried before analysis at 70°C and combusted in a Fisons EA-1108 CHN analyser (Grasshoff et al., 2009). Sulphanilamide was used as the standard.

- ### *CDOM*

Samples for CDOM analysis were collected separately in acid-rinsed amber glass bottles from 0.3 m depth and immediately stored on ice and in the dark until transfer to the laboratory. Samples were prefiltered through pre-combusted 0.7 µm pore size glass-fibre membranes (Whatman GF/F) to remove large particles and then re-filtered through a 0.2 µm Whatman nucleopore membrane filters. Loch Lomond and Loch Leven samples were measured fresh (i.e. without preservation) within 24 h following (G. Tilstone et al., 2002). Samples for Windermewre, Derwent Water, Bassenthwaite, Loch Ness, Lake Geneva, Ullswater, Coniston, Lake Vanern and Lake Balaton were preserved with a 0.5 % (vol : vol) solution of 10 g L^{-1} of sodium azide (NaN_3) (Ferrari

et al., 1996) prior to analysis, which was completed within 1 month of sample collection.

Absorbance (A) of the samples was determined on a Shimadzu UV 1601 spectrophotometer (Cuthbert and Del Giorgio, 1992; Kirk, 2010) using a 1, 4 or 10 cm path-length cuvette between 350 and 800 nm with 0.5 nm sampling interval using Milli-Q as a reference (Vodacek et al., 1997). CDOM spectral absorption coefficients (a_{CDOM}) were calculated using **equation (2-1)** (Kirk, 2010):

$$a_{CDOM}(\lambda) = 2.303 \cdot {A_{CDOM}(\lambda)}/{L} \qquad \qquad \textbf{(2-1)}$$

Where $A_{CDOM}(\lambda)$ is the measured absorption at a given wavelength and L is the cuvette path length in meters. A baseline correction was applied by subtracting the mean value of a_{CDOM} in a 5 nm window centred on 685 nm (Babin et al. 2003). This wavelength was selected because CDOM absorption is negligible and the effects of temperature and salinity on water absorption are small (Pegau et al., 1997).

The spectral slope of the CDOM absorption curve was calculated over the wavelength range of 350-500 nm ($S_{CDOM}(350–500)$) (Babin et al., 2003) using a single exponential decreasing function fitted by non-linear regression (NLR) (**equation 2-2**; Bricaud et al., 1981; Twardowski et al., 2004), where λ_{ref} is a reference wavelength (440 nm in this study).

$$a_\lambda = a_{\lambda_{ref}} \cdot e^{-S(\lambda-\lambda_{ref})} \qquad \qquad \textbf{(2-2)}$$

The E2/E3 index (250 to 365 nm absorption ratio), also known as M value, developed by De Haan and De Boer (1987) was calculated to track changes on relative size on

CDOM molecules. Decreasing ratios indicate increasing molecular size, aromaticity and humification (Peuravuori and Pihlaja, 1997).

Specific UV absorptivity at 254 nm (SUVA$_{254}$) was obtained by normalising the absorption coefficient at 254nm to DOC concentration (mg/L) (Weishaar et al., 2003a). As aromatic groups are largely responsible for absorption at this wavelength, this index indicates the degree of aromaticity of CDOM in the sample (Weishaar et al., 2003b; Helms et al., 2008).

2.2.3. Data analysis

CDOM-DOC relationship was tested by calculating univariate linear regressions between DOC concentration and each a_{CDOM} (440).

Moreover, CDOM structure and composition was inferred from the spectral slope parameter (S_{CDOM}) calculated between 350 and 500 nm (Cédric G. Fichot and Benner, 2012; Helms et al., 2008).

The UV absorbance parameter (SUVA$_{254}$) is the UV absorbance of the water sample at 254 nm normalised by the dissolved organic carbon (DOC) concentration. It is strongly correlated with DOM and an indicative of a higher abundance of aromatic compounds. And the E2:E3 ratio (M value) is the ratio of absorption at 250 nm and 365 nm. (De Haan and De Boer, 1987) and is generally used to track changes in relative size of CDOM molecules: increases in molecular size result in decreases in the E2:E3 ratio because of stronger light absorption by higher molecular weight compounds at longer wavelengths.

Finally, the relationship Chl-a to a_{CDOM} (440) relationships were also investigated.

All analyses were performed using R statistical software (R Core Team, 2017) and figures made in R using "ggplot2" (Wickham, 2016) package except for **Figure 2-1** which was created in ArcGIS v10.5.

2.3. Results

2.3.1. Optical and biogeochemical variability

Over the study lakes, the mean values of Chl-a (20.137±25.511), DOC (5.654±3.332), POC (0.832±1.350) and a_{CDOM} (440) (1.273±1.571) recorded showed a wide variability (**Table 2-3**). No DOC data were available for lakes Coniston and Geneva and no POC data were available for Lake Geneva.

Table 2-3 Water quality in different types of waters, DOC (Dissolved Organic Carbon), POC (Particulate Organic Carbon), Chl-a (Chlorophyll-a concentration) and a_{CDOM} (440) (CDOM absorption at 440nm)

Sampling site		a_{CDOM} **(440)**	**DOC (mg/L)**	**POC (mg/L)**	**Chl-a (µg/L)**
Loch Lomond	Mean	1.189	3.089	0.229	7.627
	Range	0.013-3.363	2.037-5.386	0.060-0.463	1.250-21.805
Loch Leven	Mean	0.501	6.058	1.781	57.897
	Range	0.093-1.003	3.623-21.400	0.496-3.172	10.557-100.640
Loch Ness	Mean	0.273	3.705	0.169	3.979
	Range	0.226-0.336	2.647-4.578	0.133-0.267	2.072-6.907
Bassenthwaite	Mean	1.193	2.799	0.451	17.007
	Range	0.868-1.529	2.214-3.415	0.327-0.745	6.265-36.276
Coniston	Mean	0.596	NA	0.293	9.987
	Range	0.521-0.667	NA	0.256-0.321	9.012-10.985
Derwent Water	Mean	0.835	2.126	0.321	8.691
	Range	0.507-1.181	1.691-2.684	0.234-0.419	4.900-12.284
Ullswater	Mean	0.569	1.391	0.421	13.967
	Range	0.431-0.704	0.830-1.643	0.258-0.781	9.801-19.405
Windermere	Mean	0.570	1.638	0.413	15.453
	Range	0.442-0.829	1.558-1.682	0.238-0.984	7.943-26.837
Lake Balaton	Mean	2.610	9.388	1.151	21.47
	Range	0.120-10.070	7.870-18.640	0.058-9.165	0.005-55.253
Lake Geneva	Mean	0.273	NA	NA	12.010
	Range	0.214-0.325	NA	NA	3.486-45.156
Lake Vanern	Mean	1.418	5.443	1.453	21.699
	Range	1.019-2.254	4.197-9.040	0.058-10.152	2.092-135.371
All	**Mean**	**1.273**	**5.654**	**0.832**	**20.137**
	Range	**0.013-10.070**	**0.831-21.400**	**0.055-10.152**	**0.005-135.371**

Maximum values of Chl-a were found at Lake Vanern (135.371 µg l^{-1}) and Loch Leven (100.64 µg l^{-1}). Minimum values at Loch Lomond (1.25 µg l^{-1}) and Loch Ness (2.072 µg l^{-1}). Lake Vanern showed the maximum variability in the dataset, with Chl-a concentrations ranging between 2.092 to 135.37 µg l^{-1}. Mean and extreme values per lake are shown in **Table 2-3**.

DOC concentrations varied between 0.831 mgL^{-1} at Ullswater to 21.4 mgL^{-}1 at Loch Leven. Maximum mean DOC values were found at Lake Balaton (9.388 mgL^{-1}) and minimum average values at Ullswater (1.391 mgL^{-1}). Concentrations at Lake Balaton were in the range of values previously reported (Aulló-Maestro et al., 2017) and no previous reports about Ullswater DOC content have been found to compare with this study. Highest POC values were found at Lake Vanern (10.152 mg L^{-1}) and Lake Balaton (9.165 mg L^{-1}) and minimum values at Lake Balaton (0.058 mg L^{-1}) and Loch Lomond (0.06 mg L^{-1}).

No published references have been found regarding POC at Lake Balaton, however, minimum values for Loch Lomond were lower than values previously reported for both north and south basin 0.29-0.76 mg L^{-1} (Bass, 2007), even though average values (0.229 mg L^{-}) were in the range of previous studies (Bass, 2007). Mean POC values for all the dataset varied between 0.169 (Loch Ness) and 1.781 mg L^{-1} (Loch Leven).

a_{CDOM} (440) varied between 0.013 m^{-1} at Loch Lomond to 10.07 $^{-1}$ at Lake Balaton. Maximum mean values were found at Lake Balaton (2.61 m^{-1}) and minimum average values at Lake Geneva (0.273 m^{-1}). Reference values for a_{CDOM} (440) for Lake Balaton were not found in published studies.

2.3.2. DOC vs CDOM relationship for various types of waters

The relationship between DOC and CDOM was investigated based on CDOM absorption at 440 nm. Considering the whole dataset, the relationship between a_{CDOM} (440) and DOC (n=116, R^2=0.164, p<0.05) was weak (**Figure 2-2**).
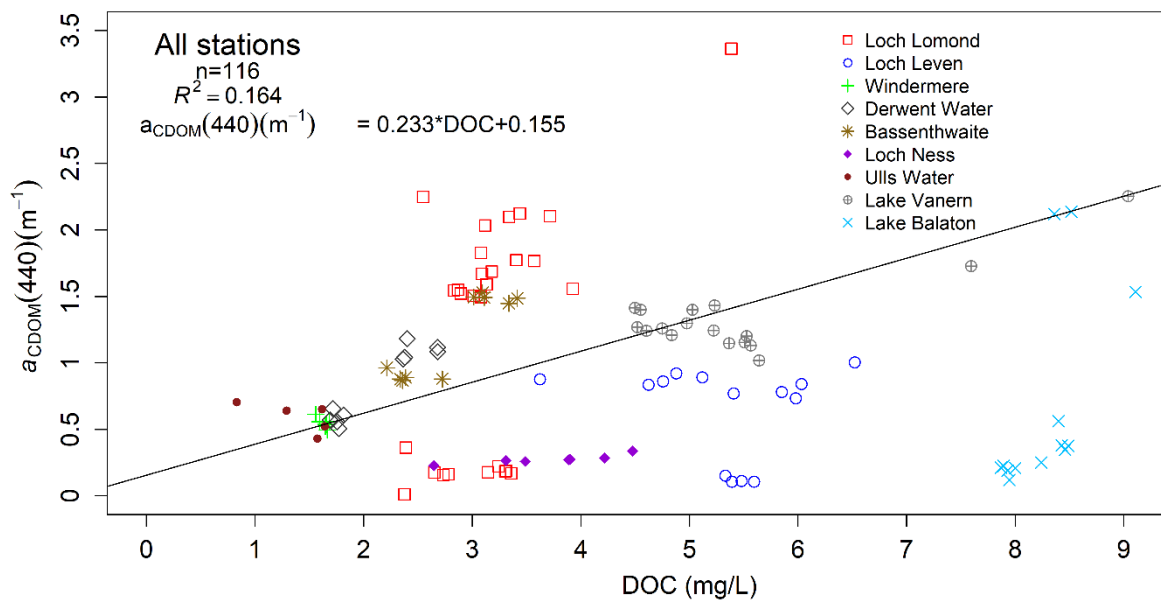
Figure 2-2 Direct relationship between a_{CDOM} (440) and DOC for all the dataset

Table 2-4 reports the statistics for the regressions using a_{CDOM} (440), with slopes ranging from -0.056 (Loch Leven) to 2.639 (Lake Balaton). No DOC data for regression were available for Coniston and Lake Geneva.

Table 2-4 Fitting equations for DOC against a_{CDOM} (440) in different types of waters. DOC data for regression was not available for Lakes Geneva and Coniston.

Site	Equations	R^2	N	p-value
Loch Lomond	a_{CDOM} (440) =0.736*DOC-0.992	0.293	31	<0.01
Loch Leven	a_{CDOM} (440) =-0.056*DOC+0.948	0.058	14	0.29
Loch Ness	a_{CDOM} (440) =0.049*DOC+0.093	0.814	7	<0.01
Bassenthwaite	a_{CDOM} (440) =0.628*DOC-0.564	0.807	10	<0.01
Coniston	NA	NA	NA	NA

Derwent Water	a_{CDOM} (440) =0.632*DOC-0.509	0.899	10	<0.01
Ullswater	a_{CDOM} (440) =-0.214*DOC+0.888	0.441	5	0.22
Windermere	a_{CDOM} (440) =-0.628*DOC-1.575	0.561	7	0.05
Lake Balaton	a_{CDOM} (440) =2.369*DOC-18.322	0.463	18	<0.01
Lake Geneva	NA	NA	NA	NA
Lake Vanern	a_{CDOM} (440) =0.185*DOC+0.412	0.609	30	<0.01
ALL	a_{CDOM} (440) =0.233*DOC+0.155	0.089	139	<0.01

When splitting the data in individual sampling sites, some significant relationships between a_{CDOM} (440) and DOC can be seen. Regression using a_{CDOM} (440) were statistically significant for Loch Lomond, Derwent Water, Bassenthwaite, Loch Ness, Lake Vanern and Lake Balaton, with coefficients of determination (R^2) ranging between 0.23 (Loch Lomond) and 0.899 (Derwent Water), all of them presented a positive correlation. The strongest correlations were found for Loch Ness, Derwent Water and Bassenthwaite (**Figure 2-3a, b** and **c**), resulting Derwent Water and Bassenthwaite divided in two clusters of lower and higher a_{CDOM} (440) and DOC.
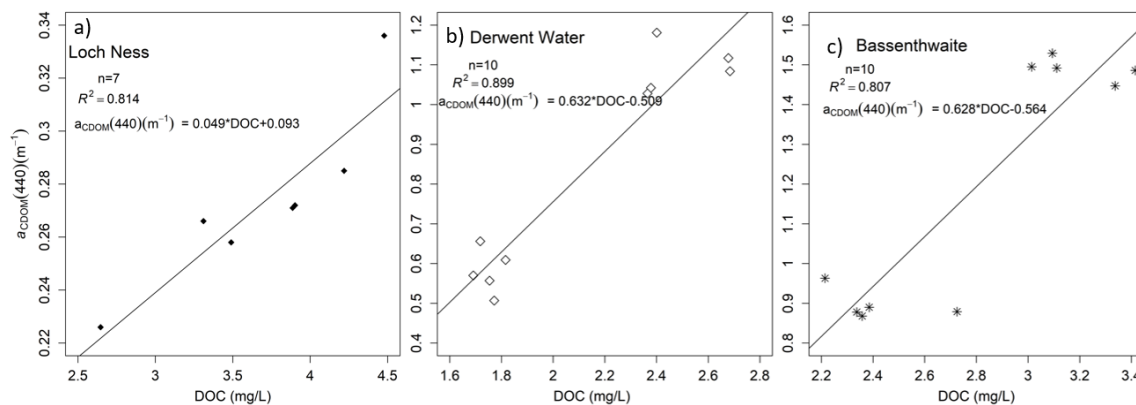
Figure 2-3 Relationships between DOC and a_{CDOM} (440) in a) Loch Ness, b) Derwent Water and c) Bassenthwaite

Lake Vanern and Lake Balaton also showed strong relationships (R^2=0.61 and 0.463 respectively; **Figure 2-4 a** and **b**).
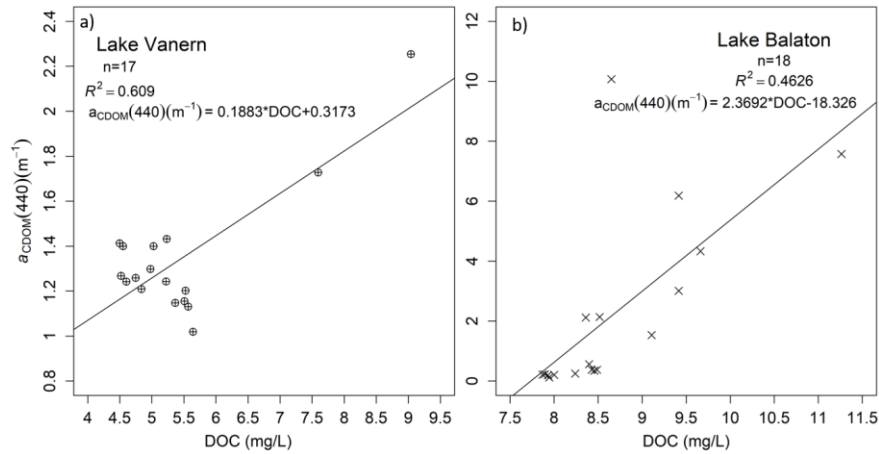
Figure 2-4 Relationships between DOC and a_{CDOM} (440) in a) Lake Vanern and b) Lake Balaton

The relationships between CDOM and DOC exhibited negative intercept for some lakes (Loch Lomond, Windermere, Derwent Water, Bassenthwaite and Lake Balaton), showing that not all DOC is chromophoric.

Moreover, it needs to be taken into account, that the association of dissolved iron with DOC affects the water colour, and spatial variations in iron concentrations lead to poor DOC-CDOM relationships (Prieur and Sathyendranath, 1981).

Moreover, strong negative relationships have been found for Windermere and Ullswater (**Table 2-4**). No DOC data were available for Lake Geneva and Coniston.

2.3.3. CDOM molecular weight and aromaticity

S_{CDOM} (350-500) values for the entire dataset ranged between -0.001 (Lake Balaton) and 0.102 (Lake Windermere) nm^{-1} (**Table 2-5**). Minimum values were found at Lake Balaton (0.001 nm^{-1}) and Lage Geneva (0.011 nm^{-1}). Highest variability was found at Loch Lomond (0.012-0.050nm^{-1}) followed by Lake Balaton (0.030 nm^{-1}).

Table 2-5 Mean and range values of a_{CDOM} (440), S_{CDOM} (350-500), [DOC], E2:E3 ratio and SUVA$_{254}$ per sampling site

		a_{CDOM} (440) (m^{-1})	S_{CDOM} (350-500) (nm^{-1})	E2:E3 ratio	SUVA254 (Lmg^{-1}m^{-1})
Loch Lomond	Mean	1.189	0.018	5.151	9.537
	Range	0.013-3.363	0.012-0.050	4.133-9.145	6.427-13.838
Loch Leven	Mean	0.501	0.017	7.222	2.693
	Range	0.093-1.003	0.015-0.028	6.390-9.356	0.105-6.333
Loch Ness	Mean	0.273	0.015	8.297	1.468
	Range	0.226-0.336	0.013-0.015	7.903-9.010	1.233-1.779
Bassenthwaite	Mean	1.193	0.017	5.415	7.673
	Range	0.868-1.529	0.015-0.017	5.191-6.003	6.204-9.088
Coniston	Mean	0.596	0.017	5.965	NA
	Range	0.521-0.667	0.016-0.018	5.771-6.141	
Derwent Water	Mean	0.835	0.017	5.349	7.281
	Range	0.507-1.181	0.016-0.018	5.515-5.631	6.160-8.558
Ullswater	Mean	0.569	0.018	5.714	9.733
	Range	0.431-0.074	0.017-0.021	5.428-6.160	7.033-16.505
Windermere	Mean	0.570	0.017	6.042	6.562
	Range	0.442-0.829	0.016-0.1018	5.524-7.632	6.176-6.917
Lake Balaton	Mean	2.610	0.015	11.243	3.252
	Range	0.120-10.070	0.001-0.016	2.736-47.197	2.252-5.604
Lake Geneva	Mean	0.273	0.012	59.278	NA
	Range	0.214-0.325	0.011-0.013	50.644-77.235	
Lake Vanern	Mean	1.418	0.017	7.083	6.590
	Range	1.019-2.254	0.015-0.019	6.279-12.864	5.051-9.690
All	**Mean**	**1.273**	**0.016**	**8.895**	**5.525**
	Range	**0.013-10.070**	**0.001 – 0.102**	**2.736-77.235**	**0.105-16.505**

S_{CDOM} (350-500) exhibited a negative correlation with a_{CDOM} (440) for Loch Ness ($R^2=0.737$), Ullswater ($R^2=0.644$), Coniston ($R^2=0.980$) and Lake Geneva ($R^2=0.364$) that has already been found in other studies (Del Castillo and Coble, 2000; C. A. Stedmon et al., 2000; Kowalczuk et al., 2003a; Yacobi et al., 2003a; Yunlin Zhang et al., 2007a) and a slight positive correlation was found at Bassenthwaite ($R^2=0.344$).

Lowest SUVA$_{254}$ values (**Table 2-5**) were found at Loch Leven (average 0.105 mg^{-1}) and highest values at Ullswater (average 9.733mg^{-1}). No SUVA$_{254}$ data were available for Coniston and Lake Geneva. As it can be seen in **Figure 2-5**, SUVA$_{254}$ also exhibited high values for Bassenthwaite, Derwent Water, Ullswater and Windermere.

Highest M value (Figure 2-5) was found for Lake Geneva (59.278), followed by Loch Leven, Loch Ness, Lake Balaton and Lake Vanern, which indicates that low molecular weight molecules dominate in this water (less light absorption). High values (higher than 8.895, the average value for all the water bodies) were found for Lake Balaton (11.243).
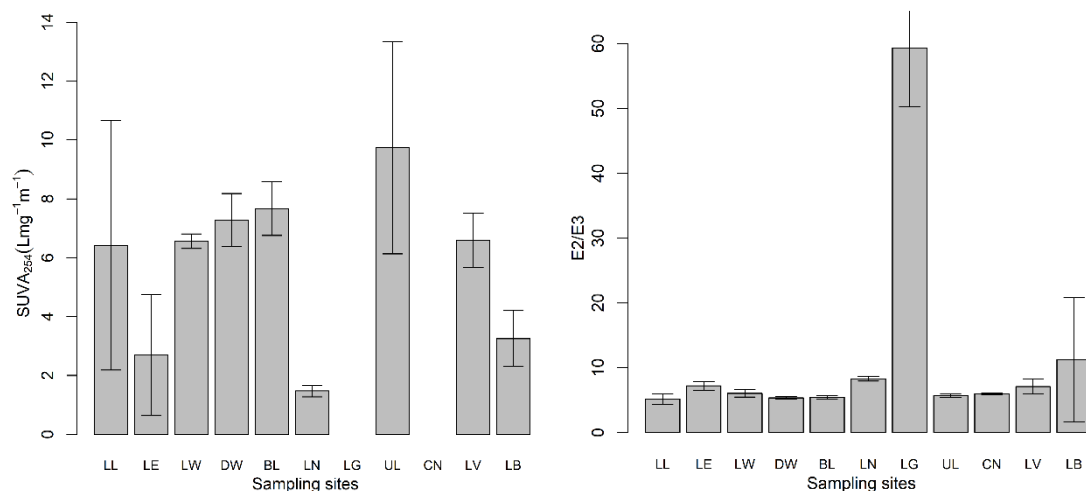
Figure 2-5 SUVA$_{254}$ and E2:E3 ratio variation per sampling site

2.3.4. a_{CDOM} to Chl-a relationship

Chl-a was not strongly related to CDOM, DOC or SUVA when all the samples were considered together ($R^2 = 0.006$, 0.172 and 0.018 respectively) but when separating samples clear differences appeared in Chl-a patterns with the three parameters.

For Loch Ness, Windermere and Derwent Water, Chl-a did not correlate with CDOM ($R^2 < 0.200$), DOC and SUVA and Chl-a variations were not large across the sampling sites.

However, Chl-a explains 57% of a_{CDOM} (440) in Loch Leven (**Figure 2-6a**), 58% Bassenthwaite (**Figure 2-6b**) and 43% in Lake Vanern (**Figure 2-6c**).
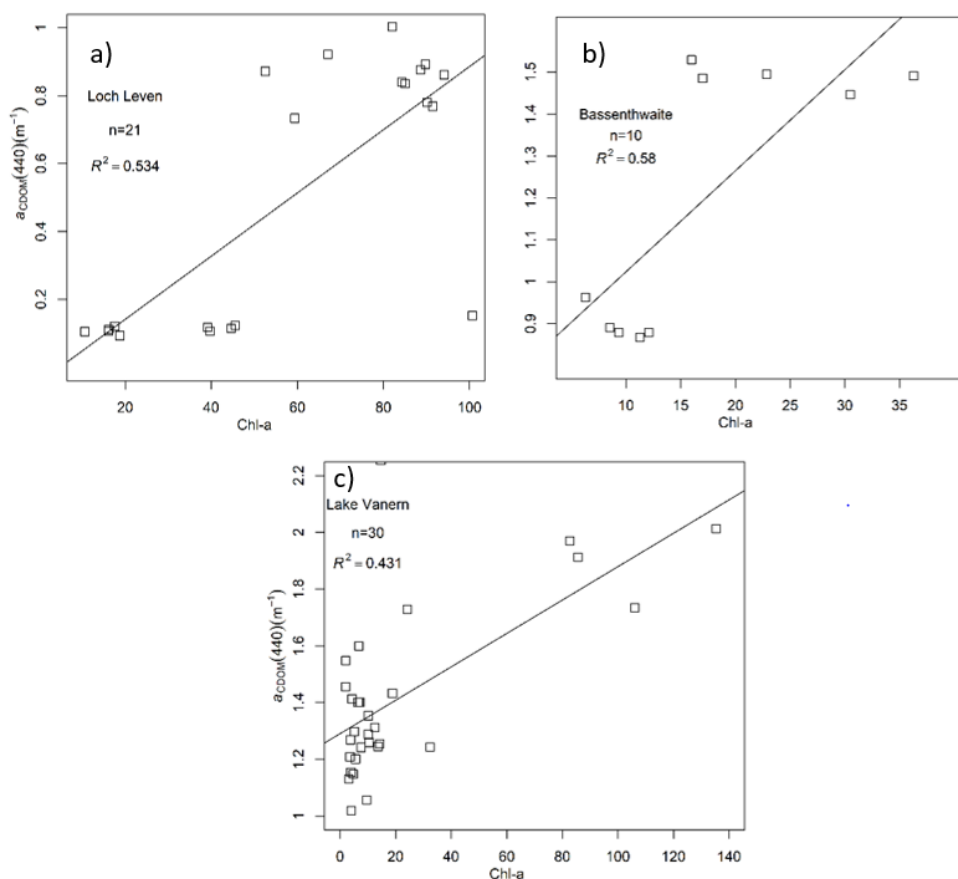
Figure 2-6 a_{CDOM} (440) to Chl-a relationship for a) Loch Leven, b) Bassenthwaite and c) Lake Vanern

2.3.5. Discussion

Different water bodies were sampled across Europe, presenting different climatic, hydrologic and land use conditions as well as very different catchments with diverse anthropogenic influence. The biological and geochemical properties of these water bodies is very diverse, presenting a large variability for each parameter measured (**Table 2-3**). The most turbid waters have generally been collected in shallow water bodies (**Table 2-2**, **Table 2-3**), which is consistent with previous findings (Song et al., 2017).

Lower DOC concentrations have been found in samples collected generally mesotrophic lakes which most of the DOC is coming from the catchment (Ullswater, Windermere, Derwent Water and Bassenthwaite; **Table 2-3**.

High DOC concentrations have been found at Lake Balaton and Loch Leven (9.388 and 6.058 respectively), both lakes with signs of eutrophication and a recently intense anthropogenic influence. The Zala wetland, responsible of about half of the total Balaton watershed, provides DOC into Balaton, whereas DOC in Loch Leven could to be the decaying of an algal bloom. Higher concentrations were found for shallower water bodies (Lake Balaton and Loch Leven), probably as a result of less dilution within the water body.

It should be noted at this stage, that DOC concentrations are strongly connected with hydrological conditions and catchment landscape features (Lee et al., 2015; Neff et al., 2006).

Generally, the relationships between CDOM and DOC in rivers and other inland waters are very variable due to the possible hydrological variability and other catchment features (Ågren et al., 2010; Spencer et al., 2012; Ward et al., 2013; Zhao et al., 2017). As

demonstrated in **Table 2-4**, the relationship between CDOM and DOC in lake waters of this study are also very variable.

For Loch Leven, Carvalho et al. (2012) showed a mean annual average Chl-a value of 15 µg l^{-1}, therefore the high values for Loch Leven found within this study are possibly in association with a phytoplankton bloom. The same is the case with Lake Vanern, with mean concentrations from existing monitoring data between 2002 and 2012 between 0.6 and 5.9 µg l^{-1} (Philipson et al., 2016), conspicuously lower than concentrations found in this study (average: 20.137 µg l^{-1}). Concentrations obtained for Loch Lomond were within values previously reported (Habib et al., 1997; Bass, 2007), and also for Loch Ness (Jones et al., 2001).

Derwent Water and Bassenthwaite show the strongest relationship between DOC and CDOM with high regression slope values (**Table 2-4**) which has been usually linked with less disturbed water bodies with low anthropogenic influence (Spencer et al., 2012). On the other hand, water bodies more heavily influenced by human activities such as Loch Leven and Lake Balaton, show less clear linkages between CDOM and DOC.

Low CDOM to DOC relationships are a possible consequence of aromaticity and coloured fractions in the DOC components (Spencer et al., 2009; Lee et al., 2015).

This general lack of co-variation can be related to the different biogeochemical and catchment characteristics, trophic status and land cover of the 11 sampling sites, suggesting large differences regarding the source and sink factors acting on CDOM dynamics (Stedmon and Markager, 2001) in these very optically different water bodies.

Lowest CDOM to DOC relationships have been found for Loch Leven, one of the most productive sampling sites of this study. Generally, in less coloured lakes, the composition of DOM has varied widely, leading to weaker relationships (Griffin et al.,

2018), but landscape modification has also historically led to increasing eutrophication of lakes, with substantial autochthonous production of low colour DOM from both phytoplankton and macrophytes (Y. Zhang et al., 2009) which may explain this result.

Most of the sampling sites present high Chl-a concentrations (>3.979 µg/L), reflecting high algal biomass and productivity typical of mesotrophic and eutrophic lakes. Chl-a, primarily an indicator of phytoplankton biomass, thus by itself cannot explain the variability in CDOM-DOC relationships introduced by macrophytic DOM.

A potential cause of the limited relationship is the sample size and range of DOC and CDOM in the study. Although representative range of reservoirs and their conditions were sampled, the sample size is limited relative to the variance (specially within water bodies), challenging even more a higher relationship.

Moreover, we aimed at defining an a_{CDOM}-DOC relationship in these inland waters and test $S_{275-295}$ for describing this variation and determine the general conditions for which CDOM may be used as a reliable proxy of DOC.

Large variations in DOC are observed for all sampling sites (1.39 – 21.4 mg/L). DOC and a_{CDOM} (440) measurements differ between lakes according to trophic status.

Highest values of s_{CDOM} (350-500) were found at Loch Lomond and Lake Balaton. Minimum values were found at Lake Balaton and Lage Geneva. Highest variability was found at Loch Lomond followed by Lake Balaton. Lowest SUVA$_{254}$ values were found at Loch Leven and Loch Ness and highest values at Ullswater, Bassenthwaite, Derwent Water and Windermere. Finally, High M values found at Lake Geneva and Lake Balaton indicate that low molecular weight molecules dominate in this water (less light absorption). Lowest M values were found at Loch Lomond, Derwent Water, Bassenthwaite, Coniston and Ullswater.

High SUVA$_{254}$ and low E2:E3 ratio values are typical of terrestrially-derived DOM, reflective of DOM from wetlands, high DOC loading rates, shallow photic zones and short residence times. Lakes with low DOC and a_{CDOM} are highly variable in SUVA$_{254}$ and M values. Major sources of DOM to oligotrophic lakes are precipitation, aerial deposition, surface waters and ground water.

High SUVA$_{254}$ values were found at Loch Leven, Windermere, Derwent Water, Bassenthwaite Lake, Ullswater and Lake Vanern. High SUVA$_{254}$ values are associated with high molecular weight, aromaticity and humification. Presence of allochthonous material into the lake is supposed to raise SUVA$_{254}$ and it is also associated with higher CDOM absorption values. Low values of S_{CDOM} (Loch Ness, Lake Geneva) along high values in absorption (Loch Ness) suggest a substantial contribution of terrestrial CDOM for Loch Ness.

Variation in DOC-CDOM has implications for remote sensing applications. Estimates of carbon pools might be inaccurate where there is high variability. Lakes of high ecological status in undisturbed catchments might show stronger DOC-CDOM relationships than those in lowland catchments with more anthropogenic disturbance. This will affect estimates for DOC from space at local, regional and global scales.

2.4. Conclusions

The central goal of this study was to examine regional variability in CDOM optical properties and CDOM-DOC relationships across a range of lakes, looking at factors that might affect this variability.

Based on the measurement of CDOM absorption and DOC laboratory analysis, the relationships between CDOM and DOC have been analysed in various types of waters

in Europe. This investigation showed that both CDOM absorption and DOC content varied significantly.

Overall, CDOM and DOC were highly correlated, particularly in Loch Ness, Bassenthwaite and Derwent Water (all sampling sites with low E2:E3 ratio, indicating composition of low aromaticity). For lakes such as Loch Leven (low SUVA254), widely affected by eutrophication, the composition of DOM might weaken the relationships between CDOM and DOC. This is also linked with autochthonous composition and low molecular weight.

The results of this chapter indicate that the relationships between CDOM absorption and DOC can vary remarkably by showing highly varied regression slopes in various types of waters.

The results of this chapter highlight that remote-sensing models for DOC estimation based on the relationship between CDOM and DOC should consider local variability and optical complexity, considering at least groups of water types according to their absorption features.

3. CHAPTER 3 - SPATIO-SEASONAL VARIABILITY OF CDOM ABSORPTION AND RESPONSES TO PHOTOBLEACHING IN A LARGE SHALLOW TEMPERATE LAKE

3.1. Introduction

3.1.1. Importance of CDOM in lakes

There are approximately 117 million lakes on Earth greater than 0.002 km^2 in surface area collectively covering about 3.7 % of its non-glacial surface (Verpoorter et al., 2014). The importance of the role that lakes play as regulators of the carbon cycle and thereby global climate has only recently been recognized (Tranvik et al., 2009), acting as both a sink (sediment storage through flocculation from dissolved to particulate organic carbon) or source for carbon (degradation and resulting mineralization to CH_4, CO and CO_2; (Benoy et al., 2007; Cole et al., 2007a; Tranvik et al., 2009). As a result they also play an important role in transforming and releasing terrestrially-derived carbon to the atmosphere and ocean (Tranvik et al., 2009). As extremely sensitive ecosystems (IPCC, 2007; Millennium Ecosystem Assessment, 2005), lakes can respond rapidly to external pressures including meteorology, climate and land use change. This has led to the emerging concept of lakes as sentinels of environmental change (Adrian et al., 2009; Schindler, 2009; Williamson et al., 2009; Williamson et al., 2009).

The optical properties of lakes provide particularly useful metrics for measuring ecosystem change (Vincent et al., 1998) as they not only convey information on the quantity of particulate and dissolved material but also its quality (Williamson et al., 2014). Furthermore, understanding how the optical properties of particulate and dissolved material in lakes influences the underwater light field and water-leaving radiative signal is important for the development and application of remote sensing techniques for lake monitoring and assessment, but also their application to lake carbon studies.

Much of the dissolved organic matter (DOM) found in lakes typically represents between 90 to 100 % of the total carbon pool ((Wilkinson et al., 2013) and is derived from terrestrial inputs, transported through streams, rivers and wetlands. This allochthonous component of the DOM originates from soils, sediments and plants and is primarily composed of humic substances. The autochthonous fraction of DOM is produced mostly by phytoplankton, zooplankton and bacterioplankton and is largely composed of fulvic acids, carbohydrates, amino acids, proteins, lipids and organic acids.

Chromophoric dissolved organic matter (CDOM) is the coloured fraction of DOM. It is one of the dominant colour-forming constituents in lakes: it not only exerts a strong influence over the underwater light field and water-leaving radiance, but it also has a number of important ecosystem functions. First of all, it absorbs light strongly in the ultraviolet (UV) spectrum limiting the penetration of biologically-damaging UV-B radiation providing protection for phytoplankton and other primary producers (Hoge et al., 1995; Laurion et al., 2000; Williamson et al., 2001; Y. Zhang et al., 2007b). In addition, CDOM can be remineralised by bacteria acting as a source of inorganic nutrients (Buchan et al., 2014),which is important for phytoplankton nutrition, thus

fulfilling an important role in the development of phytoplankton blooms and lake metabolism more widely. On the other hand, studies have also shown that light absorption by CDOM can reduce the amount and quality of photosynthetically active radiation (PAR) available to phytoplankton, thereby decreasing primary production and constraining lake metabolism (Kirk, 1994; Laurion et al., 2000, 1997; Vähätalo et al., 2005). Moreover, its conservative properties with dissolved organic carbon (DOC), means CDOM is often used as a proxy for DOC. Thus, there is substantial interest in the use of CDOM as an optical tracer of DOC due to the importance of the latter in regulating physical, chemical and biological properties of lakes. It is therefore important that we develop a better understanding of the optical properties of CDOM and how these relate to the chemical composition and concentration of DOM whether driven by changes to source relationships or through the in-lake processes and transformation of the carbon pool.

Understanding how the optical properties of CDOM vary both temporally and spatially within lakes and how the observed variability influences the underwater light field is of particular importance for the development and validation of remote sensing-based approaches for retrieving CDOM concentrations. The recent launch of new satellite missions (e.g., Sentinel-2 and -3), allied with the prospect of new hyperspectral sensors (e.g., EnMAP), has provided a new impetus for the development and application of remote sensing techniques for the assessment and monitoring of inland water quality. However, CDOM is arguably the most challenging water quality parameter for reliable estimation of remotely sensed observations (Palmer et al., 2015b) and, in spite of its importance to the physical, chemical and biological function of lakes, it remains one of the least studied parameters. Indeed, few studies have explored the application of remote sensing for the estimation of CDOM in lakes. To progress such research, an

improved understanding of the spatial and temporal variation in the optical properties of CDOM in lakes is needed.

3.1.2. Optical properties of CDOM

CDOM concentration is commonly measured by its absorption coefficient (a_{CDOM}) at 440 nm, whereas its structure and composition has been most commonly inferred from the spectral slope parameter (S_{CDOM}) calculated between two reference wavelengths (Cédric G. Fichot and Benner, 2012; Helms et al., 2008). Other optical metrics related to CDOM compositions include the E2:E3 ratio or M value, which is the ratio of absorption at 250 nm and 365 nm. (De Haan and De Boer, 1987) used E2:E3 ratio to track changes in relative size of CDOM molecules: increases in molecular size result in decreases in the E2:E3 ratio because of stronger light absorption by higher molecular weight compounds at longer wavelengths.

In addition, (Weishaar et al., 2003a) introduced the specific UV absorbance parameter ($SUVA_{254}$) defined as the UV absorbance at 254 nm normalised by the dissolved organic carbon (DOC) concentration. $SUVA_{254}$ has been shown to be strongly correlated with DOM aromaticity in a large number of aquatic environments, with higher $SUVA_{254}$ values indicative of a higher abundance of aromatic compounds. Previous studies have used $SUVA_{254}$ to explore variability in the composition of DOM in natural waters.

The compositional properties of CDOM vary over time in response to processes such as microbial decomposition and exposure to UV irradiation. Previous studies have shown the latter process, first described by (Wipple, 1914) as 'photobleaching', plays a major role in the transformation of DOM in natural waters. Exposure to solar irradiance has been shown to reduce its capacity to absorb light, the loss of absorptivity is linked to a

reduction in molecular weight (MW), alteration of its chemical composition and an increase in the bioavailability of DOM (Corin et al., 1996; Geller, 1986; Keiber et al., 1990; Lindell et al., 1995; Reche et al., 1998; Wetzel et al., 1995) with implications for lake metabolism. S_{CDOM} is also known to vary in response to photobleaching (Cédric G. Fichot and Benner, 2012; Swan et al., 2012).

Most previous studies on the origin, distribution and degradation of DOM and how this influences the optical properties of CDOM have been undertaken in oceans (Andrew et al., 2013; D'Sa et al., 2014; Hancke et al., 2014; Matsuoka et al., 2014), coastal waters (Kutser et al., 2009a; Para et al., 2013; C. a. Stedmon et al., 2000; Vantrepotte et al., 2007) or in high latitude lakes (Ficek et al., 2011a; Ylöstalo et al., 2014). Understandably, the bias towards high latitude systems partly reflects the fact this region contains a high density of humic-rich lakes. There is a relatively rich literature on DOM in temperate lakes (Müller et al., 2014; Jordan S Read and Rose, 2013; Zhang et al., 2011) but few studies have focused on large shallow lakes like Lake Balaton with a continental climate and hence our understanding of the variability in CDOM optical properties in these systems is comparatively poorer. In systems such as Lake Balaton, although the DOC pool is typically smaller than at higher latitudes it still plays a significant role in regulating light availability and therefore lake metabolism, while the influence of processes such as photobleaching is also likely to be more pronounced.

In this study we explore spatial and seasonal variability in optical properties of CDOM in Lake Balaton, a large temperate lake with a highly continental climate. We investigate how changes in spectral absorption, spectral slope coefficients, SUVA$_{254}$ and the E2:E3 ratio can be used to infer information on the concentration, source and decomposition of CDOM. The main objectives of the study were to: (1) characterize the spatial and seasonal trends in CDOM in Lake Balaton over the course of a year and

to (2) determine the origin and magnitude of the variability of different sources of CDOM.

3.2. Material and methods

3.2.1. Study site

With a surface area of 596 km^2 and a mean depth of 3.25 m, Lake Balaton in Hungary is the largest shallow lake in central Europe (**Figure 3-1a**). The region is situated on the boundaries between the Mediterranean, continental, and oceanic climatic zones (Peel et al., 2006), resulting in a climate characterised by dry summers and moderately wet winters with typical continental extremes in temperature. The first two weeks of January are the coldest periods of the year (-4 – 3 °C) whilst July and August the warmest months (15 – 28 °C). The annual precipitation in the Lake Balaton region is between 500–750 mm; most precipitation falls during the spring, while the minimum occurs during the summer. There is a secondary maximum in autumn, due to a strong cyclone activity at that time of the year. In regard to solar radiation, Lake Balaton is situated between the southern, western and central Transdanubian regions in Hungary with an annual mean of 4500 MJ m^{-2}. The highest solar radiation is received in July (650 MJ m^{-2}), while cloudy weather and shorter days mean that lowest radiation occurs in December. The maximum in sunshine duration is also reached in July with more than 250 hours, falling to a minimum of approximately 40 hours during winter months.

Lake Balaton is usually divided into four basins (south-west to north-east): Keszthely; Szigliget; Szemes; and Siófok (**Figure 3-1b**). The lake has 20 permanent and 31 temporary inflows, many of which are small streams or springs in the lake bed. The largest inflow to the lake is the Zala River, which flows through Kis-Balaton reservoir – a large semi-natural wetland system – and enters the lake in the westernmost part of

78

Keszthely basin (**Figure 3-1b**). The only outflow is the Sió channel in the northeast that connects the Siófok basin with the Danube River.

Lake Balaton has experienced eutrophication since the middle of the 18th century due to agricultural intensification and urbanisation within the catchment. Since the early 1980s, significant effort has been invested in improving its water quality (Tátrai et al., 2000). The construction of Kis-Balaton reservoir and wetland system was one of the main engineering controls built to reduce nutrient inflow from the Zala River and the overall loading within the lake. Kis-Balaton removes approximately 60 % of the annual nutrient loading to Lake Balaton (Szilágyi et al., 1990). However, nutrient inputs from the Zala River still result in high summer primary production in the eutrophic (>20 mg m^{-3} chl-a) waters in the western basins, with a steep gradient towards more mesotrophic (2 - 20 mg m^{-3} chl-a) waters in the east. The hypertrophic Kis-Balaton wetland system is believed to be responsible for much of the DOM entering the lake, largely derived from luxuriant growth and decomposition of aquatic plants. Previous research (Palmer et al., 2013; Riddick et al., 2015) has shown that CDOM is usually significantly higher close to Zala River inflow, and decreases towards the outflow but very little is known about the seasonal dynamics of CDOM in the system.

Suspended particulate matter in Lake Balaton is highly variable (spatially and temporally) due to its very shallow depth, constant mixing and susceptibility to wind-driven resuspension events (Istvánovics et al., 2004). Phytoplankton composition in the lake shows strong seasonal trends, with two annual blooms (Hajnal and Padisák, 2008; Padisak and Reynolds, 1998; Présing et al., 2008). In late summer and early autumn, cyanobacterial blooms often occur in the Keszthely basin (I), extending westwards to the Szigliget (II) and Szemes (III) basins and very occasionally to the Siófok (IV) basin (Hajnal and Padisák, 2008; Padisak and Reynolds, 1998; Présing et al., 2008). The

79

lowest phytoplankton biomass generally occurs in February when the lake can be ice-covered; a small dinoflagellate bloom may also occur in April (Mózes et al., 2006).

3.2.2. Water sampling

Spatial variability in CDOM quantity and quality was assessed over a 1-week period in July 2013 (6 stations) and a 3-week period in July 2014 (25 stations) at 31 stations over a biogeochemical gradient from the southwest in the water masses influenced by Zala River to the northeast near the outflow (**Figure 3-1c**). Five stations were also sampled in the Kis-Balaton reservoir during the same period (2 in 2013 and 3 2014). These intensive sampling campaigns were timed to coincide with the annual summer peak in DOC to capture the maximum spatial variability likely to occur in the system.

In order to capture seasonal variability in CDOM quantity and quality, water samples were collected fortnightly at 6 long-term monitoring stations on Lake Balaton over the course of seven months (March to September 2014). These comprised stations 01 and 03 from Keszthely basin (I), station 12 from Szigliget basin (II), station 20 from Szemes basin (III) and stations 25 and 30 from Siófok basin (IV) (for location of stations see **Figure 3-1c**).
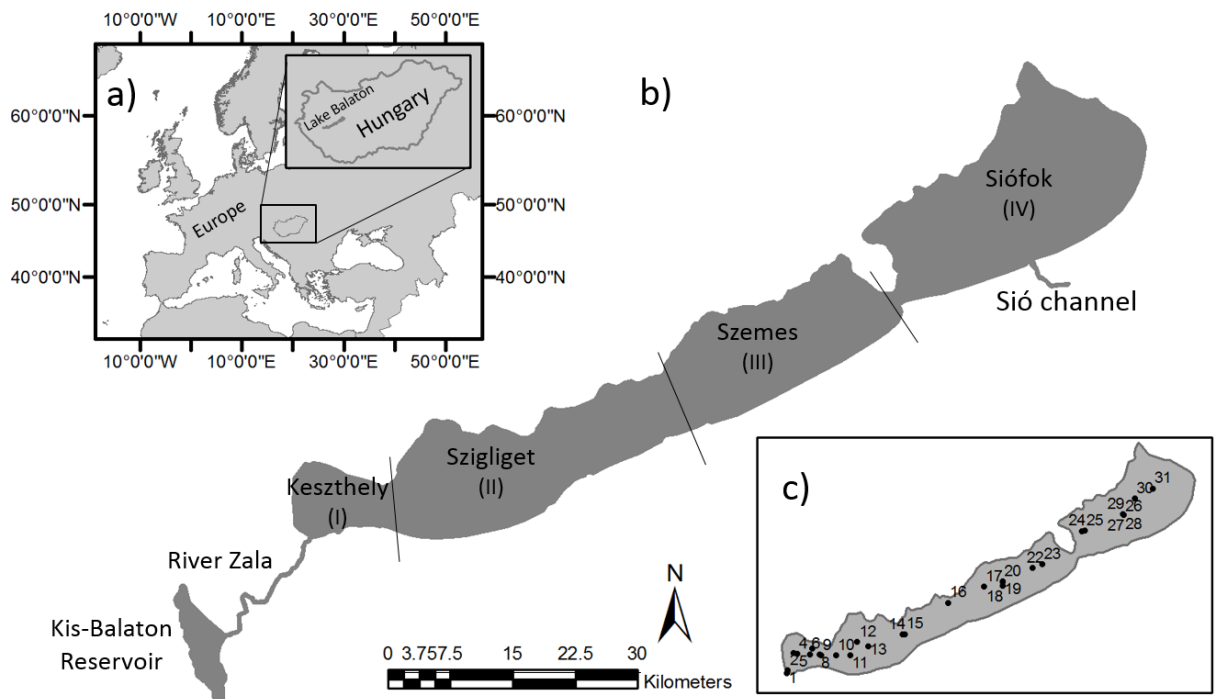
Figure 3-1 a) Location of Lake Balaton within Europe. **b)** Map of basins, Kis-Balaton Reservoir, River Zala and Sió Channel. **c)** Location of 31 sampling stations in Lake Balaton

Water samples for DOC analysis were collected in triplicate using acid-rinsed polypropylene bottles at 0.3 m depth below the surface. The samples were immediately stored on ice and in the dark until they were transferred to the laboratory for filtration. The samples were filtered through 0.7 µm pre-combusted 47 mm glass-fibre membranes (Whatman GF/F) and stored cold (4°C) and in the dark until measurement. Filters were selected for DOC measurements because of their compatibility with other POC measurements and were combusted reducing the possibility of contamination. Even though due to their large nominal pore size, these filters are expected to allow high number of bacteria, viruses and colloids through, the differences with a smaller nominal pore size are expected to be small given that this DOC was only used to correlate with a_{CDOM}. Samples for CDOM analysis were collected separately in acid-rinsed amber glass bottles from 0.3 m depth and immediately stored on ice and in the dark until transfer to the laboratory. Samples were pre-filtered through pre-combusted

0.7 μm pore size glass-fibre membranes (Whatman GF/F) to remove large particles and then re-filtered through a 0.2 μm Whatman nucleopore membrane filters. The samples collected as part of the seasonal sampling campaign were measured fresh (i.e., without preservation) within 24 hours following (Gh Tilstone et al., 2002). The samples collected during the campaigns focused on spatial variability were preserved with a 0.5 % (vol:vol) solution of 10 g L^{-1} of sodium azide (NaN$_3$) (Giovanni M Ferrari et al., 1996) prior to analysis, which was completed within 1 month of sample collection.

3.2.3. CDOM absorption

The spectral absorbance (A) of the seasonal samples was measured on a Shimadzu UV 1601 spectrophotometer (Cuthbert and Del Giorgio, 1992; Kirk, 2010) using a 1, 4 or 10 cm cuvette between 350 and 800 nm with a 0.5 nm sampling interval using ultrapure water (Milli-Q) as a reference (Vodacek et al., 1997). These samples were measured fresh in the laboratory of the Balaton Limnological Institute. Samples from campaigns focused on spatial variability were preserved immediately with 0.5 % (vol:vol) sodium azide and transported to the University of Stirling for analysis on a Cary-100 UV-visible spectrophotometer using a 1 or 10 cm cuvette between 200 and 800 nm with 0.2 nm sampling interval against ultrapure water with 0.5 % (vol:vol) sodium azide as the reference. The absorbance data were baseline corrected by subtracting the mean of a_{CDOM} in a 5 nm interval centred at 685 nm (after Babin et al. 2003). This wavelength was selected because absorption by CDOM and other dissolved constituents is negligible in the far red (Pegau et al., 1997). The CDOM spectral absorption coefficient (a_{CDOM}) was calculated as follows (Kirk, 2010):

$$a_{\text{CDOM}}(\lambda, \text{m}^{-1}) = 2.303 \cdot \frac{A_{\text{CDOM}}(\lambda)}{L} \qquad \textbf{(3-1)}$$

where $a_{CDOM}(\lambda)$ is the absorbance over a pathlength of L meters.

The absorption coefficient at 440 nm was used to express variation in CDOM quantity. This wavelength was preferred over UV wavelengths because it is more relevant to (and consistent with previous) studies on the optical properties and remote sensing of CDOM in natural waters (Carder et al., 1989; Nelson et al., 1998; Schwarz et al., 2002). The spectral slope for the interval of 350–500 nm (S_{CDOM}(350–500)) (Babin et al., 2003) was determined by fitting a single decreasing exponential function to the absorption spectra using non-linear regression (Bricaud et al., 1981; Twardowski et al., 2004) between 350 and 500 nm, as follows:

$$a_\lambda(\text{nm}) = a_{\lambda_{ref}} \cdot e^{-S(\lambda - \lambda_{ref})} \qquad\qquad 3\text{-}2$$

where λ_{ref} is a reference wavelength (440 nm in this study). This range of calculation was consistent with (Babin et al., 2003; Matsuoka et al., 2012)others and is more relevant to remote sensing studies than the use of wavelength ranges that extend into the UV spectrum.

The E2/E3 index was calculated as the ratio of the CDOM absorption coefficients at 250 and 365 nm. Previous studies have shown that decreases in this ratio are related to increases in molecular size, aromaticity and humification of DOC (Peuravuori and Pihlaja, 1997). Finally, specific UV absorptivity at 254 nm (SUVA$_{254}$) was obtained by normalising the absorption at 254 nm by the DOC concentration (mg L^{-1}) (Weishaar et al., 2003a).

3.2.4. Dissolved organic carbon (DOC)

Samples for dissolved organic carbon (DOC) were measured by thermal catalysis at 950°C in an Elementary High TOC instrument (Elementar Analysensysteme GmbH Germany) equipped with a platinum catalyst cartridge using synthetic air as the carrier gas. For spatial measurements, DOC data were only available for 18 out of 31 stations (**Table 2-1**).

3.2.5. CDOM photodegradation

In order to examine the effects of solar radiation on autochthonous and allochthonous CDOM in Lake Balaton, a 7-day in-lake incubation experiment was undertaken during mid-July 2014. CDOM samples from Lake Balaton were incubated in 65 mL capacity quartz tubes over 7 days under natural solar radiation. The mean daytime lake temperature of the lake over the experimental period was 24.6 °C. The quartz tubes were attached horizontally to a wire frame to minimise shading and submerged approximately 1 cm beneath the water surface in a sheltered bay. Fifty-six samples were taken in total of which twenty-one experimental were composed of phytoplankton-derived autochthonous CDOM ($CDOM_{auto}$) and a further 21 were comprised of CDOM of allochthonous origin ($CDOM_{allo}$). In addition, 14 dark control samples ($CDOM_{allo-dark}$ and $CDOM_{auto-dark}$) were incubated (7 allochthonous, 7 autochthonous).

The autochthonous CDOM was extracted from a strain of *Cylindrospermopsis raciborskii* (ACT 9502) previously isolated from Lake Balaton and grown under nutrient replete conditions in semi-continuous culture at 24°C and 14:10 h light/dark cycle. *Cylindrospermopsis raciborskii* dominates the phytoplankton community during summer in Lake Balaton (Présing et al., 1996), often contributing >90% of the total

biomass. A total of 3200 mL of cultured material was centrifuged in the early stationary growth phase (5 min, 4000 rpm; Hermle Z320 BHG) in order to shake off the remaining allochthonous CDOM in the supernatant and the resulting cell pellet was broken using a mini-bead beater (30 s, 3500 rpm; Biospec products) to facilitate the release of cell contents. The total cell disruption was confirmed by microscopic examination (Olympus BX51). Similar processes take place in natural environments. During some natural process the cell releases its content, for example when grazed by zooplankton, (Levine et al., 1999) or in the presence of algal viruses causing the lysis of natural phytoplankton communities (Suttle et al., 1990). The material was incubated in the dark for 5 days at 20°C to allow production of CDOM and then diluted to 0.4 % (vol:vol) with ultrapure water. The $a_{CDOMauto}$ at day 0 was 1.33 m^{-1}.

For the CDOM$_{allo}$ samples, 5 L of water was collected inside the mouth of Zala River at 1 m below the surface with an acid-rinsed amber glass bottle on day zero of the experiment. The predominately allochthonous origin of the DOM was confirmed by mass-spectrometry (Lajtha and Michener, 1994). 0.5 L of water was filtered in triplicate and the filter was dried and stored until analysis on an Isotope Ratio Mass Spectrometer (ANCA-MS, Europa Scientific Ltd., UK). The $\delta^{13}C$ values of the allochthonous samples analysed had a mean $\delta^{13}C$ signal of -33.48 ± 0.43, which is consistent with published data on the $\delta^{13}C$ signature of C3 plants.

The CDOM$_{auto}$ and CDOM$_{allo}$ samples were filtered through a pre-combusted 47 mm diameter glass fibre filter paper (Fisher Brand MF300, nominal pore size 0.7 μm) previously rinsed with ultrapure water to remove particulate matter including bacteria. The samples were re-filtered using 0.2 μm porosity Whatman nucleopore membrane filters. The quartz tubes were acid-washed for 24 h, and then rinsed repeatedly with ultrapure water. The tubes were then filled with the CDOM samples and sealed with

parafilm to prevent contamination. The dark samples were wrapped with black vinyl tape (resistant to UV radiation). Data on the total solar UV-radiation during the experiment were obtained from the Hungarian Meteorological Service.

One $CDOM_{allo}$ and one $CDOM_{auto}$ sample were collected and analysed in triplicate at daily time steps and their absorption and fluorescence spectra were measured. CDOM absorption coefficients were measured according to the methods detailed above. Subsamples for fluorescence measurements were stored cold (4 °C) and in the dark after preservation with a 0.5 % (vol:vol) of 10 g L^{-1} sodium azide (NaN_3) (Giovanni M Ferrari et al., 1996) until further analysis.

Spectral fluorescence signatures (SFS) were measured using an Instant Screener (ISC) analyser (Laser Diagnostic Instruments Ltd., Tallinn, Estonia). Measurements were made using a 1 cm quartz cuvette at excitation wavelengths from 240 to 360 nm and at emission wavelengths from 260 to 575 nm with a 5 nm slit-widths for excitation and emission wavelengths. Ultrapure water with 0.5 % NaN_3 was used as a reference. The fluorescence signals of the samples were examined in two spectral regions. "Protein-like" fluorescence ($F_n(280)$) was excited at a wavelength of 280 nm, with the emission peak recorded in the range 350 ± 5 nm. "Humic-like" fluorescence ($F_n(355)$) was excited at 355 nm and its emission was measured at 450 ± 5 nm (Vignudelli et al., 2004; Vodacek et al., 1997). The fluorescence data were expressed as QSU (Quinine sulfate units; (Coble et al., 1998).

3.3. Results

3.3.1. Seasonal variability

- *CDOM optical properties*

There was some (pronounced in basin 1, noticeable in basin 2 and low in basin 4) seasonal variability in the CDOM concentration measured in Lake Balaton throughout a year (**Figure 3-2**, **Table 3-1**). It should be stressed that seasonal changes were only measured for one year and may not represent the typical seasonal cycle observed over longer time periods. High a_{CDOM} (440) values were observed throughout the year at the mouth of the Zala River in the Keszthely basin at ST01 (**Table 3-2**), with concentrations increasing from an annual minimum in spring (3.69 m^{-1} in March) to a peak in August (9.01 m^{-1}) during the warmest and driest period of the year (Anda and Varga, 2010). Values of a_{CDOM} (440) decreased for ST03 (0.64 m^{-1} in June – 1.43 m^{-1} in March) and were consistently lower and less variable in the other lake basins with a maximum value of 0.63 m^{-1} observed at ST12 (Szigliget) in September and a minimum value of 0.06 m^{-1} at ST30 (Siófok) in June.

Table 3-1 Seasonal variability of a_{CDOM} *(440)* for permanent stations

Month	ST01	ST02	ST03	ST04	ST05	ST06
3	3.694	1.435	NA	NA	0.265	NA
4	5.485	1.244	0.617	0.468	0.228	0.302
5	6.831	0.912	0.603	0.615	0.221	0.329
6	6.872	0.637	0.417	0.152	0.145	0.062
7	7.547	0.670	0.419	0.274	0.088	0.111
8	9.005	0.746	0.507	0.431	0.258	0.189
9	6.172	0.930	0.633	0.265	0.196	0.170
MAX	9.005	1.435	0.633	0.615	0.265	0.329
MIN	3.694	0.637	0.417	0.152	0.088	0.062
MEAN	6.515	0.939	0.533	0.367	0.200	0.194

Table 3-2 Values of CDOM absorption coefficient at 440nm, CDOM slope coefficient between 350 and 500nm, DOC concentration, E2:E3 ratio, SUVA254 and mean distance of the basin to River Zala. Values obtained for CDOM seasonal variation.

Station	Basin	a_{CDOM} (440) (m^{-1}) Min - Max Season Season (Mean±SD)	S_{CDOM} (350-500) (nm^{-1}) Min - Max Season Season (Mean±SD)	[DOC] mg·L^{-1} Min - Max Season Season (Mean±SD)	Distance to River Zala (Km)
01	Keszthely	3.69 - 9.01 Summer - Spring (6.52±1.54)	0.0161 - 0.0181 Spring - Summer (0.0173±0.0006)	10.02 - 19.70 Summer - Winter (16.08±2.88)	0.48
03		0.64 - 1.43 Spring - Summer (0.94±0.28)	0.0187 - 0.0221 Summer - Summer (0.0201±0.0011)	8.97 - 12.67 Autumn - Spring (10.15±1.04)	3.59
12	Szigliget	0.42 - 0.63 Autumn - Summer (0.53±0.09)	0.0185 - 0.0230 Summer - Summer (0.0211±0.0016)	8.88 - 10.85 Autumn - Spring (9.51±0.66)	14.95
20	Szemes	0.15 - 0.61 Spring - Summer (0.37±0.15)	0.0175 - 0.0275 Summer - Summer (0.0213±0.0035)	8.23 - 9.00 Summer - Autumn (8.76±0.23)	39.73
25	Siófok	0.09 - 0.26 Spring - Summer (0.20±0.06)	0.0185 - 0.0279 Summer - Summer (0.0215±0.0033)	7.63 - 8.54 Summer - Spring (8.13±0.25)	62.86
30		0.06 - 0.33 Spring - Summer (0.19±0.10)	0.0158 - 0.0300 Summer - Spring (0.0219±0.0049)	7.82 - 8.36 Autumn - Spring (8.01±0.18)	69.16

The lowest and highest S_{CDOM} (350-500) coefficients were observed in Keszthely (I) basin and ranged from 0.0161 nm^{-1} in August at ST01 to 0.0221 nm^{-1} in June at ST03 (**Figure 3-2**). S_{CDOM} was more variable with increasing distance from the inflow; all the stations except for ST01 demonstrated a maximum in early or mid-summer month (June-July) and minima in spring and autumn (**Table 3-2**). The maximum value for S_{CDOM} (350-500) was 0.0300 nm^{-1} at ST30 in June and the minimum observed was 0.0158 nm^{-1} at ST30 in May, highlighting the high variability of this parameter near the outflow. The mean (and range) in S_{CDOM} (350-500) for Lake Balaton in the summer period was 0.0211 nm^{-1} (0.0174 to 0.0229 nm^{-1}), higher than values reported in several other spatial variation studies including Lake Erie (C. Binding et al., 2008; O'Donnell et al., 2010) and Lake Chapman (O'Donnell et al., 2013).
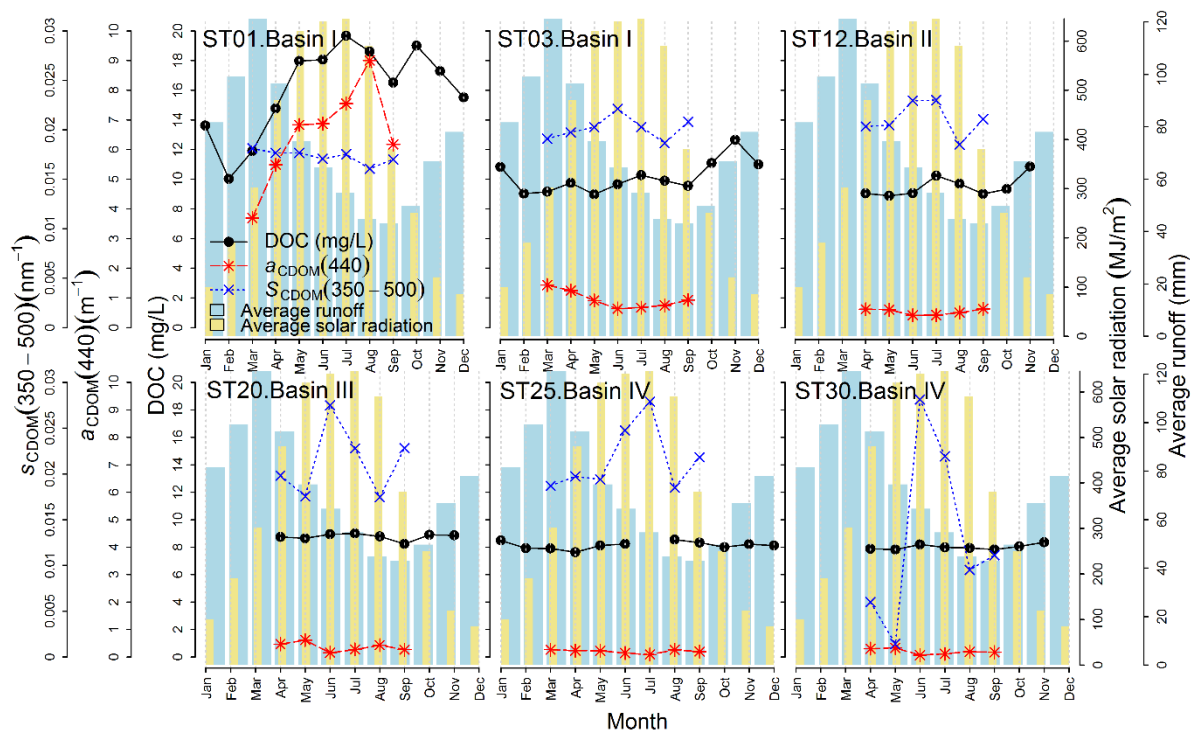
Figure 3-2 Seasonal a_{CDOM} (440), SCDOM(350-500) and DOC concentration variation in Lake Balaton between January and December 2014 and seasonal variability of runoff in Balaton region (Hungary), monthly means from 1921 to 2007 (modified from (Anda and Varga, 2010).

S_{CDOM} (350-500) values for Keszthely and Siófok basins were negatively correlated with a_{CDOM} (440) (**Figure 3-3**a & b) (R^2=0.78, p<0.001 for the Keszthely basin and R^2=0.92, p<0.001 for the Siófok basin). The relationship between S_{CDOM} and a_{CDOM} in the Szigliget and Szemes basins was also negative (R^2=0.91, p=0.01 for Szigliget and R^2=0.79, p=0.01 for Szemes) (**Figure 3-3b**).
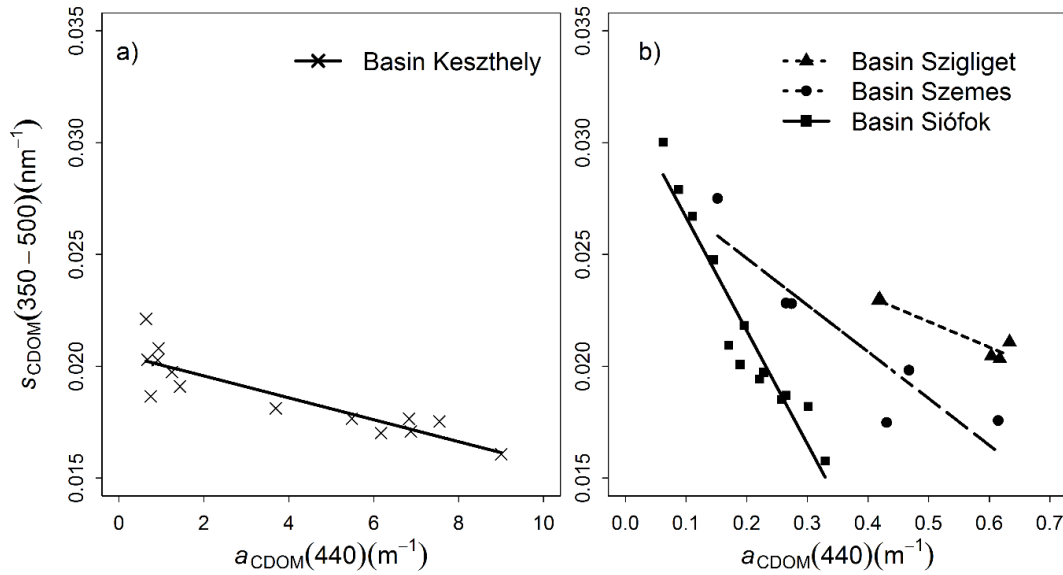
Figure 3-3 Plot of S_{CDOM} (350-500) as a function of a_{CDOM} (440) using the seasonal sampling data for **(a)** basin Keszthely, S_{CDOM} (350-500) = -0.0005·a_{CDOM} (440) + 0.0205, R^2=0.7833, p<0.001 and **(b)** basin Szigliget, S_{CDOM} (350-500) = -0.0114·a_{CDOM} (440) + 0.0277, R^2=0.9122, p=0.011; basin Szemes, S_{CDOM} (350-500) = -0.0209·a_{CDOM} (440) + 0.0209, R^2=0.7932, p=0.0108 and basin Siófok, S_{CDOM} (350-500) = -0.0507·a_{CDOM} (440) + 0.0317, R^2=0.9154, p<0.001.

- ▪ *DOC*

Seasonal variation in DOC was measured at six permanent sampling stations (Stations 01 and 03 from Basin Keszthely (I), Station 12 from Basin Szigliget (II), Station 20 from Basin Szemes (III), Stations 25 and 30 from Basin Siófok (IV). DOC concentrations ranged from 7.63 at ST25 in April to 19.70 mg L^{-1} at ST01 in July with a mean value of 10.1 mg L^{-1} (**Table 3-2**). The highest concentrations were observed at ST01 (where the Zala River enters the lake) in summer (July: mean 19.7 mg L^{-1},

August: mean 18.6 mg L^{-1}) with a slightly smaller secondary peak in early autumn

(October: mean 18.9 mg L^{-1}) (**Figure 3-2**). However, a slightly different trend was

observed in the central part of Keszthely basin at ST03, where DOC started increasing

at the end of the summer reaching a maximum in November (12.7 mg L^{-1}). For stations

furthest from the main inflow, DOC concentrations remained relatively consistent

during the course of the year, with two small peaks at ST12 in July and November.

DOC concentrations at ST20, 25 and 30 were significantly lower at the $p<0.5$ level than

ST01, 03 (ANOVA ($F_{(1,57)}$ = 31.63, $p<0.001$).

Table 3-3 Values of CDOM absorption coefficient at 440nm, CDOM slope coefficient between 350 and 500nm, DOC concentration, E2:E3 ratio, SUVA254 and mean distance of the basin to River Zala. Values obtained for CDOM spatial variation (values July 2014).

Basin	a_{CDOM} (440) (m^{-1}) Min - Max (Mean)	S_{CDOM} (350-500) (nm^{-1}) Min - Max (Mean)	[DOC] $mg·L^{-1}$ Min - Max (Mean)	E2:E3 ratio Min - Max (Mean)	SUVA$_{254}$ ($L·mg^{-1}·m^{-1}$) Min - Max (Mean)	Mean distance to River Zala (Km)
Kis-Balaton	2.45 - 4.66 (3.58)	0.0186 - 0.0191 (0.0189)	---		---	
Kestzthely	0.57 - 7.89 (1.49)	0.0174 - 0.0212 (0.0199)	10.9 - 8.85 (9.66)	34.1 - 11.1 (15.9)	4.45 - 3.59 (4.04)	3.84
Szigliget	0.33 - 4.31 (1.00)	0.0190 - 0.0214 (0.0209)	9.63 - 8.50 (8.85)	28.8 - 14.4 (18.9)	4.35 - 3.24 (3.70)	17.4
Szemes	0.26 - 0.34 (0.294)	0.0211 - 0.0221 (0.0215)	9.07 - 8.03 (8.56)	44.3 -18.4 (27.2)	3.82 - 2.62 (3.12)	40.0
Siófok	0.17 - 0.21 (0.193)	0.0203 - 0.0229 (0.0215)	8.99 - 8.14 (8.66)	62.0 - 24.1 (42.2)	3.13 - 2.47 (2.69)	60.5

3.3.2. Spatial variability

- ***CDOM optical properties***

We observed an a_{CDOM} gradient across the lake (**Figure 3-4a**) with higher a_{CDOM} (440) values in Kis-Balaton and the Keszthely basin (I) (where the Zala River enters into the lake) decreasing rapidly towards the northeastern basins near the outflow. The a_{CDOM} (440) coefficients were markedly different between basins ranging from 0.17 to 7.89 m-1 with the highest value observed in Keszthely basin at the mouth of Zala River (**Figure 3-4a** and **Figure 3-5a**) (**Table 3-3**).
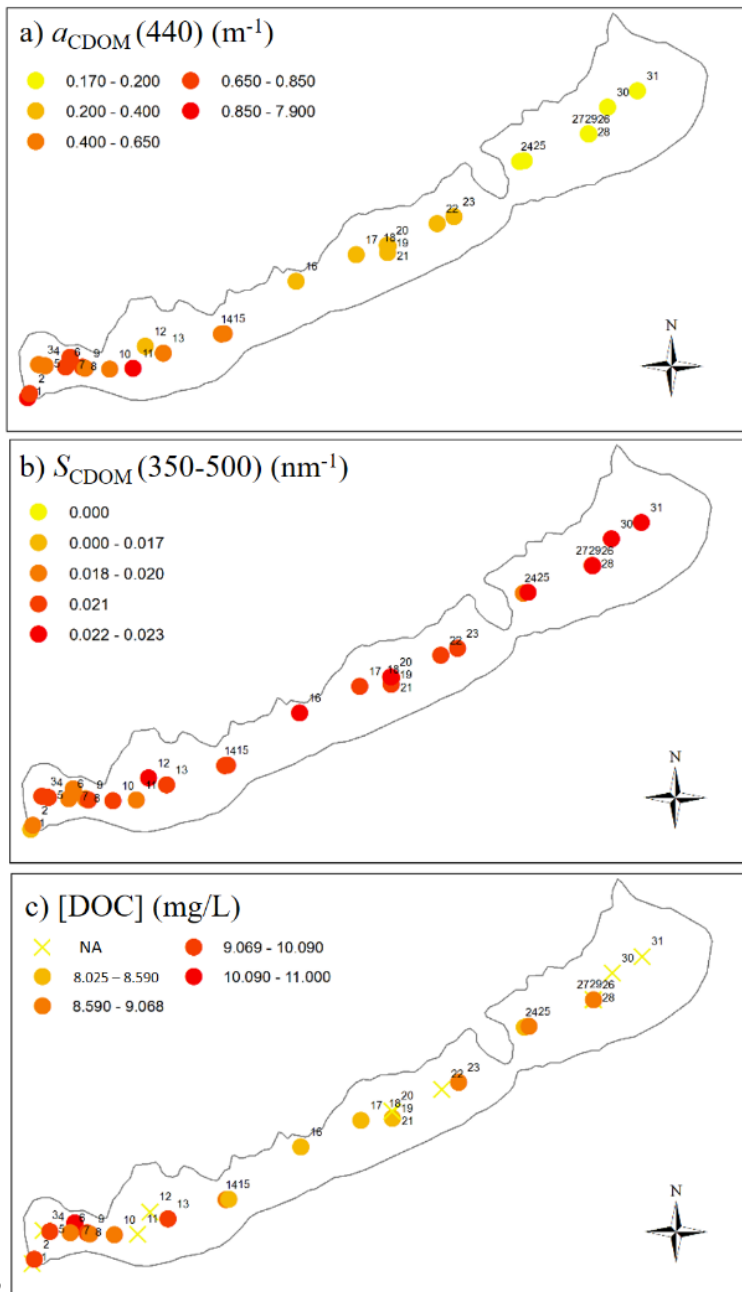
Figure 3-4 a) Spatial a_{CDOM} (440) variation in Lake Balaton per station. b) Spatial SCDOM (350-500) variation in Lake Balaton per station. c) Spatial DOC concentration in Lake Balaton per station. Data derived from measurements made in July 2014.

S_{CDOM} coefficients showed marked variability (0.0174-0.0229 nm^{-1}) compared to previous studies in inland and marine waters (e.g. Helms et al., 2008). There was no consistent trend in S_{CDOM} coefficients across the lake although the lowest values generally occurred in the western basin near the inflow (**Figure 3-4b**, **Figure 3-5b**). In Kestzthely (I) basin and the western parts of Szigliget (II) basin nearest the inflow of

the Zala River, higher variability was observed with lower S_{CDOM} coefficients more than elsewhere in the lake. In our study, S_{CDOM} (350-500) exhibited a negative correlation with a_{CDOM} (440) (**Figure 3-6a & b**) as has been shown in previous studies (e.g., (C. a. Stedmon et al., 2000), (Castillo and Coble, 2000); (Yacobi et al., 2003b); (Rochelle-Newall et al., 2004); (Yunlin Zhang et al., 2007b); (Kowalczuk et al., 2003b).
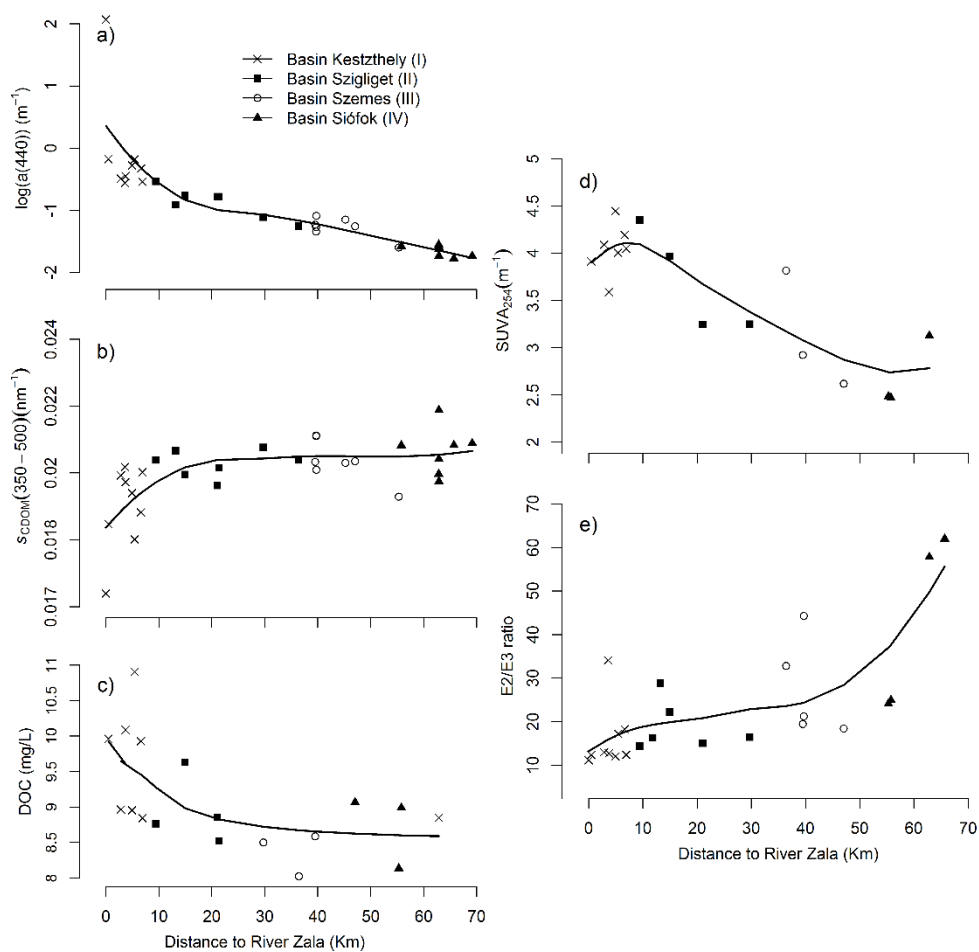
Figure 3-5 Scatterplots against distance to the main inflow [Km] with loess curve fitted to data. (a) Variation of CDOM absorption coefficient at 440 nm (a_{CDOM} (440)) [m-1], (b) CDOM slope coefficient between 350 and 500 mm (SCDOM (350-500)) [nm-1] variation, (c)

The E2:E3 ratio varied significantly (R^2=0.47, p<0.001) between the mouth of the river (11.1) and the main outflow (62.0) as specified in **Table 3-3**. SUVA$_{254}$ varied between 2.47 L mg^{-1} m^{-1} at ST25 in the Siófok basin to 4.45 L mg^{-1} m^{-1} at ST06 in the Keszthely

basin (**Table 3-3**). **Figure 3-5d** and 6e shows that $SUVA_{454}$ decreased with distance from the inflow of the River Zala (R^2=0.713, p<0.001), whereas E2:E3 ratio increases with increased with distance from the main inflow.
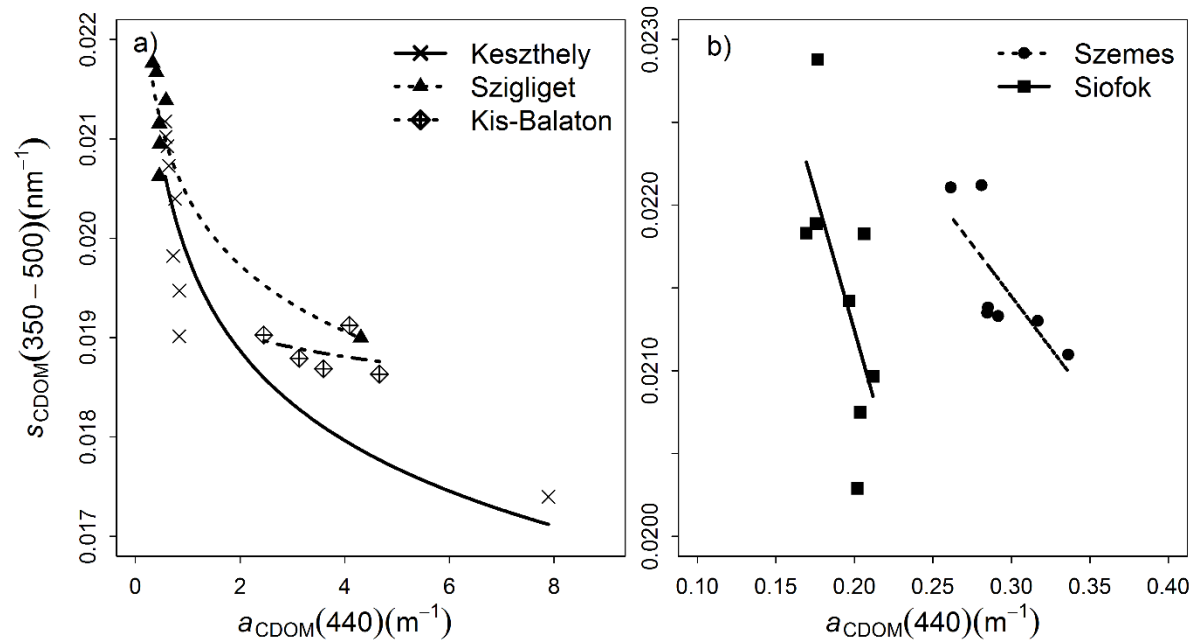
Figure 3-6 Plot of S_{CDOM} (350-500) as a function of a_{CDOM} (440) spatial variation. **a)** Kis Balaton, S_{CDOM} (350-500) = 0.019266*a_{CDOM} (440)$^{-0.017362}$; basin Keszthely, S_{CDOM} (350-500) = 0.019817*a_{CDOM} (440)$^{-0.070820}$ and basin ^{Szigliget}, S_{CDOM} (350-500) = 0.020418*a_{CDOM} (440)$^{-0.070820}$. **b)** Basins Szemes, S_{CDOM} (350-500) = -0.01252·a_{CDOM} (440) + 0.02521 and Siofok, S_{CDOM} (350-500) = -0.03330·a_{CDOM} (440) + 0.027900.

▪ *DOC*

Concentrations ranged from a minimum of 8.03 at ST17 (Basin III) to 10.9 mg L^{-1} at ST07 (Basin 1) with a mean value of 9.66 in the Keszthely basin (I), 8.85 for the Szigliget basin (II), 8.56 for the Szemes basin (III) and 8.66 for the Siófok basin (IV). DOC concentrations slowly decreased with increasing distance from Zala River (**Figure 3-4c**, **Figure 3-5c**), similarly to the trends observed for a_{CDOM} (440), but with greater variability through the system than for S_{CDOM} (coefficient of variation (CV) for S_{CDOM} = 0.053) and smaller than for a_{CDOM} (440) (CV for a_{CDOM} (440) = 2.065). DOC concentrations showed a strong and positive relationship with a_{CDOM} (440) coefficients

over the entire dataset (**Figure 3-7**) (R^2=0.945, p<0.001) although for individual basins this relationship was only significant for Keszthely (R^2=0.952, p= <0.001).
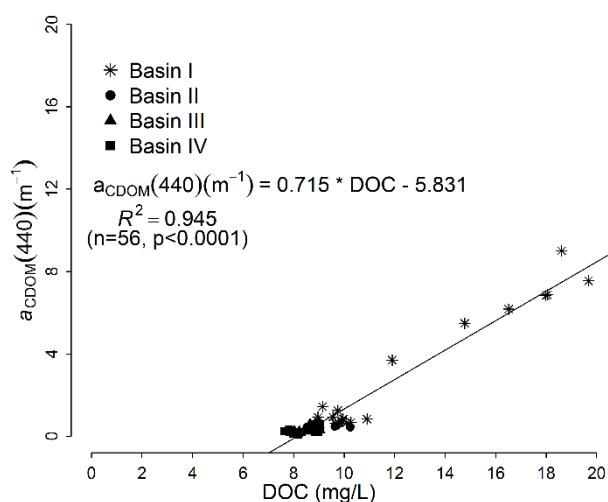
Figure 3-7 Scatterplot of a_{CDOM} (440) plotted as a function of DOC concentration (mg/L). Line is a regression curve by least squares fit.

3.3.3. CDOM photodegradation experiment

Ultraviolet irradiance during the photobleaching experiment ranged from 7.79 to 42.9 MJ m^{-2} per day with a mean of 32.4 MJ m^{-2} per day (**Figure 3-8**a). The exposure of CDOM to natural solar UV radiation resulted in marked alterations to its absorption properties (**Figure 3-8b**). a_{CDOM} (440) remained relatively constant in the dark control samples (7.04 to 6.18 m^{-1}) for the allochthonous treatment from days 0 to 7 (**Figure 3-8b**) indicating minimal bacterial degradation of CDOM. However, the CDOM$_{allo}$ samples exposed to natural solar radiation demonstrated considerable a reduction in absorption (ANOVA, F (1,14) = 12.70, p=0.003; **Figure 3-8b**) in the visible part of the spectrum (440 nm) with regard to the dark samples. After 7 days, a_{CDOM} (440) for the allochthonous samples decreased from 7.04 to 3.36 m^{-1}; this equates to a rate of loss of 1.49 m^{-1} d^{-1} and a 42 % net decrease in absorption from day 0. The difference observed between the control samples and those exposed to natural solar radiation is indicative of a strong photobleaching effect, although it is also possible that bacterial degradation

was enhanced in the light. In contrast, there was no discernible, systematic change in the CDOM$_{auto}$ samples over time. They showed an increase in $a_{CDOM}(440)$ during the first 3 days (**Figure 3-8b**) from 1.22 to 1.34 m^{-1}, but subsequently showed a decrease in absorption from 1.34 to 0.312 m^{-1} during the last 4 days, which equates to a 77 % decrease (1.03 m^{-1}) from the value at day 3.
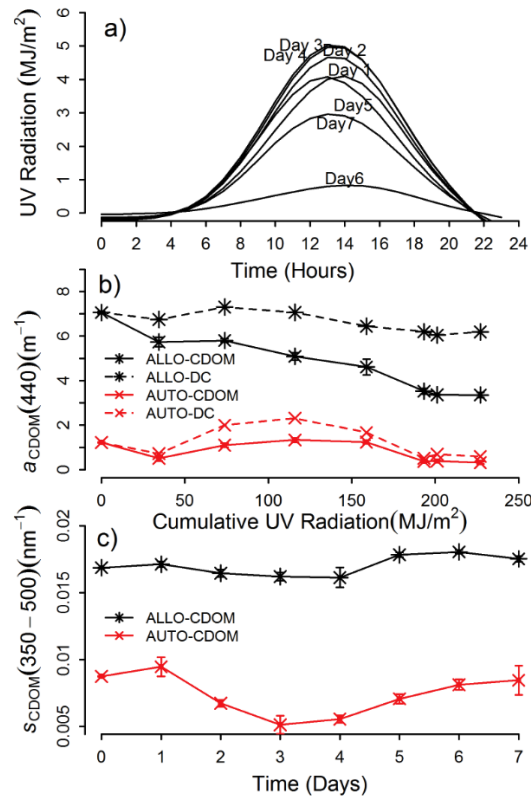
Figure 3-8 a) Ultraviolet irradiance during the photobleaching experiment. **b)** Variation of S_{CDOM} (350-500) per day. **c)** Variation of a_{CDOM} (400) accumulated UV radiation.

The autochthonous control samples (CDOM$_{auto-dark}$) varied in $a_{CDOM}(440)$ from 1.22 to 0.596 m^{-1}; in the absence of photobleaching the decrease in $a_{CDOM}(440)$ might be explained by residual bacterial activity (although the samples were filtered to minimise bacterial contamination before exposure).

Photodegradation also modified the spectral slope coefficient of the samples (**Figure 3-8c**). The values of S_{CDOM} (350-500) for the CDOM$_{allo}$ samples remained stable, varying less than 0.001 nm^{-1} per day. However, for the CDOM$_{auto}$ treatment, S_{CDOM}

coefficients decreased conspicuously until the third day (from 0.009 to 0.005 nm^{-1}) and then increased with further irradiation from day 3 to day 7 until recovering to its original value (from 0.0051 to 0.0084 nm^{-1}). Both the spectral slope (ANOVA, $F_{(1,14)}$ = 63.20, $p<0.001$) and absorption coefficient (ANOVA, $F_{(1,11)}$ = 208.65, $p<0.001$) values for $CDOM_{auto}$ were significantly lower than those for $CDOM_{allo}$.

Humic-like fluorescence as indicated by $F_n(355)$ decreased gradually for the $CDOM_{allo}$ samples with increasing cumulative UV radiation and exposure time (**Figure 3-9a**) from 41.1 to 17.5 QSU (42.6 % of the original value). Interestingly, no marked changes or clear trend was observed in $F_n(280)$ (**Figure 3-9b**), suggesting protein-like fluorescence was less susceptible to degradation by natural solar radiation.
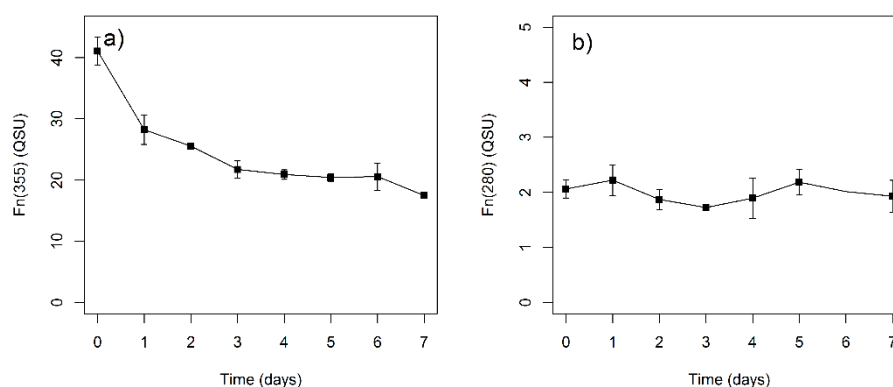
Figure 3-9 Changes in humic-like fluorescence (Fn (355)) and protein-like fluorescence (Fn (280)) for allochthonous CDOM samples with time during photobleaching experiment. Bars = ±Standard Deviation.

There were more than ten orders of magnitude difference in fluorescence intensity between $CDOM_{allo}$ and $CDOM_{auto}$ samples, presumably driven by the difference in concentration. Given the low concentrations of CDOM, after Milli-Q correction, there was no measurable fluorescence signal for the autochthonous samples.

3.4. Discussion

3.4.1. Dynamics of dissolved organic carbon

CDOM is the coloured fraction of DOC and is often the dominant light absorbing component in lakes, particularly at blue and green wavelengths. Previous research has shown that CDOM can be responsible for up to 80 % of light absorption in Lake Balaton Riddick et al. (2015) in spite of the fact that the lake also has high concentrations of phytoplankton and non-algal particles (NAP). The high input of DOC from the Zala River results in elevated concentrations in the western basin relative the remainder of the lake (from 0.169 m^{-1} near the outflow to 7.89 m^{-1} at the mouth of the Zala river). High DOC concentrations were largely confined to the waters nearest the inflow but the at times the influence of this input could be observed across the westernmost basin and as such must exert influence over metabolic processes in this part of the lake. In comparison to published data from other large systems such as Lake Erie (O'Donnell et al., 2010); 0.19-2.0 m^{-1}), Lake Champlain (O'Donnell et al., 2013); 0.5-1.15 m^{-1}) and lakes Peipsi, Vättern and Vänern (Reinart et al., 2004); 0.33-3.82 m^{-1}) the magnitude of variability in a_{CDOM} (440) observed in this study was markedly greater (although these previous studies might not have captured the full range of a_{CDOM}(440) variation), which is perhaps surprising given the northerly latitude of some of these lakes (Curtis, 1998). However, the magnitude variability in a_{CDOM}(440) observed in this study is not too dissimilar from that reported previously in other systems such as Lake Taihu (Zhang et al., 2011).

The seasonal pattern in CDOM absorption and DOC concentration varied considerably in the western basin, but was relatively constant in other basins. The annual peak(s) in a_{CDOM} (440) and DOC occurred in spring and/or autumn some stations (e.g., ST03, ST12, ST30) were broadly coincident with or lagged slightly behind the annual runoff

maxima suggesting a seasonal trend that was partly driven by the flushing of organic matter from catchment soils during high flow events. This pattern is common in many temperate and boreal lakes where DOC export from catchments is driven by the availability of flushable terrestrial carbon sources and the seasonality of precipitation and/or snowmelt.

Conversely, at the station nearest to the inflow of the River Zala the main peak in a_{CDOM} (440) and DOC occurred in summer (August and July respectively) with a smaller secondary peak in DOC the autumn. The summer peak in a_{CDOM} (440) and DOC at the inflow of the River Zala was clearly related to the proximity of the station to the mouth of the River Zala and a high input of humic-rich water from the Kis-Balaton wetland complex. In wetlands, high production of DOC can occur during the growing season due to leaching from plants and biological degradation of organic detritus (Freeman et al., 2004; Pinney et al., 2000). In our study system, this summer peak in DOC production also coincides with the annual rainfall minimum and the period of lowest flow into the lake, resulting in a concentrated input of humic-rich water and elevated CDOM absorption at the inflow of the Zala and across the western basin.

It is also notable that the effect of this humic-rich water from the River Zala on the biogeochemistry and light climate in Lake Balaton diminishes rapidly through the system in summer. This can be partly attributed to the dilution of the inflow with less humic water, but also the rapid degradation of the highly biologically and photochemically reactive DOC originating from Kis-Balaton during a period when microbial activity is high due to warm water temperatures and UV irradiance is at its maximum. The collective residence time of the Keszthely and Szigliget basins (0.25 and 0.72 years respectively; (Somlyódy, L., & van Straten, 2012) explains why the

highly humic and labile components of the DOC entering the lake from the River Zala are largely degraded before reaching the Szemes basin with only the most recalcitrant DOC fractions persisting beyond the westernmost basins. The resulting differences in CDOM composition are clearly reflected in the variability in the CDOM absorption characteristics (S_{CDOM}, $SUVA_{254}$ and E2:E3) observed through the system. These findings agree with other field and experimental studies which have shown that CDOM can be rapidly degraded by photobleaching in summer (Del Vecchio and Blough, 2002; Vodacek et al., 1997; Yunlin Zhang et al., 2009a).

The mean (and range) in S_{CDOM} (350-500) for Lake Balaton in summer was 0.0211 nm^{-1} (0.0174 to 0.0229 nm^{-1}), higher than values reported for several other systems including Lake Erie (C. Binding et al., 2008; O'Donnell et al., 2010) and Lake Chapman (O'Donnell et al., 2013) (**Figure 3-2** & **Figure 3-5b**). The values reported by (C. E. Binding et al., 2008; O'Donnell et al., 2013) were more comparable to the mean slopes observed for the humic-rich waters encountered in Kis-Balaton (0.0189 nm^{-1}) and the Keszthely basin (0.0199 nm^{-1}). However, it should be stressed that some of this variation could in part be explained by the different wavelength ranges used in the calculation of S_{CDOM}. The magnitude of spatial variability in Lake Balaton was more comparable to that reported for northern Lake Taihu, where S_{CDOM} was found to vary between 0.0127 to 0.0190, from 0.0159 to 0.0220 and from 0.0122 to 0.0174 nm^{-1} for the wavelength domains 280 to 500 nm, 280 to 360 nm and 360 to 400 nm respectively (Y. Zhang et al., 2007a) and between 0.0180 to 0.0281 nm^{-1} (for S_{CDOM} (280-500)) in (Zhang et al., 2011).

Very few studies have investigated seasonal variation in S_{CDOM} in lakes. In the present study, seasonal variation in S_{CDOM} (350-500) was greatest in the eastern basin furthest from the inflow ranging from 0.0158 nm^{-1} to 0.0300 nm^{-1} (**Table 3-2**, **Figure 3-2**) with

a mean annual value of 0.0205 nm^{-1}. The range observed in Lake Balaton was greater than previously reported in other lake systems. (Ylöstalo et al., 2014) for instance reported a mean (range) of 0.0182 nm^{-1} (0.0155-0.0200 nm^{-1}) for 15 boreal lakes in Southern Finland within the summer months. Interestingly, there is more variation in S_{CDOM} in lakes and other optically complex inland waters (Kowalczuk et al., 2003b; Y. Zhang et al., 2007a) than shelf sea environments despite the fact the latter are globally diverse and far more extensive (Babin et al., 2003).

The structural modifications in DOM and its coloured fractions that are in part conveyed through variation in S_{CDOM} result from interplay between the input of allochthonous DOC from the catchment, the production of autochthonous DOC from the microbial digestion of phytoplankton cells and the rate at which these materials are degraded biologically and photochemically (Nelson et al., 1998; Vantrepotte et al., 2007; Yamashita and Tanoue, 2004; Yunlin Zhang et al., 2009b)(Yamashita et al., 2013). Newly produced autochthonous CDOM typically has a higher S_{CDOM} coefficient compared to humic-rich allochthonous material (Bracchini et al., 2010). Photobleaching also results in an increase in S_{CDOM}. The majority of sampling stations in Lake Balaton exhibited higher slope coefficients during the summer months, which could be attributed to an increase in new autochthonous DOC production from the growth and decay of phytoplankton during the summer bloom period and intense photobleaching of humic-rich material received from the catchment. Seasonal variability in S_{CDOM} was notably lower at the inflow of the River Zala than in the easternmost basins, which again probably reflects the marked effect that intense summer photobleaching has on the structural composition of dissolved organic matter as it slow moves through the system.

Noticeably, while a_{CDOM} (440) and S_{CDOM} (350-500) demonstrated a strong inverse relationship over the entire dataset, the slope of this relationship varied significantly between the different basins in the lake. The slope of the relationship highest in the eastern basin and lower in the west near the inflow where DOC concentrations were the highest. The relationship between a_{CDOM} (440) and S_{CDOM} is known to be influenced by both its provenance and any subsequent transformations (Carder et al., 1989; Helms et al., 2008) that take place. The observed trends in Lake Balaton are likely to be a result of the mixing of water rich in allochthonous carbon from the River Zala with more dilute and autochthonous carbon sources in the main lake and the progressive degradation of this material via photobleaching as it moves through the system. Comparable trends have been found by (Y. Zhang et al., 2007a) in the Yunnan Plateau lakes.

E2:E3 ratio variation found in this study have also been shown in previous studies (Helms, 1998; Santos et al., 2014). In coastal waters E2:E3 values are typically within the range 8.70±1.4 and 13.5±1.6 (nearshore – offshore in Georgia Bight; (Helms et al., 2008). In inland and transitional waters, E2:E3 ratios as high as 14.6 have been reported in Lake Taihu (Zhang et al., 2011) and up to 26.9 in Chesapeake Bay (Helms et al., 2008). E2:E3 values for Lake Balaton were significantly higher and more variable than previously reported varying between 11.0 and 72.0, with the highest values near the outflow indicating the CDOM here was less humified and had a lower molecular weight. Increasing values of E2:E3 ratio have been reported by other authors indicating a decrease in colour as well as in molecular weight (Helms et al., 2008; Peuravuori and Pihlaja, 1997).

Similar trends were also observed in SUVA$_{254}$. In Lake Balaton, SUVA$_{254}$ varied between 2.5 mg^{-1} m^{-1} in the easternmost basin and 4.5 L mg^{-1} m^{-1} near the mouth of the

River Zala. This again indicates that water entering from the river contained high molecular weight dissolved organic carbon with a high content of aromatic substances (Weishaar et al., 2003a), whereas the compounds comprising the DOC in the central and eastern parts of the lake had a lower molecular size and aromaticity. The $SUVA_{254}$ values measured in Lake Balaton were broadly comparable to those reported for other lake systems. For example, (Song et al., 2013) reported a maximum value of 8.7 ± 2.8 (L mg^{-1} m^{-1}) for 26 inland water bodies in China. $SUVA_{254}$ values were lower than those reported for marine waters where the relative contribution of autochthonous carbon sources is often greater. The sensitivity of $SUVA_{254}$ to changes in the carbon provenance is shown by (Asmala et al., 2013) who obtained a range $SUVA_{254}$ values of 3.58 ± 0.33 5.41 ± 0.40 L mg^{-1} m^{-1} in three Baltic Sea estuaries whereas measurements taken from stations on the sea shelf varied between 1.87 ± 0.09 and 3.47 ± 0.27 L mg^{-1} m^{-1}.

3.4.2. CDOM photobleaching

The spatio-seasonal variability in CDOM absorption in Lake Balaton strongly suggests that photobleaching plays a key role in the processing and degradation of dissolved organic carbon as it flows through the system. Rapid degradation of allochthonous CDOM was observed (**Figure 3-8**), which was especially pronounced at the time of year with the highest solar radiation but probably also enhanced by mineralisation by bacterial activity as a response to high water temperatures during the summer period. Dilution processes alone cannot explain the loss of DOC; therefore, it must also be due to in-lake transformation. The processing and transformation of DOC by photobleaching not only influences carbon cycling, but it also is accompanied by an increase in the transparency of the water column (Osburn et al., 2009) and changes in

the optical properties (Yamashita et al., 2013) that have wider implications for the underwater light climate and primary production.

The in-lake incubations conducted in Lake Balaton provide further substantiation for the critical role of photochemistry in the turnover of CDOM. We observed rapid changes in the absorption properties of CDOM in response to exposure to natural UV irradiation. In the allochthonous CDOM treatments, the rate of degradation resulted higher than that obtained for Lake Taihu by Zhang et al. (2013) who reported a 22 % decrease over 9 days. Bacterial degradation was not noticeable in the allochthonous samples as there was almost no difference in $a_{CDOM}(440)$ for the dark treatment compared to the initial value (**Figure 3-8d**) although we cannot exclude the possibility of enhanced bacterial degradation in light exposed treatments (Kragh et al., 2008).

Photodegradation also modified the spectral slope (**Figure 3-8b**) of the CDOM absorption spectra. Both the spectral slope and absorption coefficient for autochthonous CDOM were significantly lower than for allochthonous samples (ANOVA, F (1,27) = 6.55, p=0.01). During our experiment, S_{CDOM} (350-500) did not follow a systematic trend in the allochthonous samples, varying less than 0.0007 m^{-1} per day. However, for the autochthonous treatment, it decreased conspicuously until the third day (from 0.0087 to 0.0051 m^{-1}) but then increased again from day 3 to day 7 until it almost returned to its original value (from 0.0051 to 0.0084m^{-1}). The increase in slope matches with an increase in a_{CDOM} (440) and has been considered by (Helms et al., 2008) to be a result of transformation from high to low molecular weight CDOM and is considered to be a response to photo-induced decomposition (Grzybowski, 2000; Moran et al., 2000; Yamashita et al., 2013). The initial decrease in slope during the early part of the experiment echoes observations by (Yamashita et al., 2013) and (C.G. Fichot and

Benner, 2012) whom attributed this phenomena to microbial degradation of bioavailable CDOM (Nelson et al., 2004).

The fluorescence spectra also indicate a marked difference in composition between the allochthonous and autochthonous material. The decomposition of CDOM into lower molecular weight compounds under UV-B radiation (Lepane et al., 2003) results in a significant loss of both absorption and fluorescence. The negligible fluorescence signal observed for the autochthonous CDOM samples in this study is likely due to its low concentration. In contrast, the humic-like fluorescence signal measured from allochthonous samples was initially high but decreased over the experimental period from 41.07 to 17.48 QSU (57.5 % decrease). Similarly, we observed a reduction in protein-like fluorescence from 2.06 to 1.93 QSU (6.31 % decrease; **Figure 3-9b**) over the 7 days of the experiment. This agrees strongly with the results of previous studies showing the fluorescence signal from humic compounds is rapidly lost through photobleaching, whereas aromatic-like fluorescence is generally not as susceptible to photo-degradation. Helms et al. (2013) for example reported an 84% decrease in humic-like fluorescence in response to photobleaching compared to an only 47 % decrease in aromatic-like fluorescence after 68 days of continuous irradiation in a UV solar simulator.

3.4.3. Implications for underwater light field

The absorption of light by CDOM is a major determinant of water transparency in lakes and the availability of light for primary production (Kirk, 1994; Laurion et al., 2000, 1997; Vähätalo et al., 2005). Absence of measurements of the underwater light field makes it difficult to attribute its effect to this particular case, but there clearly exists evidence that the dynamic nature of dissolved organic carbon in lakes results in marked spatio-seasonal variation in both the magnitude and wavelength-dependency of light

absorption by chromophoric substances. This variability undoubtedly has implications not only for the quantity of light available to photosynthetic organisms but also its quality. High concentrations of CDOM result in intense absorption of light at blue and green wavelengths but the intensity of absorption decreases exponentially with wavelength. This not only has implications for the productivity of the system (Cory et al., 2015), but also for the photo-physiology and species composition of the phytoplankton community. The intense absorption of UV light by CDOM protects phytoplankton from physiological damage and reduces the need for phytoplankton cells to manufacture UV-protective pigments. This can result in chromatic acclimation with phytoplankton in high CDOM waters investing less in UV-protective pigments (Riddick et al., 2015).

The magnitude of variability in the spectral dependency of CDOM absorption also has implications for bio-optical models of the underwater light field that are used to underpin remote sensing algorithms for estimation of CDOM in lakes and other inland waters. Existing bio-optical models (Lee et al., 2002a) commonly extrapolate absorption by CDOM in the blue to longer wavelengths using a fixed slope coefficient. We demonstrate here that even within a single lake system significant variability can occur in S_{CDOM}. Failure to accommodate variability in S_{CDOM} in bio-optical models will lead to errors not only in the estimation of CDOM absorption but also in the contributions of other optically-active substances (e.g., chlorophyll, non-algal particles) to light absorption and scattering within the water column. In Lake Balaton, the variability observed in S_{CDOM} (0.0174 - 0.0289 nm^{-1}) could produce errors up to 180 % and 900 % on estimates of a_{CDOM} at wavelengths in the blue (350 nm) and red (650 nm) respectively. This suggest that new approaches are needed to incorporate knowledge on the variability in S_{CDOM} into adaptive bio-optical modelling frameworks for optically-

complex waters to improve our ability to model the underwater light field and increase the performance of physics-based remote sensing algorithms for CDOM retrieval.

3.5. Conclusions

This study revealed the high spatial and seasonal variability in the quantity and quality of CDOM that can exist within a large, temperate shallow lake. The variation was strongly driven by the allochthonous input of dissolved carbon from the Zala River and its rapid transformation as it moves through the system. The variability in the quantity and quality of CDOM was strongly reflected in a number of readily measured optical parameters including S_{CDOM}, E2:E3 ratio and $SUVA_{254}$, which collectively pointed towards a marked decrease in the molecular weight of dissolved carbon compounds, a reduction on its aromatic content and a decrease in the degree of humification as water moved through the system from the main inflow to outflow.

Photobleaching was found to be a major factor controlling the in-lake transformation and degradation of CDOM, and a key process influencing the spatial structure CDOM throughout the system. The photobleaching rate coefficient for allochthonous CDOM was found to be higher than for autochthonous CDOM due to the greater photoreactivity of terrestrially-derived compounds. CDOM in Lake Balaton is mainly terrestrial in origin and is thus rapidly degraded by exposure UV irradiation. The implied importance of photobleaching to carbon dynamics is consistent with previous studies conducted in other inland water bodies (Zhang et al. 2013) as well as other studies carried out in shelf seas (Babin et al., 2003) and the open ocean ((Helms et al., 2013).

More widely, these results provide an insight on the potential contribution of wetlands to DOM and CDOM in lakes, not only in terms of the concentration of CDOM but also

its seasonality. The seasonal trend in CDOM observed close to the main inflow was significantly different from that observed elsewhere in the system. Notwithstanding the fact that most of the CDOM in Lake Balaton would seem to be terrestrial in origin, we did observe an increase in a_{CDOM} (440) in autumn following the breakdown of phytoplankton blooms on the lake.

The observed spatial and temporal variability in the optical properties of CDOM in this study has important implications for biogeochemical cycling in Lake Balaton but also for bio-optical models of the underwater light climate in lakes and their application in the parametrization of algorithms for optical remote sensing of CDOM and other optically-active constituents.

4. CHAPTER 4 – REMOTE SENSING OF COLOURED DISSOLVED ORANIC MATTER IN LAKES: OPTIMISING RETRIEVAL ALGORITHMS FOR GLOBAL APPLICATION

4.1. Introduction

Lakes and in particular, small inland water bodies, play an important role in the global carbon cycle (Cole et al., 2007b) affecting climate and acting as indicators of climate warming (Williamson et al., 2009). Dissolved organic carbon (DOC) is one of the predominant forms of carbon in most lakes (Tranvik et al., 2009) and coloured dissolved organic matter (CDOM) is one of the major contributors to light and heat absorption in fresh and near-shore coastal waters (Soppa et al., 2019), being commonly used as a proxy for DOC (Hoge et al., 1993; Williamson et al., 2001).

CDOM contributes significantly to and often dominates light absorption in freshwaters, particularly at wavelengths <500 nm (Fichot et al., 2007; Nelson and Siegel, 2013) playing an important role in photo-processes (Smith et al., 1992; Herndl et al., 1993; Häder et al., 1998; Aulló-Maestro et al., 2017). In waters with high concentrations of CDOM (humic waters), light does not penetrate more than 30-50 cm in the water column (Gareis et al., 2010), making deeper waters dark and protected from sunlight, limiting photo-degradation processes. All this can lead to reductions in water transparency to UV and photosynthetically active radiation (PAR, 400-700 nm) that can influence food web structure and, ultimately, ecosystem services. This "browning", can result not only in increases in DOC concentrations but also in its colour and its effects, which depend and vary with the initial colour of the lake (Jordan S. Read and Rose, 2013). The shading of CDOM can increase thermal stratification, deplete oxygen and alter the structure of the pelagic food web inhibits photosynthesis reducing food supply

for higher trophic levels and in recent decades, it has also been associated with increasing pH (Williamson et al., 2016).

Moreover, the absorption spectrum of CDOM contributes significantly to subsurface radiative transfer processes and therefore, to water-leaving radiative signals measured from space.

Optical remote sensing provides a valuable tool to measure CDOM absorption (a_{CDOM}) at large spatial scales (Tranvik et al., 2009). However, much of the research on the development of algorithms for the retrieval of CDOM absorption from optical satellite data has focussed on marine systems, particularly open ocean waters and generally in brown lakes. The markedly different and highly complex optical properties that characterise inland waters mean that algorithms developed for open ocean waters may not perform adequately in inland waters given the potential interference from high concentrations of suspended material of biogenic and minerogenic origin not typically found in open oceans.

Many CDOM retrieval algorithms have been developed using both empirical and analytical approaches (IOCCG, 2006). Some authors have obtained CDOM absorptivity at 440 nm (a_{CDOM} (440)) estimations from satellite radiometry using ratios of remote sensing reflectance (R_{rs}) in the red and blue parts of the spectrum ($_{rs}670/R_{rs}410$, Bowers et al., 2000) and others showed that a_{CDOM} (440) can be derived using the ratio of R_{rs} in the red and blue-green parts of the spectrum (e.g., $R_{rs}665/R_{rs}490$ in Binding and Bowers, 2003). Empirical approaches such as Kutser et al. (2005), Del Castillo and Miller (2008), Ficek et al. (2011) and Mannino et al. (2008) or combination of multiple band ratios such as Griffin et al. (2011) and Carder et al. (1999), require adequate data to parametrise the model and are usually focused on specific lake types. Semi-analytical approaches such as Lee et al., 2002 and 2009, matrix inversion methods (MIM, Siegel

et al., 2002) and artificial neural networks (ANN, Tanaka et al., 2000) require more knowledge about specific inherent optical properties being also specific for regional environments. A summary of bio-optical models previously used to estimate a_{CDOM} can be found at Zhu et al. (2014), while Brezonik et al. (2015) presents an overview of the factors affecting the measurement of CDOM from remote sensing. However, previous validation efforts have been based on small datasets, being therefore a need to determine the most accurate algorithms for wide ranges of optical water types (OWTs) is still needed.

In this study we present the first extensive algorithm validation over 250 inland water bodies. In total 35 algorithms (24 empirical and 11 semi-analytical) were assessed. A previous validation study have focused on specific water bodies with particular characteristics (Zhu et al., 2014 evaluated fifteen algorithms on water from Kawkawling and Saginaw rivers and Lake Huron). The validation and training dataset (https://www.limnades.org/home.psp) used to investigate a_{CDOM} retrieval algorithms was developed with simultaneous measurements of *in situ* chlorophyll-a (Chl-a), total suspended matter (TSM), CDOM absorption (a_{CDOM}) and *in situ* hyperspectral R_{rs}. The dataset is clustered in 13 optical water types following Spyrakos et al. (2018).

This chapter aims to evaluate the accuracy of a_{CDOM} algorithm performance over a wide range of OWTs examining the influence that specific parameters such as Chl-a and other optically active constituents had on the estimation performance. Moreover, to improve the overall performance of a selection of algorithms by its reparameterization, improving at the same time the ability to select the most appropriate algorithms and parametrisations for specific scenarios. Finally, a robust selection of candidate algorithms will be proposed for a_{CDOM} retrieval in more than 1000 lakes globally. To this end, the study was organised as follows: (1) existing algorithms with original

parametrisations were tested over a wide range of OWTs; (2) best performing

algorithms were calibrated by empirically adjusting model coefficients using in-situ

measurements as training dataset, globally and per OWT.

4.2. Methods

4.2.1. Data

The data used in this study were obtained from the LIMNADES database

(https://www.limnades.org/home.psp).

The database was compiled from a variety of natural and artificial inland aquatic

systems including lakes, reservoirs, rivers and floodplains in 13 individual datasets. It

provides in-situ measurements of water parameters such as a_{CDOM} (440), Chl-a and total

suspended matter (TSM). Corresponding measurements of hyperspectral R_{rs} (λ) (sr^{-1})

at a 3nm spectral resolution were also provided. Primary input for CDOM algorithms is

generally remote sensing reflectance, R_{rs} (λ) (sr^{-1}).

In total, 1809 measurements of in-situ hyperspectral Rrs (λ) were identified that had

contemporaneous measurements of aCDOM, Chl-a and TSM. These data represent 281

lakes in 12 OWTs according to the classification of Spyrakos et al. (2018).

Table 4-1 summarises the data for the a_{CDOM} in-situ samples available showing a list of the datasets from inland water systems used from the LIMNADES dataset.

Table 4-1 OWTs used for the algorithm validation

OWT	Number of Lakes	Number of Samples
1	4	21
2	46	261
3	13	95
4	39	315
5	14	159
6	27	224
7	11	25
8	20	106
9	35	162
10	10	50
11	27	167
12	35	224
Total	**281**	**1809**

The data were classified in 12 spectrally distinct OWTs following (Spyrakos et al., 2018b). The original scheme identified 13 different OTWs, according to a specific combination of biogeochemical characteristics, but in this study, a_{CDOM} (440) data were only available for 12 OWTs, as OWT-13 (spectra from very high biomass waters with scums) had no contemporaneous a_{CDOM} (440) measurements. **Figure 4-1** shows R_{rs} (λ) spectra for every water type (apart from OWT-13).
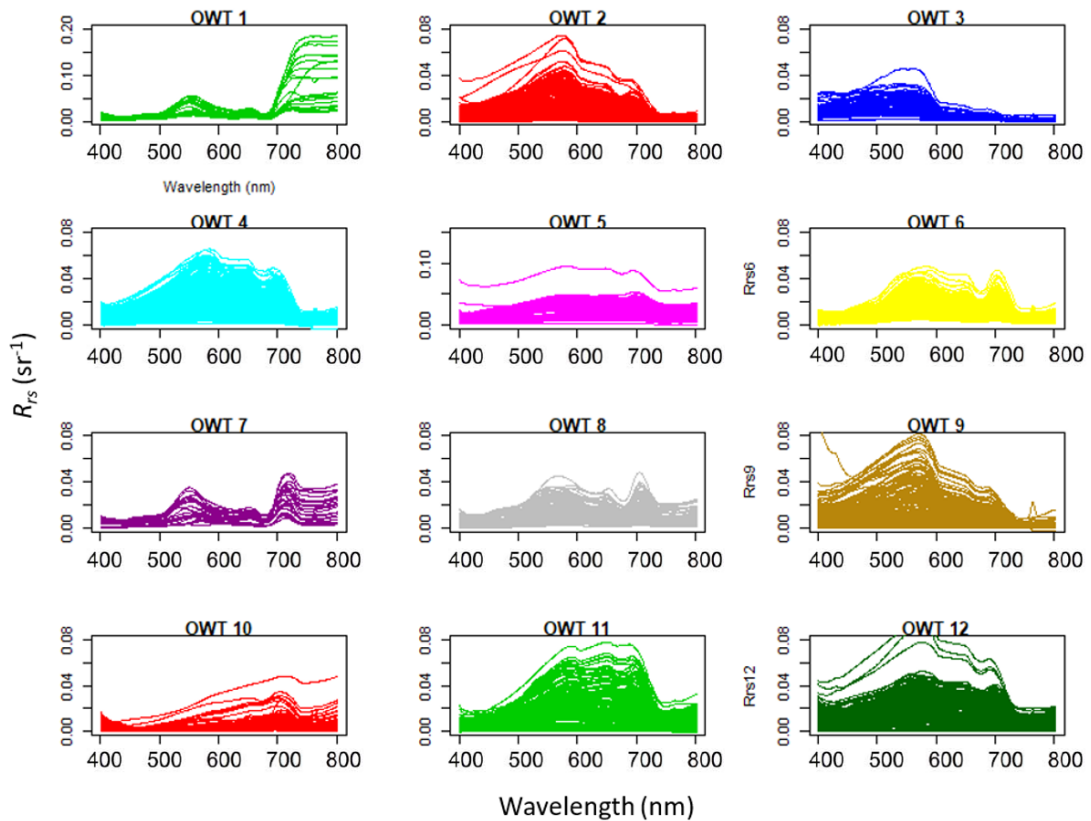
Figure 4-1 The R_{rs} (λ) spectra per OWT used in this study for the

4.2.2. Satellite data simulation

The majority of CDOM algorithms have been developed for application to ocean colour

satellite platforms such us the Medium Resolution Imaging Spectrometer (MERIS) that

was part of ESA's Envisat payload, the Moderate Resolution Imaging Spectrometer

(MODIS) on NASA's Aqua/Terra and NASA's Sea-viewing Wide Field-of-view

Sensor (SeaWiFS). In addition, some algorithms have also been developed for

application to lower spectral and radiometric resolution sensors primarily for terrestrial

applications but offering spatial resolutions more suitable for the observation of inland

waters and near-shore marine systems such as Landsat ETM and Advanced Land

Imager (ALI) and Landsat Operational Land Imager (OLI).

Hyperspectral R_{rs} (λ) from LIMNADES database for 1809 stations was spectrally

resampled to the wavebands of MERIS, MODIS, SeaWiFS, Landsat TM, Landsat ETM

and Landsat OLI sensors, using the specific spectral response functions and used as

117

input to the models. Estimated a_{CDOM} (440) was at the end compared with in-situ values from LIMNADES database to determine the performance of the algorithms.

4.2.3. CDOM estimation Algorithms

A group of 35 published and well documented algorithms representing the two major categories of CDOM retrieval algorithms were selected: 24 empirical (EMP) and 11 semi-analytical (SA). The algorithms were developed for a range of different water types, for specific remote sensing sensors, utilising different reflectance bands and retrieving CDOM absorption coefficients at different wavelengths. The specifications of the algorithms are summarised in

Table 4-2. Algorithms with different versions were treated as different algorithms and evaluated independently.

Table 4-2 Compilation of algorithm, sensor, input R$_{rs}$ (λ), band ratios and outputs

Model	Type	Algorithm name	Sensor	Input R$_{rs}$ (λ) (nm)	Band ratio	Output	Reference(s)
1		D'Sa & Miller-1		443, 510	443/510		
2		D'Sa & Miller-2		412, 510	412/510	a_{CDOM} (412)	D'Sa and Miller
3		D'Sa & Miller-3		510, 555	510/555		
18		DelCastillo-Miller		510, 670	510/670	a_{CDOM} (412)	Del Castillo & Miller (2008)
5		D'Sa		510, 555	510/555	a_{CDOM}	D'Sa et al. (2006)
6		Johannessen-1				a_{CDOM} (323)	
7		Johannessen-2				a_{CDOM} (338)	
8		Johannessen-3	SeaWiFS				Johannessen et al. (2003)
9		Johannessen-4		412, 555	412/555	a_{CDOM} (323)	
10		Johannessen-5					
11		Johannessen-6				a_{CDOM} (338)	
12		Mannino-1				a_{CDOM}	
13	Emp	Mannino-2		490, 555	490/555	a_{CDOM}	
14		Mannino-3				a_{CDOM}	Mannino et al.
15		Mannino-4				a_{CDOM}	
16		Mannino-5		490, 551	490/551	a_{CDOM}	
17		Mannino-6	Aqua-MODIS			a_{CDOM}	
21		Carder-1		412, 443, 551	412/551, 443/551		Carder et al., (1999)
22		Carder-2		443, 488, 551, 667	443/551, 488/551, 667/551	a_{dg} (443)	
4		Kutser	ALI		565/660	a_{CDOM}	Kutser et al. (2005)
19		Ficek			570/655	a_{CDOM}	Ficek et al. (2011)
20		Griffin	Landsat-		560/660	a_{CDOM}	Griffin et al. (2011)
23		Lee-1	SeaWiFS, CZCS	440, 490, 555	440/555, 490/555		Lee et al. (1998)
24		Lee-2		490, 510, 555	490/555, 510/555	a_T (440)	
25		GSM01	SeaWiFS	Full spectrum		a_{CDM} (440)	(Maritorena et al., 2002)
26		QAAv4-Lee1					
27		QAAv4-Lee2				a_{dg} (443)	Lee et al., (2002)
28		QAAv4-Lee3					
29		QAAv4-Le	SeaWiFS, Aqua-MODIS, MERIS, Hyperspectral		---		
30	SA	QAAv4-Zhu1				*missing*	
31		QAAv4-Zhu2				*missing*	Zhu et al. (2011)
32		QAAv4-Zhu3					
33		QAAv5-Lee				a_{CDOM} (440)	Lee et al. (2009)
34		QAAv5-Mishra					Mishra et al.,
35		QAA-CDOM					Zhu and Yu (2013)

120

Models 1, 2 and 3

Models 1, 2 and 3 refer to the two-band ratio algorithms of D'Sa and Miller (2003) described for SeaWiFS bands. It takes as an input R_{rs} (λ) measured at 412 (R_{rs} (412)), 443 (R_{rs} (443)), and 510 (R_{rs} (510)):

$$a_{CDOM}(412) = 0.417 \cdot \left(\frac{R_{rs}(443)}{R_{rs}(510)}\right)^{2.025}, \tag{4-1}$$

$$a_{CDOM}(412) = 0.403 \cdot \left(\frac{R_{rs}(412)}{R_{rs}(510)}\right)^{1.388}, \tag{4-2}$$

$$a_{CDOM}(412) = 0.547 \cdot \left(\frac{R_{rs}(443)}{R_{rs}(510)}\right)^{2.225}. \tag{4-3}$$

Model 4

Model 4 refers to the ALI B2/B3 ratio algorithm developed by (Kutser et al., 2005) that retrieves a_{CDOM} (420) from Advanced Land Imager (ALI) images.

$$a_{CDOM}(420) = 5.13 \cdot \left(\frac{B2}{B3}\right)^{-2.67}, \tag{4-4}$$

being B2 (525-605 nm) and B3 (630-690 nm).

Model 5

Model 5 refers to D'Sa et al. (2006) empirical algorithm calibrated using coastal waters impacted by the Mississippi River. It retrieves CDOM absorption at 412 nm from SeaWiFS bands;

$$a_{CDOM}(412) = 0.227 \cdot \left(\frac{R_{rs}(510)}{R_{rs}(555)}\right)^{-2.022}. \tag{4-5}$$

Models 6, 7, 8, 9, 10 and 11

Models 6 to 11 refer to the band ratio set of algorithms proposed by Johannessen et al. (2003) developed for the Bering Sea, the Mid-Atlantic Bight, Delaware and

Chesapeake Bay applied to SeaWiFS images to calculate a_{CDOM} at 323, 338 and 380 nm.

The equations of the best fit regression lines for the Bering Sea and from the coast to the Gulf stream in the Mid-Atlantic Bight:

$$a_{CDOM}(323) = 0.7060 \cdot \left(\frac{R_{rs}(412)}{R_{rs}(555)}\right)^{-1.07} - 0.00714, \qquad (4\text{-}6)$$

$$a_{CDOM}(338) = 0.5182 \cdot \left(\frac{R_{rs}(412)}{R_{rs}(555)}\right)^{-1,12} - 0.00190 \qquad (4\text{-}7)$$

and

$$a_{CDOM}(380) = 0.2935 \cdot \left(\frac{R_{rs}(412)}{R_{rs}(555)}\right)^{-1.24} - 0.00171. \qquad (4\text{-}8)$$

The equations of the best fit regression lines to the bay data are:

$$a_{CDOM}(323) = 0.2405 \cdot \left(\frac{R_{rs}(412)}{R_{rs}(555)}\right)^{-1.07} + 0.0463, \qquad (4\text{-}9)$$

$$a_{CDOM}(338) = 0.1564 \cdot \left(\frac{R_{rs}(412)}{R_{rs}(555)}\right)^{-1.12} + 0.171 \qquad (4\text{-}10)$$

and

$$a_{CDOM}(380) = 0.0553 \cdot \left(\frac{R_{rs}(412)}{R_{rs}(555)}\right)^{-1.24} + 0.400. \qquad (4\text{-}11)$$

Models 12, 13, 14, 16, 16 and 17

Models 12 to 17 refer to the band-ratio empirical algorithm developed by Mannino et al. (2008) to retrieve surface ocean CDOM (a_{CDOM} (355), a_{CDOM} (412) and a_{CDOM} (443)) from NASA's MODIS-Aqua;

$$a_{CDOM}(355) = -0.2847 \cdot ln\left(\frac{0.3662 \cdot R_{rs}(490)}{R_{rs}(551)} + 0.0514\right), \qquad (4\text{-}12)$$

$$a_{CDOM}(412) = -0.1243 \cdot ln\left(\frac{0.4264 \cdot R_{rs}(490)}{R_{rs}(551)} + 0.0241\right), \qquad (4\text{-}13)$$

$$a_{CDOM}(443) = -0.0762 \cdot ln\left(\frac{0.4502 \cdot R_{rs}(490)}{R_{rs}(551)} + 0.0150\right), \tag{4-14}$$

and SeaWiFS satellite sensors;

$$a_{CDOM}(355) = -0.2746 \cdot ln\left(\frac{0.3273 \cdot R_{rs}(490)}{R_{rs}(555)} + 0.0436\right), \tag{4-15}$$

$$a_{CDOM}(412) = -0.1201 \cdot ln\left(\frac{0.3848 \cdot R_{rs}(490)}{R_{rs}(555)} + 0.0205\right), \tag{4-16}$$

$$a_{CDOM}(443) = -0.0736 \cdot ln\left(\frac{0.4077 \cdot R_{rs}(490)}{R_{rs}(555)} + 0.0127\right), \tag{4-17}$$

Model 18

Model 18 refers to the two band ratio algorithm developed by Del Castillo and Miller (2008) for the estimation of a_{CDOM} (412) at the Mississippi River Plume from SeaWiFS imagery;

$$a_{CDOM}(412) = -0.90 \cdot \left(\frac{R_{rs}(510)}{R_{rs}(670)}\right) + 2.34. \tag{4-18}$$

Model 19

Model 19 refers to the two-band empirically derived ratio algorithm of Ficek et al. (2011) for 15 Pomeranian lakes and the Baltic Sea;

$$a_{CDOM}(440) = 3.65 \cdot \left(\frac{R_{rs}(570)}{R_{rs}(655)}\right)^{-1.93}$$
(4-19)

Model 20

Model 20 refers to the empirical algorithm developed for Landsat satellite data by Griffin et al. (2011):

$$a_{CDOM}(440) = exp^{\left(-1.145 + 26.529 \cdot TM3 + 0.603 \cdot (TM2/TM1)\right)}, \tag{4-20}$$

where TM1= 0.45-0.52µm, TM2= 0.52-0.60 µm and TM3= 0.63-0.69 µm.

Models 21 and 22

Models 21 and 22 refer to the empirical moderate-resolution imaging spectrometer algorithms for Chl-a and absorption developed by (Carder et al., 1999):

$$a_{dg}(443) = 10^{(-1.144-0.738\cdot\rho15-1.386\cdot\rho15^2-0.644\rho25+2.451\cdot\rho25^2)} \qquad (4\text{-}21)$$

and

$$a_{dg}(443) = 10^{(0.043-0.185\cdot\rho25-1.081\cdot\rho35+1.234\cdot\rho65)}, \qquad (4\text{-}22)$$

$$\text{where } \rho15 = \left(R_{rs}(412)\Big/R_{rs}(551)\right), \qquad (4\text{-}23)$$

$$\rho25 = \left(R_{rs}(443)\Big/R_{rs}(551)\right), \qquad (4\text{-}24)$$

$$\rho35 = \left(R_{rs}(488)\Big/R_{rs}(551)\right) \qquad (4\text{-}25)$$

$$\text{and } \rho65 = \left(R_{rs}(667)\Big/R_{rs}(551)\right). \qquad (4\text{-}26)$$

Models 23 and 24

Refers to the empirical algorithm for light absorption by ocean water based on colour developed by Lee et al. (1998):

$$\log a_T(440) = (A_0 + A_1 \cdot \rho25 + A_2 \cdot \rho25^2 + B_1 \cdot \rho35 + B_2 \cdot \rho35^2), \qquad (4\text{-}27)$$

where $A_0 = -0.674$, $A_1 = -0.531$, $A_2 = -0.745$, $B_1 = -1.469$, $B_2 = 2.375$,

$$\rho25 = \log\left(R_{rs}(440)\Big/R_{rs}(555)\right) \qquad (4\text{-}28)$$

and

$$\rho35 = \log\left(R_{rs}(490)\Big/R_{rs}(555)\right). \qquad (4\text{-}29)$$

Model 25

Model 25 refers to the semi-analytical Garber-Siegel-Maritorena (GSM01) inversion model developed by Garver & Siegel (1997) and updated by Maritorena et al. (2002)

and based on an underlying quadratic relationship relating $R_{rs}(\lambda)$ to the IOPs of the water body;

$$R_{rs}(\lambda) = \frac{t^2}{n_w^2} \sum_{i=1}^{2} g_i \left(\frac{b_b(\lambda)}{b_b(\lambda) + a(\lambda)} \right)^i \qquad \textbf{(4-30)}$$

In turn, IOPs are partitioned into their contributing components where $b_b(\lambda) = b_{bw}(\lambda) + b_{bp}(\lambda)$ for water and SPM and $a(\lambda) = a_w(\lambda) + a_{ph}(\lambda) + a_{CDOM}(\lambda)$ for water, phytoplankton and CDOM. The IOP spectra are then parameterized as a known shape with an unknown magnitude using the following expressions;

$$a_{ph}(\lambda) = Chla \times a_{ph}^*(\lambda), \qquad (4\text{-}31)$$

$$a_{cdom}(\lambda) = a_{cdom}(\lambda) \times \exp{-S(\lambda - \lambda_0))}, \qquad (4\text{-}32)$$

$$b_{bp}(\lambda) = b_{bp} \lambda_0) \times \left(\frac{\lambda_0}{\lambda} \right)^Y \qquad (4\text{-}33)$$

Inversion of the model produces simultaneous estimates of the unknown quantities of Chl-a, CDOM and b_{bp} from $R_{rs}(\lambda)$ by application of a nonlinear least square optimisation routine. Global parameters, $a_w(\lambda)$, $b_{bw}(\lambda)$, n_w, t, and g_i were taken from the literature (Pope & Fry, 1997; Smith & Baker, 1981; Gordon et al., 1988), while $a*ph$, S and Y were derived empirically from the SeaWiFs Bio-Optical Algorithm Mini-Workshop (SeaBAM) in-situ dataset.

Model 26, 27 and 28

Models 26, 27 and 28 refer to the QAA method devised by Lee et al. (2002), developed primarily for optically deep waters.

Total absorption is estimated from subsurface $R_{rs}(\lambda)$ (sr^{-1}) a given wavelength.

$$a(\lambda) = \frac{(1 - u(\lambda))\left(b_{bw}(\lambda) + b_{bp}(\lambda) \right)}{u(\lambda)} \qquad (4\text{-}34)$$

where

$$u(\lambda) = \frac{-g_0 + \sqrt{(g_0)^2 + 4g_1 \times r_{rs}(\lambda)}}{2 \times g_1}, \quad (4\text{-}35)$$

$$b_{bp}(\lambda) = b_{bp}(555) \cdot \left(\frac{555}{\lambda}\right)^Y, \quad (4\text{-}36)$$

$$Y = 2.2 \cdot \left\{1 - 1.2 \cdot exp\left[-0.9 \cdot \frac{r_{rs}(440)}{r_{rs}(555)}\right]\right\} \quad (4\text{-}37)$$

$$b_{bp}(555) = \frac{u(555) \cdot a(555)}{1 - u(555)} - b_{bw}(555), \quad (4\text{-}38)$$

$$a(555) = 0.0596 + 0.2 \cdot [a(440)_i - 0.01], a(440)_i = \exp(-2.0 - 1.4\varphi + 0.2\varphi^2), \varphi = ln\left[\frac{r_{rs}(440)}{r_{rs}(555)}\right], \quad (4\text{-}39)$$

$$r_{rs}(\lambda) = \frac{R_{rs}(\lambda)}{(0.52 + 1.7 \cdot R_{rs}(\lambda))} \quad (4\text{-}40)$$

and $g_o = 0.0895$, $g_l = 0.1247$.

The absorption signal is then decomposed into CDOM and phytoplankton components using known relations and empirical estimations;

$$a_{dg}(\lambda) = a_{dg}(443) \cdot \exp{-S(\lambda - 443))}, \quad (4\text{-}41)$$

$$a_{ph}(\lambda) = a(\lambda) - a_w(\lambda) - a_{cdom}(\lambda) \quad (4\text{-}42)$$

The slope of CDOM, *S*, was derived empirically from samples collected from aquaculture ponds in Mississippi.

Model 29

Model 29 refers to the calibration and adaptation of the QAA-V4 algorithm for highly turbid eutrophic waters and was described by Le et al. (2009) with 710 nm used as a reference wavelength instead of 555.

$$u(\lambda) = \frac{-g_0 + \sqrt{(g_0)^2 + 4g_1 \times r_{rs}(\lambda)}}{2 \times g_1}, \quad (4\text{-}43)$$

$$b_{bp}(\lambda) = b_{bp}(710) \cdot \left(\frac{710}{\lambda}\right)^Y, \quad (4\text{-}44)$$

$$Y = 2.2 \cdot \left\{1 - 1.2 \cdot exp\left[-0.9 \cdot \frac{r_{rs}(560)}{r_{rs}(750)}\right]\right\} \quad (4\text{-}45)$$

$$b_{bp}(710) = \frac{u(710) \cdot a(710)}{1 - u(710)}, \tag{4-46}$$

$$a(555) = 0.0596 + 0.2 \cdot [a(440)_i - 0.01], \tag{4-47}$$

$$r_{rs}(\lambda) = R_{rs}(\lambda) \Big/ (0.52 + 1.7 \cdot R_{rs}(\lambda)) \tag{4-48}$$

and $g_o = 0.0895$, $g_l = 0.1247$.

In this case, the absorption of suspended solid and phytoplankton is negligible, the absorption is dominant by pure water, and the reflectance can be accurately measured. Pure water backscattering coefficient can also be neglected.

Model 30, 31 and 32

Models 30, 31 and 32 refer to an adaptation of the QAA-V4 algorithm so-called *Extended Quasi-Analytical Algorithm* (QAA-E), the first model which separates a_g, the absorption coefficient a of CDOM, from a_{dg} (a of CDOM and nonalgal particles) based on two absorption-backscattering relationships. It was developed by Zhu et al. (2011) and in this model, the water absorption and backscattering coefficients, a(λ) and b$_b$(λ), are expressed as

$$a(\lambda) = a_w(\lambda) + a_{ph}(\lambda) + a_g(\lambda) + a_d(\lambda) \tag{4-49}$$

and

$$b_b(\lambda) = b_{bw}(\lambda) + b_{bp}(\lambda), \tag{4-50}$$

Where the subscripts, w, ph, g and d denote the contributions of pure sea water, phytoplankton, CDOM and NAP respectively, and p in the backscattering term means the total particulate backscattering coefficients including both phytoplankton and NAP.

Model 33

Model 33 refers to the update of the Quasi-Analytical algorithm developed by Lee et al. (2009), QAAv5;

$$a(\lambda) = \frac{(1-u(\lambda))\left(b_{bw}(\lambda)+b_{bp}(\lambda)\right)}{u(\lambda)}$$

(4-51)

where

$$u(\lambda) = \frac{-g_0+\sqrt{(g_0)^2+4g_1 \cdot r_{rs}(\lambda)}}{2 \cdot g_1}$$

(4-52)

and $g_o = 0.089$, $g_l = 0.125$. The absorption signal is then decomposed into CDOM and

phytoplankton components using known relations and empirical estimations;

$$a_{cdom}(\lambda) = a_{cdom}(443) \cdot \exp -S(\lambda - 443)),$$

(4-53)

$$a_{ph}(\lambda) = a(\lambda) - a_w(\lambda) - a_{cdom}(\lambda)$$

(4-54)

Model 34

Model 34 refers to the method developed by Mishra et al. (2013) for the retrieval of

cyanobacteria in turbid waters. As a first step, total absorption and particulate

backscattering are estimated from subsurface R_{rs} (λ) (r_{rs}, sr^{-1}) at a given wavelength;

$$a(\lambda) = \frac{(1-u(\lambda))\left(b_{bw}(\lambda)+b_{bp}(\lambda)\right)}{u(\lambda)}$$
(4-55)

where

$$u(\lambda) = \frac{-g_0+\sqrt{(g_0)^2+4g_1 \times rrs(\lambda)}}{2 \times g_1}$$

(4-56)

and $g_o = 0.089$, $g_1 = 0.125$. The absorption signal is then decomposed into CDOM and

phytoplankton components using known relations and empirical estimations;

$$a_{cdom}(\lambda) = a_{cdom}(443) \times \exp -S(\lambda - 443)),$$

(4-57)

$$a_{ph}(\lambda) = a(\lambda) - a_w(\lambda) - a_{cdom}(\lambda)$$

(4-58)

The slope of CDOM, *S*, was derived empirically from samples collected from

aquaculture ponds in Mississippi.

Model 35

Model 35 refers to the quasi-analytical algorithm (QAA-CDOM) developed by Zhu and Yu (2013) to invert CDOM absorption from Earth Observing-1 (EO-1) Hyperion satellite images. It was developed from original QAA algorithm with the goal of improving its performance for a wide range of water conditions, particularly turbid water sin estuarine and coastal regions. To derive a (440) from R_{rs} (λ), QAA-v4 executes the following six steps:

a) Estimating R_{rs} (λ);

$$r_{rs}(\lambda) = \frac{R_{rs}(\lambda)}{T + \gamma Q \cdot R_{rs}(\lambda)},$$
(4-59)

where T=0.52 and $\gamma Q = 1.7$

b) Calculating u(λ);

$$u(\lambda) = \frac{-g_0 + \sqrt{(g_0)^2 + 4g_1 \cdot r_{rs}(\lambda)}}{2 \cdot g_1},$$
(4-60)

where g0=0.0895 and g1=0.1247 and u(λ) is defined by ;

$$u(\lambda) = \frac{b_b(\lambda)}{a(\lambda) + b_b(\lambda)}$$
(4-61)

c) Estimating a (555);

$$a(555) = a_w(555) + 10^{h_0 + h_1 \cdot X + h_2 \cdot X^2}$$
(4-62)

with

$$X = log\left(\frac{R_{rs}(440) + R_{rs}(490)}{R_{rs}(555) + 2 \cdot \frac{R_{rs}(640)}{R_{rs}(490)} \cdot R_{rs}(640)}\right)$$
(4-63)

where h0=-1.226, h1=-1.214 and h2=-0.35.

d) Calculating b_{bp} (555)

$$b_{bp}(555) = \frac{u(555) \cdot a(555)}{1 - u(555)} - b_{bw}(555).$$
(4-64)

e) Calculating b_{bp} (440)

$$b_{bp}(440) = b_{bp}(555) \cdot \left(\frac{555}{440}\right)^Y \qquad \text{(4-65)}$$

with

$$Y = y_0 \cdot \left(1 - y_1 \cdot exp\left(y_2 \cdot \frac{r_{rs}(440)}{r_{rs}(555)}\right)\right), \qquad \text{(4-66)}$$

where y_0=2.2, y_1=1.2 and y_2=-0.9.

f) Calculating a (440)

$$a(440) = \frac{(1-u(440)) \cdot \left(b_{bw}(440) + b_{bp}(440)\right)}{u(440)}. \qquad \text{(4-67)}$$

4.2.4. Model version denotations

The algorithms were validated using three different approaches: (1) original algorithms (OPA) – in first instance, the original algorithm (published parametrisation) was applied over the entire dataset and over every of the 12 OWTs independently; (2) globally re-parametrised algorithms (GPA) – subsequently, and assuming that the optimal relationship is linear, we re-calibrated the algorithm coefficients by regressing the estimated absorption coefficients against the in-situ data from the complete LIMNADES dataset; and (3) re-parametrisation by OWT (TPA) – finally, the best performing algorithms for each OWT were re-calibrated.

Optimisation algorithms (models 25, 34 and 35) were re-parametrised from the start of the analysis, so no original version was available to apply.

4.2.5. Quantitative statistical methodology

To test the performance of each algorithm, the following statistical tests that are commonly used good indicators for performance. Every statistic was assessed independently.

Pearson's correlation coefficient (r)

The correlation coefficient (r-value) is calculated according to

$$r = \frac{1}{N-1}\sum_{i=1}^{N}\left[\frac{X_i^M - \left(\frac{1}{N}\sum_{j=1}^{N}X_j^M\right)}{\left\{\frac{1}{N-1}\sum_{k=1}^{N}\left[X_k^M - \left(\frac{1}{N}\sum_{l=1}^{N}X_l^M\right)\right]^2\right\}^{1/2}}\right] x \left[\frac{X_i^E - \left(\frac{1}{N}\sum_{m=1}^{N}X_m^E\right)}{\left\{\frac{1}{N-1}\sum_{n=1}^{N}\left[X_n^E - \left(\frac{1}{N}\sum_{o=1}^{N}X_o^E\right)\right]^2\right\}^{1/2}}\right], \quad (4\text{-}68)$$

where, X is the variable and N is the number of samples. The superscript E denotes the estimated variable (from the model) and the superscript M denotes the measured variable (from LIMNADES database).

Bias

The error between model and measurement can be expressed according to

$$Error_{log} = log\left(x^{model}\right) - log\ x^{measured})\qquad\qquad (4\text{-}69)$$

Bias is a systematic error that arises due to the sample selection, therefore, the closer the algorithm bias is to zero, the better the retrieved data corresponds with the in-situ data. It is important also to look at the 95% confidence interval, even when the bias is very close to zero, a much larger value of this interval will imply lower confidence in the retrieved bias.

$$bias_{log} = Mean\left(Error_{log}\right)\qquad\qquad (4\text{-}70)$$

Mean Absolute Percentage Error

It is an accuracy measure of the forecast quality and is calculated as:

$$MAPE = mean(log_{10}APE), \text{ being } APE = 100 \cdot \left|\frac{x_i^{model} - x_i^{measured}}{x_i^{measured}}\right|. \qquad (4\text{-}71)$$

As a percentage relative error measure, it is considered a better index than absolute error measures (e.g. RMSE) in comparing model performance among data which mean could differ considerably.

Slope and intercept of the regression between in situ data and the estimated variable

Slope (S) and intercept (I) were obtained from type-2 regression. The closer the intercept is to the reference value of zero and the closer the slope is to the reference value of one, the better the fit between variables. In addition to it, the standard deviation has been also computed.

$$log_{10}CDOM_{mod} = S \times log_{10}CDOM_{meas} + I \qquad (4\text{-}72)$$

Percentage of possible retrievals

$$\eta = \frac{N_{model}}{N_{measured}} \cdot 100 \qquad (4\text{-}73)$$

where *n* is the number of observations (Arnone et al., 2006), x^{model} is the variable of interest derived from the proposed models and $x^{measured}$ is the same variable observed from *in situ* measurements.

RMSE (Root Mean Squared Error)

The absolute root mean square error (RMSE) is used to provide a description of the difference between estimated and in-situ a_{CDOM} (440) and it is defined as follows:

$$RMSE = \sqrt{\frac{\sum_{i=1}^{n}[\log(x_i^{estimated}) - \log x_i^{in-situ}]^2}{n-2}} \qquad (\ 4\text{-}74)$$

4.3. Results

4.3.1. *In situ* biogeochemical characteristics of the dataset

The distribution of a_{CDOM} (440) measurements is shown in **Figure 4-2**, as well as Chl-a and TSM. The mean a_{CDOM} (440) was 1.470 m^{-1} (median=0.900 m^{-1}). The mean Chl-a value of 58.785 mg m^{-3} (median=16.055 mg m^{-3}) which suggests the distribution of Chl-a is biased by some very high values from highly eutrophic systems.
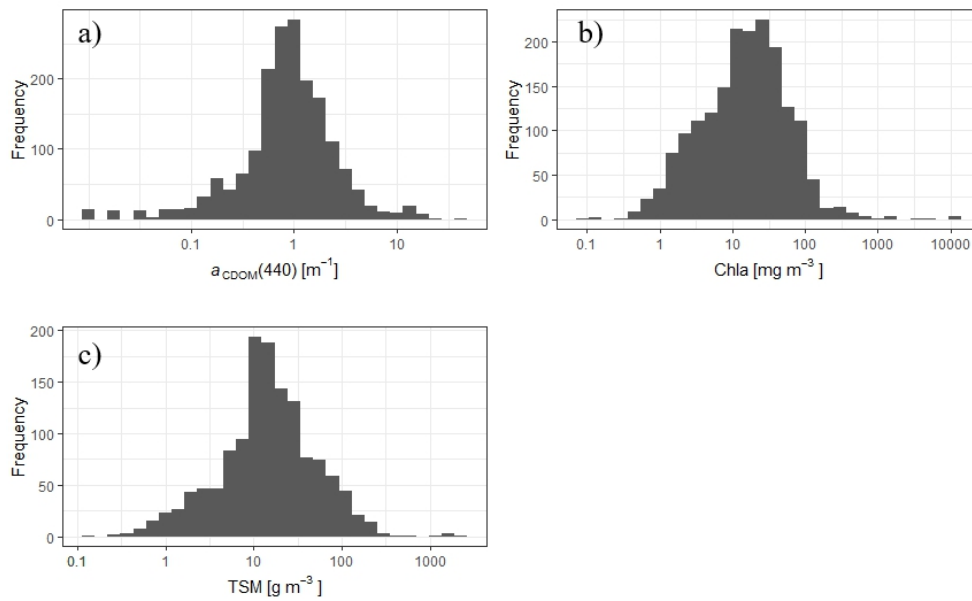
Figure 4-2 Distribution of a) a_{CDOM} (440), b) Chl-a and c) TSM

The dataset shows large differences in biogeochemical and optical water properties between the optical water types. **Table 4-3** shows average measured TSM and Chl-a concentrations, CDOM absorption coefficients and spectral slopes (400-500) for the 12 OWTs.

Table 4-3 Biogeochemical and optical water properties of the dataset (average values)

OWT	Number of samples	a_{CDOM} (440) (m^{-1}) Average Min-max	S_{CDOM} (400-500 nm)	Chl-a (mg/m³) Average Min-max	TSM samples	TSM (mg L⁻¹) Average Min-max
1	21	7.40 0.530-10.2	-0.006	2070 43.1-13296	21	340 20.4-1833
2	261	0.748 0.010-2.82	-0.007	11.6 0.150-55.4	169	8.50 0.400-45.9
3	95	0.155 0.020-1.03	-0.008	1.65 0.160-6.17	61	1.55 0.150-11.0
4	315	1.21 0.010-3.39	-0.007	17.8 0.100-97.6	234	17.6 1.30-110
5	159	1.52 0.320-7.61	-0.007	36.9 0.900-943	154	88 1.88-286
6	224	1.30 0.010-4.19	-0.008	49.6 7.80-125	135	12.8 1.55-43.8
7	25	3.034 0.630-17.9	-0.007	417 19.3-1842	23	153 5.00-2533
8	106	1.20 0.010-3.04	-0.007	142.4 19.3-3443	57	42.2 4.35-500
9	162	0.317 0.010-1.38	-0.008	5.59 0.540-23.2	128	9.22 0.910-58.4
10	51	9.00 0.840-42.5	-0.006	16.1 0.510-115	49	29.8 0.650-423
11	167	2.69 0.400-15.3	-0.007	19.7 0.800-86.5	134	27.4 4.00-113
12	224	1.02 0.030-5.71	-0.007	28.2 1.70-223	192	34.0 2.00-124

The range of a_{CDOM} (440) was large (0.172 m^{-1} for OWT-9 to 9.001 m^{-1} for OWT-10) and the mean/median Chl-a varied from 5.589 mg/m^3 to 2072.753 mg/m^3 (for OWT 9 and 1 respectively). OWT-1, -7 and -8 exhibit highest values of Chl-a and lower values are represented by OWT-3 and -9, consistent also with low values of TSM (1.511 and 9.098 mg L^{-1}).

4.3.2. Performance of original algorithms

▪ *Full dataset*

Overall, the performance of the original CDOM algorithms (OPA) tested varied greatly within the complex set of OWTs included in this study.

The RMSE, calculated on log values, for the retrieval of a_{CDOM} varied between 0.269 and 1.438 For clarity, we considered RMSE values in the first quartile (Q1 < 0.365) to represent comparatively "good" performance , values falling into the second quartile (0.365 < Q2 < 0.490) to perform "moderately good" and those with values falling into the third quartile (Q3 > 0.615) and above to perform "poorly". Generally, semi-analytical algorithms (mean RMSE= 0.516, max. RMSE=1.060, min. RMSE=0.270) marginally outperformed the empirical models (average RMSE=0.562, max. RMSE=1.440, min. RMSE=0.290). In addition, 25 algorithms generated invalid CDOM estimates (i.e. negative a_{CDOM}(440) values) when existing model parameters where used (models 1, 2, 3, 5, 6, 7, 8, 9, 10, 11, 12, 13, 14, 15, 16, 17, 21, 24, 26, 27, 28, 30, 31, 32 and 33) and they were excluded from further comparison and discussion.

In total, 10 algorithms retrieved valid CDOM estimates (models 4, 18, 19, 20, 22, 23, 25, 29, 34 and 35), and from those, only 7 generated R^2>0.25 (models 4, 19, 22, 25, 29, 34 and 35) and were moved to reparameterization. Within these 7 algorithms, only 3

produced RMSE<0.365 (models 4, 34 and 35). Moreover, the highest R^2 was obtained by models 4 and 19 (R^2=0.432 and 0.486 respectively).

Figure 4-3 shows the distributions when comparing modelled $\log_{10}(a_{CDOM}(440))$ with in-situ measurements for each of the 7 best ranked models.
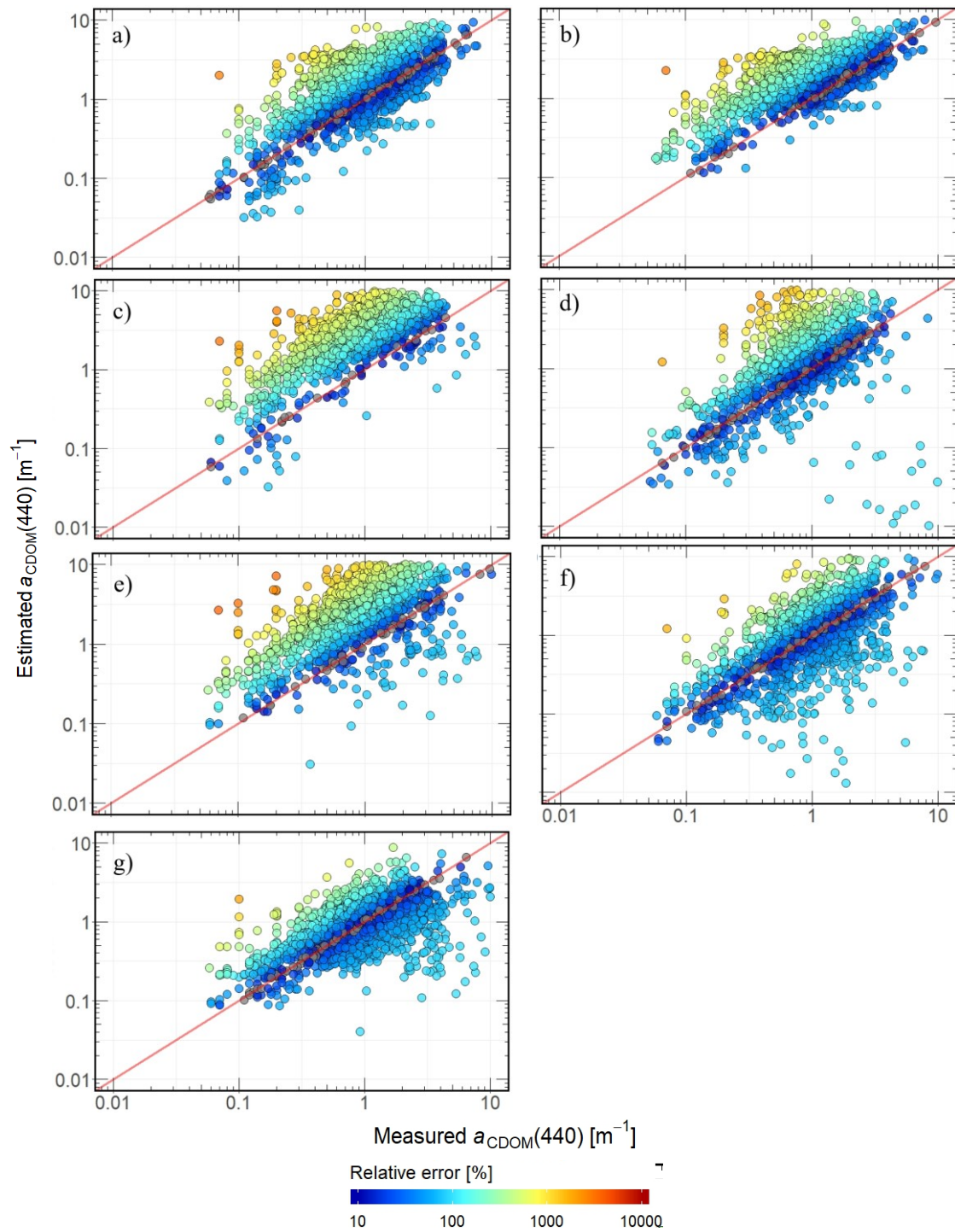
Figure 4-3 OPA Algorithms that retrieved valid a_{CDOM} (440) a) Model-4 (Kutser), b) Model-19 (Ficek), c) Model-22 (Carder-2), d) Model-25 (GSM01), e) Model-9 (QAAv4-Le), f) Model-34 (QAAv5-Mishra), g) Model-35 (QAAv5-CDOM).

Table 4-4 shows the error statistics generated when comparing modelled $\log_{10}(a_{CDOM}$ (440)) with in-situ measurements for each of the ranked models.

Table 4-4 Statistic for OA over the entire dataset, excluding those that produced negative values

Model	R^2	SLOPE	INTERCEPT	RMSE	MAPE	BIAS	N
Kutser	0.432	0.665	-0.376	0.346	219.855	0.211	59.714
Ficek	0.486	0.920	-0.659	0.366	140.693	0.271	59.714
Carder-2	0.420	0.218	`-0.317	0.570	14433	-1.43	59.69
GSM01	0.230	0.227	-.0421	1.060	32560	0.47	100
QAAv4Le	0.298	0.573	-0.703	0.485	528.613	0.469	59.714
QAAv5Mishra	0.304	0.514	-0.183	0.341	247.583	0.062	59.714
QAAv5CDOM	0.270	0.723	-0.031	0.325	158.664	-0.008	59.714

- ***Performance per OWT***

The performance of the original algorithms (OPA) was also examined within each individual OWT by comparing retrieved $\log_{10}(a_{CDOM}(440)$ using the original algorithm parametrisation against the in-situ measurements. Algorithm performance showed high variability between the tested models and between the different OWTs, with values of RMSE ranging from 0.040 (Carder-2, OWT-11) to 6.690

(Carder-1, OWT-10).

The performance of the algorithms was again considered by examination of the distribution of RMSE values. Those algorithms falling in Q1 are considered to have comparatively good performance, retrieving RMSE <0.320, those with moderate performance in Q2 retrieved RMSE between 0.320 and 0.470, while those with poor performance in Q3 had RMSE >0.470.

Overall, 13 algorithms performed well or moderately well across more than 6 OWTs (models 4, 5, 6, 9, 10, 12, 13, 14, 18, 19, 20, 29, 35) achieving RMSE < 0.470, even though, model 9 did not work for OWT-1 and model 18 did not retrieve any value for OWT-3. 14 models performed bad for more than 6 OWTs (models 1, 2, 3, 15, 16, 17, 21, 25, 26, 30, 31, 32, 33 and 34).

When looking at every cluster separately, OWTs 1 and 10 have only 2 algorithms performing well or moderately well, whereas OWT-2, and -9 have at least 29. Best performing algorithms per OWT are represented in **Table 4-5**. Higher values of RMSE where found for OWT-1, -10 and -11 (2.072, 6.688 and 2.487 respectively) and lowest values for OWT-6, -8 and -11 (0.068, 0.122 and 0.039 respectively).

Finally, for OWT-3 and 4 three algorithms did not retrieve any value (models 3, 17 and 18 for OWT3 and models 20, 21 and 24 for OWT-4). For OWT 1, models 9 and 17 did not retrieve any value and for OWT-12, model 17 did not retrieve any value.

Algorithms with good performance per OWT, were assumed as best performing and moved forward for re-parametrisation for OWTs 1 to 9, 11 and 12. For OWT-10, moderately good performance algorithms Carder-2 and QAAv4-Le (models 22 and 29) were moved to reparameterization given that no good RMSE valued were retrieved by any model.

Table 4-5 RMSE of OPA per OWT. Dark green show good performance algorithms, light green show moderately goodperformance algorithms, in orange we show algorithms with poor performance and in red, algorithms that did not retrieve any value.

OWT	1	2	3	4	5	6	7	8	9	10	11	12
N	21	255	95	314	159	222	25	106	149	50	167	224
Model							RMSE					
1	1.692	0.653	0.435	0.813	0.417	0.659	0.629	0.726	0.526	0.916	1.183	0.851
2	1.091	0.664	0.331	0.883	0.832	0.791	0.756	0.827	0.483	0.959	1.116	0.866
3	1.296	0.677	NA	0.918	0.541	0.617	0.600	0.631	0.406	1.434	1.162	0.826
4	0.818	0.334	0.348	NA	0.350	0.196	0.316	0.308	0.414	0.747	0.310	0.262
5	0.935	0.351	0.178	0.465	0.592	0.329	0.391	0.360	0.308	1.019	0.723	0.427
6	0.275	0.316	0.175	0.411	0.619	0.099	0.354	0.123	0.317	0.648	0.521	0.456
7	0.486	0.363	0.170	0.500	0.676	0.230	0.393	0.201	0.313	0.798	0.704	0.514
8	0.518	0.414	0.169	0.555	0.734	0.289	0.424	0.246	0.316	0.857	0.795	0.566
9	NA	0.301	0.181	0.392	0.620	0.068	0.275	0.122	0.310	0.704	0.512	0.450
10	0.454	0.341	0.174	0.470	0.680	0.184	0.377	0.195	0.309	0.824	0.674	0.509
11	0.498	0.382	0.170	0.537	0.734	0.236	0.409	0.234	0.312	0.881	0.774	0.561
12	0.971	0.291	0.231	0.313	0.578	0.252	0.425	0.348	0.305	1.348	0.507	0.385
13	0.993	0.292	0.220	0.316	0.604	0.258	0.437	0.356	0.305	1.398	0.523	0.405
14	0.959	0.300	0.250	0.283	0.586	0.230	0.418	0.343	0.321	1.411	0.483	0.372
15	1.374	0.473	0.254	0.644	0.946	0.533	0.677	0.616	0.433	1.888	0.906	0.752
16	1.554	0.577	0.497	0.759	1.195	0.630	0.866	0.786	0.562	1.311	1.061	0.988
17	NA	0.300	NA	0.813	0.126	0.783	0.386	0.673	0.228	0.848	1.092	NA
18	0.823	0.330	0.217	0.340	0.463	0.188	0.280	0.293	0.363	0.627	0.376	0.360
19	2.072	0.904	0.385	NA	1.333	1.050	1.183	1.190	0.593	6.688	1.667	1.172
20	0.540	0.484	0.251	0.131	0.534	0.356	0.293	0.499	0.491	2.083	0.039	0.461
21	0.811	0.308	NA	0.267	0.249	0.199	0.289	0.272	0.345	0.680	0.342	0.209
22	0.708	0.381	0.249	0.296	0.452	0.206	0.245	0.321	0.463	0.440	0.333	0.393
23	0.694	0.376	0.300	0.324	0.411	0.288	0.409	0.494	0.401	0.686	0.381	0.252
24	0.708	0.372	0.291	NA	0.416	0.288	0.428	0.480	0.392	0.628	0.382	0.258
25	0.899	0.437	0.292	0.270	1.284	0.398	0.505	0.774	0.595	2.303	2.487	0.731
26	1.269	0.354	0.187	0.554	0.812	0.335	0.654	0.474	0.313	0.776	0.773	0.773
27	1.514	0.345	0.186	0.380	0.809	0.332	0.590	0.462	0.311	0.805	0.701	0.620
28	1.255	0.358	0.187	0.377	0.794	0.324	0.657	0.464	0.316	0.762	0.710	0.602
29	0.619	0.517	0.265	0.369	0.432	0.455	0.373	0.589	0.466	0.336	0.619	0.359
30	0.698	0.326	0.296	0.603	0.838	0.381	0.567	0.498	0.402	0.721	0.687	0.795

OWT	1	2	3	4	5	6	7	8	9	10	11	12
N	21	255	95	314	159	222	25	106	149	50	167	224
Model						RMSE						
31	1.041	0.332	0.276	0.307	0.852	0.475	0.631	0.507	0.338	0.705	0.688	0.742
32	1.313	0.279	0.422	0.982	0.451	1.060	0.589	0.487	0.291	0.707	0.735	0.678
33	1.041	0.332	0.276	0.519	0.852	0.475	0.631	0.507	0.338	0.705	0.688	0.742
34	1.468	0.345	0.186	0.510	0.788	0.326	0.577	0.454	0.314	0.793	0.678	0.604
35	0.814	0.322	0.184	0.297	0.473	0.223	0.342	0.357	0.312	0.718	0.300	0.267

Good	Moderately good	Poor	Not performing

4.3.3. Performance of reparametrized algorithms

- *Full dataset (GPA)*

When reparametrizing the 7 best performing original algorithms (models 4, 19, 22, 25, 29, 34 and 35), with the entire training dataset (we are working now with a reduced set of algorithms having removed the non-performers based on the results achieved using the original parameterisations), the overall performance slightly improves (**Table 4-6**, mean RMSE=0.54 and mean R^2=0.33). No noticeable differences in overall algorithm performance was observed between empirical and semi-analytical models. Overall, performance of the set of algorithms improved with reparameterization (GPA) (**Table 4-6**). Similarly happened for most models individually, the reparameterization causes algorithm performance to improve (**Table 4-6**). It needs to be taken into account at this stage, that models 25, 34 and 35 were re-parametrised from the start of the analysis, so no original version was available to apply.

Table 4-6 Performance of OPA and GPA over the 7 best OPA algorithms

	OPA				GPA			
	RMSE	**MAPE**	**Bias**	**R^2**	**RMSE**	**MAPE**	**Bias**	**R^2**
MAX	1.058	32560.038	0.563	0.486	1.058	32560.038	0.521	0.562
MIN	0.325	140.693	-0.008	0.233	0.267	47.628	-0.033	0.233
AVERAGE	0.499	6918.298	0.293	0.348	0.442	4838.794	0.182	0.369

	Improves	Worsen	Stays

Only one algorithm individually improved both its RMSE and its R^2 (Carder-2, **Table 4-7**, **Figure 4-4**), retrieving also the best R^2 value of the entire reparameterization exercise for all OWTs (R^2=0.50).

Table 4-7 Performance of reparameterization

Model	RMSE	MAPE	Bias	R^2
4 - Kutser	0.304	188.474	0.152	0.432
19 – Ficek	0.293	82.472	0.115	0.483
22 – Carder-2	0.267	47.268	-0.033	0.562
25 – GSM01	1.058	32560.038	0.466	0.233
29 – QAAv4-Le	0.507	586.696	0.521	0.298
34 – QAAv5-Mishra	0.341	247.583	0.062	0.304
35 – QAAv5-CDOM	0.325	158.664	-0.008	0.270
Improves	**Worsen**	**Stays**		
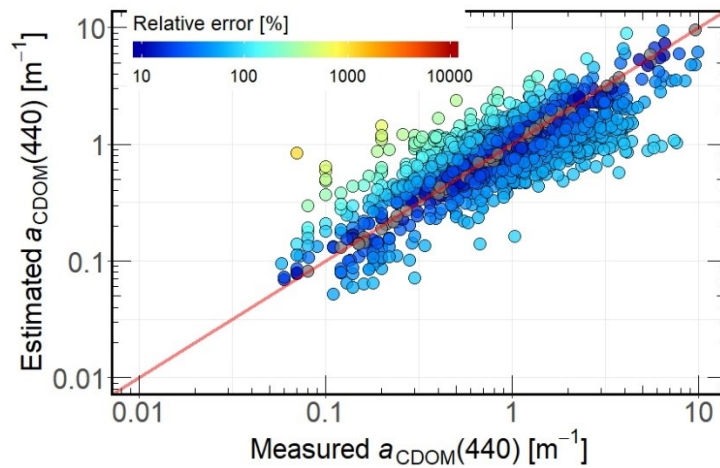
Figure 4-4 Estimated a_{CDOM} (440) against in-situ values for the reparametrized version of model 22

■ *Performance per OWT (TPA)*

The reparameterization within OWT groups (TPA) was performed for those original good performing algorithms (those with RMSE values <0.365 for OWT 1 to 9, 11 and 12 and RMSE<490 for OWT-10). **Table 4-8** provides the situation of reparameterization per model and per OWT showing also retrieved RMSE of reparametrized forms. a_{CDOM} (440) generated using the OWT training subsets (TPA) were compared to outputs from OPA models for the corresponding OWT assigned spectra.

Algorithm performance is highly variable across the tested models, with RMSE values ranging between 0.151 (22_Carder-2, OWT-3) to 1.577 (Lee-1, OWT-3). Values under Q1 (0.198) were considered good, between Q1 and Q2 (0.198 < RMSE < 0.269),

moderate and higher than Q2 (RMSE > 0.269), poor. Following this scheme, no algorithms demonstrated good or moderately good performance for OWT-2, -5 and -9. For OWT-3, 21 algorithms performed good or moderately good (models 5 to 15, 18, 20, 22, 24, 26 to 29, 34 and 35), for OWT-6 , 16 algorithms performed good or moderately good (4, 6 to 14, 18, 21 to 24 and 35), 5 algorithms for OWT-4 and 12 (models 12, 13, 14, 20 and 21; models 4, 21, 23, 24 and 35), 2 models for OWT-7 and -11 (21 and 22; 4 and 20) and one model for OWT-10 (22).

Several models are found to perform reasonably well across more than three or more OWT. Best performing algorithms have been selected from those best RMSE values with $R^2 > 0.25$ (for those OWTs with no models retrieving $R^2 > 0.25$, best R^2 have been selected)

Table 4-8 Performance of algorithm reparameterization in respect to the original parameters of every algorithm per OWT and RMSE values. In bold, best RMSE value for each model and OWT. In bold, best performing algorithms per OWT

OWT		1	2	3	4	5	6	7	8	9	10	11	12
N		21	255	95	314	159	222	25	106	149	50	167	224
Algorithm	Model						RMSE						
DSa-Miller-1	1												
DSa-Miller-2	2												
DSa-Miller-3	3												
Kutser	4						0.190	0.299	0.282			**0.228**	0.216
DSa	5			0.176						0.322			
Johannessen-1	6	**0.264**	0.276	0.198			0.238		0.654	0.430			
Johannessen-2	7			0.198			0.238		0.654	0.430			
Johannessen-3	8			0.198			0.238		0.654	0.430			
Johannessen-4	9		0.307	0.206			0.256	0.465	0.648	0.562			
Johannessen-5	10			0.206			0.256		0.648	0.562			
Johannessen-6	11			0.206			0.256		0.648	0.562			
Mannino-1	12		0.300	0.173	0.266		0.196			0.320			
Mannino-2	13		0.300	0.173	0.266		0.196			0.320			
Mannino-3	14		0.300	0.173	0.266		0.196			0.320			
Mannino-4	15			0.173									
Mannino-5	16												
Mannino-6	17		0.300			0.198				0.320			
DelCastillo-Miller	18			0.165			0.192	0.311	0.281				
Ficek	19												
Griffin	20			0.179	1.208			0.921				0.254	
Carder-1	21	**0.251**			1.208	**0.157**	0.189	0.244	0.274				**0.200**
Carder-2	22			**0.151**	0.260		**0.179**	**0.211**	**0.261**		0.268		
Lee-1	23			1.577	**0.324**		0.188						0.203
Lee-2	24			0.160			0.190						0.209
GSM01	25			0.292	0.270								
QAAv4-Lee-1	26			0.187						0.315			
QAAv4-Lee-2	27			0.186						0.314			
QAAv4-Lee-3	28			0.187			0.319			0.316			
QAAv4-Le	29			0.259							0.337		
QAAv4-Zhu-1	30			0.302									
QAAv4-Zhu-2	31			0.292	0.511								

Algorithm	Model	1	2	3	4	5	6	7	8	9	10	11	12
OWT		1	2	3	4	5	6	7	8	9	10	11	12
N		21	255	95	314	159	222	25	106	149	50	167	224
							RMSE						
QAAv4-Zhu-3	32		0.279							0.317			
QAAv5-Lee	33			0.292									
QAAv5-Mishra	34			0.186						0.314			
QAAv5-CDOM	35		0.322	0.184	0.297		0.223			**0.312**		0.300	0.267

Corresponding error and regression statistics for the best performing models across OWTs are shown in **Table 4-9**. It is clear that significant variability in performance is observed across each water type, even for best performing algorithms.

Table 4-9 Corresponding error and regression statistics for the best performing models across OWTs

OWT	Model	RMSE	BIAS	MAPE	R^2	SLOPE	INTERCEPT
OWT-1	6_Johannessen-1	0.264	0.155	201.562	0.296	0.871	-0.125
OWT-2	21_Carder-1	0.251	-0.003	168.689	0.149	0.434	0.003
OWT-3	22_Carder-2	0.151	-0.006	43.005	0.328	0.490	0.006
OWT-4	22_Carder-2	0.571	-0.002	96.241	0.199	0.434	0.002
OWT-5	21_Carder-1	0.157	-0.005	38.110	0.610	0.435	0.005
OWT-6	22_Carder-2	0.179	0.008	92.034	0.151	0.478	-0.015
OWT-7	22_Carder-2	0.211	0.005	64.134	0.314	0.434	-0.005
OWT-8	22_Carder-2	0.261	0.514	399.096	0.099	0.251	-0.295
OWT-9	35_QAAv5CDOM	0.312	0.215	244.460	0.159	0.666	0.055
OWT-10	22_Carder-2	0.268	-0.006	65.450	0.471	0.434	0.003
OWT-11	4_Kutser	0.228	0.062	58.364	0.253	1.095	-0.233
OWT-12	21_Carder-1	0.200	0.004	57.561	0.123	0.434	-0.004

4.3.4. Performance of the ensemble algorithm

Based on an objective evaluation and individual error statistics, the best performing algorithm selection for inland waters per OWT are shown in **Table 4-10** indicating the corresponding parametrisation. The selected choice of models is varied and from the 12 groups, five models identified as best performers appear in their OPA form and seven in their OTA form.

When considering the whole dataset comparison, the performance improves with TPA form, what could be an effect of the variation in the number of observations.

Table 4-10 Recommended model for each defined OWT ordered by OWT group median a_{CDOM} (440). Parameters for semi-analytical algorithms were the slope of the corresponding OWT

OWT	Model	Architectural approach	a	b	c	d	e
1	Johannessen-1 (TPA)	Band-ratio	-649	-0.035	686		
2	21_Carder-1 (TPA)	Semi-analytic	-1.62	-0.736	0.212	-3.73	-3.87
3	22_Carder-2 (TPA)	Semi-analytic	-0.363	1.59	-7.00	0.965	
4	22_Carder-2 (TPA)	Semi-analytic	-0.505	-1.65	-2.66	0.765	
5	22_Carder-1 (TPA)	Semi-analytic	0.648	0.407	-3.75	2.60	8.98
6	22_Carder-2 (TPA)	Semi-analytic	0.174	-0.629	-0.407	1.58	
7	22_Carder-2 (TPA)	Semi-analytic	0.549	-1.05	-1.98	1.7	
8	22_Carder-2 (TPA)	Semi-analytic	0.006	-0.363	0.120	0.933	
9	35_QAAv5-CDOM (TPA)	Semi-analytic	0.0180				
10	22_Carder-2 (TPA)	Semi-analytic	0.149	-0.686	-2.24	2.07	
11	4_Kutser (TPA)	Band-ratio	2.33	-1.68			
12	21_Carder-1 (TPA)	Semi-analytic	0.545	1.33	2.49	3.48	5.79
ALL	Carder-2 (TPA)	Semi-analytic	-0.0600	-0.449	0.730	1.35	

4.3.5. Influence of other OACs on CDOM retrieval

The corresponding histogram of residuals for Carder-2 in its original and reparametrized form is shown in **Figure 4-5**.
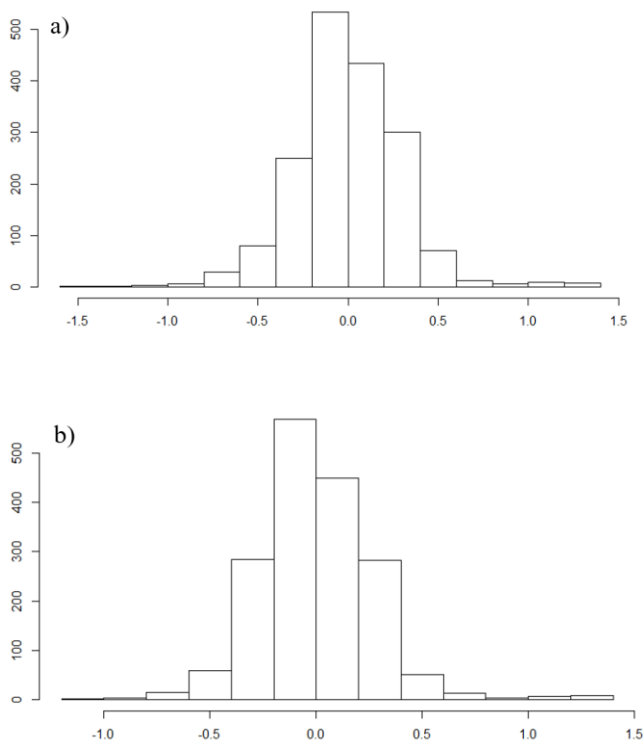
Figure 4-5 Histogram of residuals for model outputs in its original and reparametrized form

No correlation was found between a_{CDOM} (440) and Chl-a measurements (**Figure 4-6**) or TSM (**Figure 4-7**).
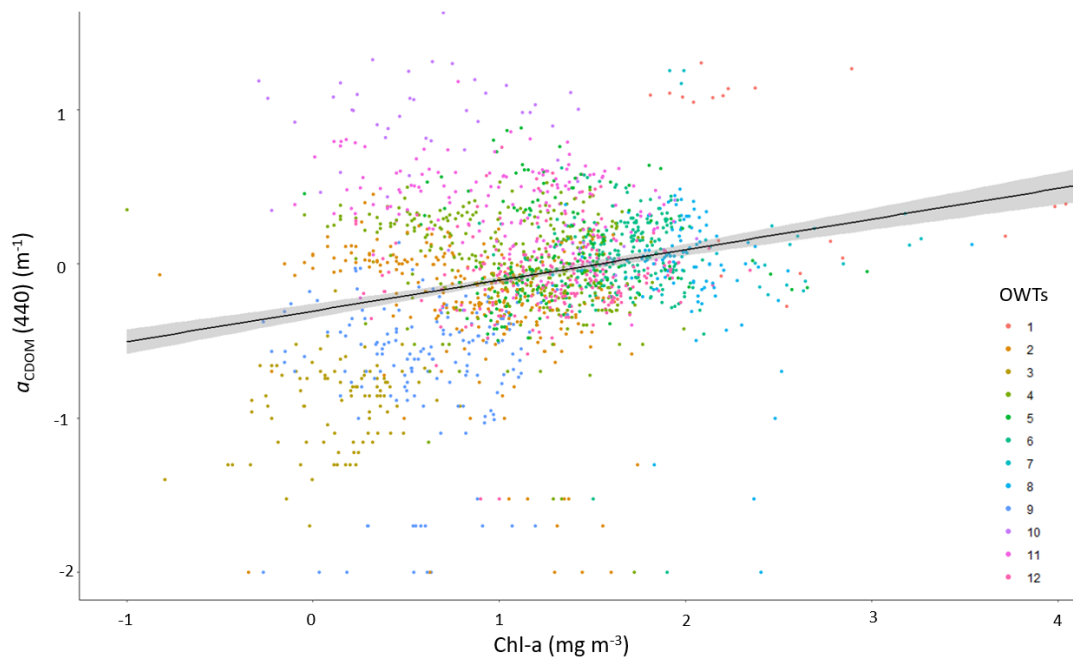
Figure 4-6 Correlation between a_{CDOM} (440) and Chl-a (R^2=0.0008, Y=0.0001x + 1.4672).
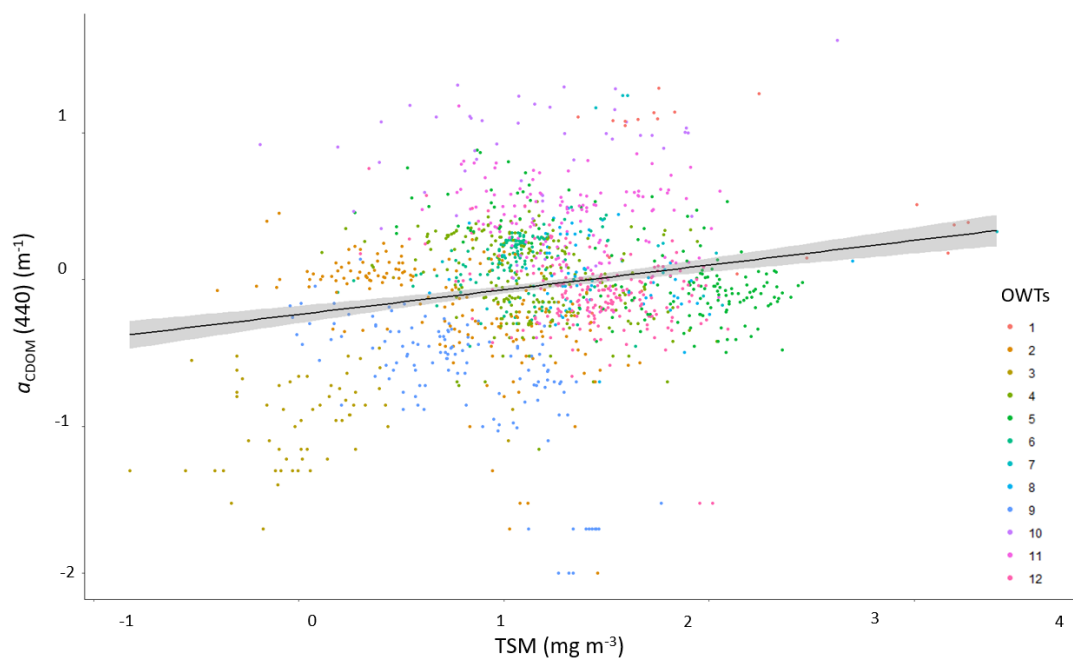
Figure 4-7 Correlation between a_{CDOM} (440) and TSM (R^2=0.003, Y=0.001x+1.856).

4.4. Discussion

This chapter shows how the accuracy of remote sensing-based retrievals of a_{CDOM} (440) can improve, mostly by targeting specific OWTs in algorithm development.

For original parametrisations across the entire dataset the accuracy of the models was very variable **Figure 4-3**. Of the 35 algorithms tested, 9 produced good estimations (RMSE values within the first quartile) when original parametrisation was used, and a further 14 algorithms produced poor estimations. The remainder performed moderately. In addition, 25 algorithms generated invalid CDOM estimates (i.e. negative a_{CDOM} (440) values) when existing model parameters were used.

In total, 10 algorithms retrieved valid CDOM, and from those, only 7 were reparametrized (those with $R^2>0.25$). Within these 7 algorithms the highest R^2 was obtained by models 4 and 19 ($R^2 = 0.432$ and 0.486 respectively).

It must be noted that several of the OWTs were under-represented by the *in situ* data resulting in poorer error statistics for OWTs 1, 7 and 10. These results can be useful for highlighting the areas that require further attention in terms of data needs: hypereutrophic waters (OWT 1), highly productive waters with high cyanobacteria abundance and elevated reflectance at red/near-infrared spectral region (OWT 7) and CDOM-rich waters (OWT 10).

OWT 10 differ from the rest of the OWTs on having lower reflectance values between 400 and 600 nm and a peak around 700 nm. Is made up of data collected from rivers and lakes with high CDOM concentrations (0.84 - 42.27 m^{-1}) with strong absorption even at shorter wavelengths (<500 nm), at the red part of the spectrum. Kutser et al. (2016) and Toming et al. (2016) highlighted the use of 705 nm bands (such as Sentinel-2 band 5) for estimation of CDOM in high coloured water bodies such as boreal and

artic lakes. Even though care needs to be taken when using CDOM for the remote estimation of DOC, given that in these water bodies, relationship CDOM-DOC is demonstrated to vary seasonally (Kutser et al., 2016a; K. Toming et al., 2016).

For almost every model validated, the reparametrized version produced more accurate results. The reparametrized version of model 22 was the best performer for most of the individual OWTs. Highest R^2 was obtained by reparametrized versions of models 4 and 19. Model 4 was developed by Kutser et al. (2005) for the estimation of CDOM in lake waters over large geographic areas and using Landsat-ALI. a_{CDOM} (420) values of this study varied between 0.68 and 11.13 m^{-1}. On the other hand, Ficek et al. (2011) developed Model 19 from data of the Pomeranian lakes and the Baltic Sea with the algorithm being trained on data with a_{CDOM} (440) between 0.1 and 17.4 m^{-1} and chlorophyll a concentrations between 1.3 and 336 mg m^{-3}. Both models 4 and 19 and Green/Red based empirical algorithms.

Improvement in the final error statistics was achieved by applying the best performing algorithm for each OWT indicated in **Table 4-9**, producing an improvement in log transformed RMSE of 10 % on average between the 12 OWTs. This demonstrates that improvement on the retrieval of algorithm performance can be achieved by focusing on OWTs during algorithm development. Moreover, it shows that algorithms perform very differently across OWTs in spite of the fact they are all Case 2 waters.

For hypereutrophic waters with cyanobacterial blooms and abundant vegetation (OWT-1), Blue-Green ratio based algorithms outperformed semi-analytic as well as empirical algorithms based on different wavelength ratios. For waters with diverse reflectance shape and marginal dominance of pigments and CDOM over inorganic suspended particles, sediment-laden waters and turbid, moderately productive waters with cyanobacteria presence, a double Blue-Green ratio based empirical algorithm

outperformed the rest. A double Blue-Green ratio and a Red-Green ratio was the best algorithm for application in clear waters, turbid waters with high organic content, waters with balanced effects of optically active constituents at short wavelengths, high productive waters with high cyanobacteria abundance and high reflectance at red/near-infrared spectral region, productive waters with cyanobacteria presence and Rrs peak close to 700 nm and for CDOM-rich waters. For waters high in CDOM, cyanobacteria presence and high absorption by NAP (Non-Algal Particles), a Green-Red ratio based algorithm outperformed the others. And finally, a semi analytic algorithm worked best for waters with high Rrs at short wavelengths.

The errors were still high for retrievals of several OWTs (4, 5, 6, 8, 9, and 11), what could constitute a first step for further research on a_{CDOM} algorithm validation and development, focusing on these OWTs.

As a consequence of was has been exposed, a dynamic approach to algorithm selection is needed to optimise retrievals. Neil et al. (2019) reached similar conclusions for Chl-a algorithms.

4.4.1. Band effects on algorithm performance

The information regarding the spectra needed for a_{CDOM} retrieval across several water types has a relevant importance on the performance of the algorithms. The spectral characteristics determine the degree to which the collected spectra influence the algorithm output: (i) band selection and (ii) band ratios. Zhu et al. (2014) have previously demonstrated that bandwidth might not influence the accuracy of the retrievals, probably given that CDOM absorption extend over a broad spectral range; even though, bands need to target those spectral regions where Chl-a absorption is lowest.

The results of this chapter illustrate that the performance of the algorithms in optically complex inland waters can be improved by selecting the appropriate bands with longer wavelengths than those typically selected for ocean environments. Model 22 performed for the full dataset far better than its predecessor model 21 (which produced negative retrievals) when a second band at 667 nm was incorporated. These longer wavelengths (>600 nm) are generally more appropriate for CDOM-rich inland waters.

Empirical algorithms based on band ratios generally improve their accuracy when incorporating at least one band >565 nm (e.g. models 4, 18, 19, 20 and 22). It was a generality that original algorithms based only on shorter wavelengths generated as a result negative, therefore, invalid a_{CDOM} estimates.

4.4.2. Methodological considerations

This chapters looks at the accuracy retrieved by several bio-optical models designed to retrieve a_{CDOM} (440) from measurements of water colour in optically complex inland waters. a_{CDOM} (440) was calculated from an extensive database of *in situ* R_{rs} measurements resampled to the wavebands of MERIS, MODIS, SeaWiFS, Landsat TM, Landsat ETM and Landsat OLI sensors.

Some of the observations from this dataset have been already used in previous studies to parametrise some of the algorithms tested in this chapter, therefore the influence of data dependency on the results need to be acknowledged.

Spyrakos et al. (2018) provides with a full description of the individual datasets with corresponding measurements and processing protocols. The validation dataset comprised 1809 R_{rs} measurements with corresponding concentrations of Chl-a, TSM and a_{CDOM} (440). a_{CDOM} (440) measurements were made following generally accepted methods, and it needs to be acknowledged that variability in a_{CDOM} (440) quantification

methods and interlaboratory protocols may contribute to uncertainty to the final retrieval (Hooker et al., 2005). However, usually refinement and optimisation of methodologies are required when applied to inland waters in order to approach optical complexities, what difficulties the standardisation of protocols. Moreover, all the datasets used in this study have been validated by data providers and quality checked before inclusion in the LIMNADES database.

Improvements in the accuracy of CDOM retrieval is demonstrated by calibrating best performing original models with OWT specific coefficients. With this, best performing OWTs were 3 (model 22, RMSE=0.151), 5 (model 21, RMSE=0.157) and 6 (model22, RMSE=0.179).

Finally, and even though this study focuses on OWTs defined by Spyrakos et al. (2018), it is recognised that these might not represent all water typed occurring in natural waters and that OWTs may be defined by alternative methods such as Moore et al. (2014).

4.4.3. Proposed solution for CDOM remote sensing

4.5. Conclusions and future perspectives

In this chapter, a series of a_{CDOM} (440) retrieval models have been validated using a dataset of in-situ measurements collected from over 185 inland waters to determine the most effective for recovering concentrations of a_{CDOM} (440) in optically complex environments.

CDOM content in complex inland waters usually present a wide range given their surrounding terrestrial characteristics and seasonal differences. CDOM levels in our sites vary between 0.172 m^{-1} (OWT-9) 9.001 m^{-1} (OWT-10).

The complexity of inland water bodies is currently a challenge to current remote sensing algorithms used to estimate parameters such as a_{CDOM} and even though this study does not attempt to be a full validation exercise for every bio-optical model developed for retrieving a_{CDOM} (440) from remote sensing estimations, it identifies several key observations with respect of current algorithms.

A total of 35 algorithms were explored and ranked based on their relative statistical performance and several final conclusions can be made:

- The most suitable and accurate models for estimating a_{CDOM} (440) within the whole range of water bodies were models 35, 34, 4, 19, 29, 22 and 25.

- The very big variability of performance of the tested algorithms emphasises the importance of model selection and validation and the risks of applying models across wide ranges of water bodies of different biogeochemical and physical characteristics.

- The overall performance was improved when reparametrizing algorithms within different OWTs.

- This research work aims to contribute to the remote monitoring of inland waters from space.

Given that this analysis has been carried out based on a series of *in situ* R_{rs} assuming them correspondent with true water-leaving reflectance, the next steps would be to transfer the results to satellite data such as Sentinel-3 OLCI.

Moreover, several OWTs were under-represented by the dataset analysed in this study, highlighting some areas that require further attention in terms of data needs: hypereutrophic waters (OWT 1), highly productive waters with high cyanobacteria

abundance and elevated reflectance at red/near-infrared spectral region (OWT 7) and

CDOM-rich waters (OWT 10).

5. CHAPTER 5 – CONCLUSSIONS AND FUTURE RESEARCH

The central goal of this PhD Thesis was to contribute with the knowledge of remote sensing of CDOM in inland water bodies. It delves into the role of lakes within the current climate change and the carbon cycle and reviews the physical principles that support the remote estimation of water quality parameters from space. The Thesis is structured to approach its objectives by trying to reply to three main questions.

In the first place, and taking into account the remote estimation of DOC is usually made through estimation of CDOM optical properties, we have looked at how the last one varies regionally and how this variation affects to the CDOM-DOC relationships across a range of lakes.

Subsequently, the Thesis looks at how the origin, distribution and degradation of CDOM vary both temporally and spatially within a shallow temperate lake and how the observed variability influences the underwater light field.

Finally, to evaluate the current accuracy of existing a_{CDOM} algorithms over a wide range of OWTs examining the influence that specific parameters such as Chl-a and other optically active constituents had on the estimation performance. Moreover, we intended to improve the overall performance of a selection of algorithms by its reparameterization, improving at the same time the ability to select the most appropriate algorithms and parametrisations for specific scenarios. A robust selection of candidate algorithms have been proposed for a_{CDOM} retrieval in more than 1000 lakes globally.

The presence of a significant relationship between CDOM and DOC has been documented in several inland waters in the recent years (Vodacek et al., 1997; Mannino et al., 2008; Harvey et al., 2015; Vantrepotte et al., 2015; Specchiulli et al., 2018; Li et al., 2018; Shao et al., 2019). Some studies evidence the constant behavior of the

relationship in waters dominated by terrestrial discharges given the conservative mixing of CDOM and DOC. However, a wide variability in the link at both seasonal and regional scale has also been proved. Based on the measurement of CDOM absorption and DOC laboratory analysis from a multi-year dataset of samples from contrasting lakes across Europe, the relationships between CDOM and DOC were analysed in various types of waters. This investigation showed that both CDOM absorption and DOC content varied significantly regionally and generally in accordance to the origin of its carbon content.

Overall, CDOM and DOC were highly correlated, particularly in sampling sites with composition of high aromaticity and allochthonous carbon compositions. For lakes historically affected by eutrophication, we found that the composition of DOM might weaken the relationships between CDOM and DOC fact that could be linked with the autochthonous composition and low molecular weight.

It can also be inferred from the results obtained, that CDOM optical properties and the CDOM-DOC relationship present high seasonal discrepancies that should be taken into account. Therefore and based on these conclusions, remote-sensing models for DOC estimation based on the relationship between CDOM and DOC should consider local and seasonal variability as well as optical complexity, considering at least groups of water types according to their absorption features. However, in order to better understand the implications of these results, future studies could deepen in the limitations on using CDOM as a proxy for DOC in different inland waters.

Subsequently, the Thesis looks at how the origin, distribution and degradation of CDOM and how it varies both temporally and spatially within a shallow temperate lake and how the observed variability influences the underwater light field.

In this context, photobleaching is understood as the decomposition of CDOM as a result of its exposition to UV irradiation. It has been found to be a major factor controlling the in-lake transformation and degradation of CDOM, and a key process influencing the spatial structure CDOM throughout the system. The variability in the quantity and quality of CDOM found pointed towards a marked decrease in the molecular weight of dissolved carbon compounds, a reduction on its aromatic content and a decrease in the degree of humification as water moved through the system from the main inflow to outflow.

Wetlands are important transitional zones between the terrestrial and aquatic environment. They are broadly recognized as substantial sources of aromatic CDOM to fluvial networks. They supply organic matter to downstream waters so that there is a significant relationship between the proportion of wetlands contributing and the concentration of DOM in destination waters. This study strengthen the general recognition of the potential contribution of water draining from wetlands often containing high concentrations of darkly coloured DOM, not only in terms of the concentration of CDOM but also its seasonality.

We also found a spatial and temporal variability in the optical properties of CDOM. In this study, this has important implications for bio-optical models of the underwater light climate in lakes and their application in the parametrization of algorithms for optical remote sensing of CDOM and other optically-active constituents.

Finally, we evaluated the current accuracy of existing a_{CDOM} algorithms over a wide range of OWTs examining the influence that specific parameters such as Chl-a and other optically active constituents had on the estimation performance. Several CDOM estimation algorithms have been developed in the last times, including empirical band ratios (Carder et al., 1999; D'Sa and Miller, 2003; Johannessen, 2003; D'Sa et al.,

2006; Del Castillo and Miller, 2008; Mannino et al., 2008), semi-analytical models (Lee et al., 2002b, 2009; Zhu et al., 2011; Mishra et al., 2013; Zhu and Yu, 2013), matrix inversion methods (MIM) based on the Hydrolight® radiative transfer model (Campbell and Phinn, 2010) and artificial neural networks (Hieronymi et al., 2017).

This exercise arises as a response to the need of validating existing remote sensing models on a wider group of water bodies with higher variability in their optical properties than what has been done until now. Moreover, we have intended to improve the overall performance of a selection of algorithms by its reparameterization, improving at the same time the ability to select the most appropriate algorithms and parametrisations for specific scenarios. A robust selection of candidate algorithms are proposed for a_{CDOM} retrieval in more than 1000 lakes globally.

We present the first extensive CDOM algorithm validation exercise based on the validation of a series of a_{CDOM} (440) models over a dataset of in-situ measurements collected from over 185 inland waters to determine the most effective for recovering concentrations of a_{CDOM} (440) in optically complex environments.

The complexity of inland water bodies is currently a challenge to current remote sensing algorithms used to estimate parameters such as a_{CDOM} and even though this study does not attempt to be a full validation exercise for every bio-optical model developed for retrieving a_{CDOM} (440) from remote sensing estimations, it identifies several key observations with respect of current algorithms.

The performance of the algorithms in optically complex inland waters can be improved by selecting the appropriate bands with longer wavelengths than those typically selected for ocean environments. These longer wavelengths (>600 nm) are generally more appropriate for CDOM-rich inland waters.

Empirical algorithms based on band ratios generally improve their accuracy when incorporating at least one band >565 nm. It was a generality that original algorithms based only on shorter wavelengths generated as a result negative, therefore, invalid a_{CDOM} estimates.

This research work aims to contribute to the remote monitoring of inland waters from space.

Given that this analysis has been carried out based on a series of *in situ* R_{rs} assuming them correspondent with true water-leaving reflectance, the next steps would be to transfer the results to satellite data such as Sentinel-3 OLCI.

Moreover, several OWTs were under-represented by the dataset analysed in this study, highlighting some areas that require further attention in terms of data needs: hypereutrophic waters, highly productive waters with high cyanobacteria abundance and elevated reflectance at red/near-infrared spectral region and CDOM-rich waters.

BIBLIOGRAPHY

ACIA, 2004. "Impacts of a Warming Arctic-Arctic Climate Impact Assessment." Impacts of a Warming Arctic-Arctic Climate Impact Assessment, by Arctic Climate Impact Assessment.

Adrian, R., Reilly, C.M.O., Zagarese, H., Baines, S.B., Hessen, D.O., Keller, W., Livingstone, D.M., Sommaruga, R., Straile, D., Van Donk, E., 2009. Lakes as sentinels of climate change. Limnol. Oceanogr. 54, 2283–2297. https://doi.org/10.4319/lo.2009.54.6_part_2.2283

Ågren, A., Haei, M., Köhler, S.J., Bishop, K., Laudon, H., 2010. Regulation of stream water dissolved organic carbon (DOC) concentrations during snowmelt; the role of discharge, winter climate and memory effects. Biogeosciences 7, 2901–2913. https://doi.org/10.5194/bg-7-2901-2010

Anda, A., Varga, B., 2010. Analysis of precipitation on Lake Balaton catchments from 1921 to 2007. Idojaras Q. J. Hung. Meteorol. Serv. 114, 187–201.

Andrew, A. a., Del Vecchio, R., Subramaniam, A., Blough, N. V., 2013. Chromophoric dissolved organic matter (CDOM) in the Equatorial Atlantic Ocean: Optical properties and their relation to CDOM structure and source. Mar. Chem. 148, 33–43. https://doi.org/10.1016/j.marchem.2012.11.001

Arnone, R., Babin, M., Barnard, A.H., Boss, E., Cannizzaro, J.P., Carder, K.L., Chen, F.R., Devred, E., Doerffer, R., Du, K., Hoge, F., Kopelevich, O. V, Platt, T., Poteau, A., Roesler, C., Sathyendranath, S., 2006. Reports of the International Ocean-Colour Coordinating Group Remote Sensing of Inherent Optical Properties : Fundamentals, Tests of Algorithms, and Applications, IOCCG Report 5. https://doi.org/10.1006/jmbi.1998.2073

Arst, H., Kutser, T., 1994. Data processing and interpretation of sea radiance factor measurements. Polar Res. 13, 3–12. https://doi.org/10.3402/polar.v13i1.6676

Asmala, E., Autio, R., Kaartokallio, H., Pitkänen, L., Stedmon, C. a., Thomas, D.N., 2013. Bioavailability of riverine dissolved organic matter in three Baltic Sea estuaries and the effect of catchment land use. Biogeosciences 10, 6969–6986. https://doi.org/10.5194/bg-10-6969-2013

Aulló-Maestro, M.E., Hunter, P., Spyrakos, E., Mercatoris, P., Kovács, A., Horváth, H., Preston, T., Présing, M., Torres Palenzuela, J., Tyler, A., 2017. Spatio-seasonal variability of chromophoric dissolved organic matter absorption and responses to photobleaching in a large shallow temperate lake. Biogeosciences 14, 1215–1233. https://doi.org/10.5194/bg-14-1215-2017

Aurin, D.A., Dierssen, H.M., Twardowski, M.S., Roesler, C.S., 2010. Optical complexity in Long Island Sound and implications for coastal ocean color remote sensing. J. Geophys. Res. 115, C07011. https://doi.org/10.1029/2009JC005837

Babin, M., Stramski, D., Ferrari, G.M., Claustre, H., Bricaud, A., Obolensky, G., Hoepffner, N., 2003. Variations in the light absorption coefficients of phytoplankton, nonalgal particles, and dissolved organic matter in coastal waters around Europe. J. Geophys. Res. Oceans 1978–2012 108. https://doi.org/10.1029/2001JC000882

Bass, A.M., 2007. Stable isotopic insight into pelagic carbon cycling in Loch Lomond: a large, temperate latitude lake.

Benoy, G., Cash, K., McCauley, E., Wrona, F., 2007. Carbon dynamics in lakes of the boreal forest under a changing climate. Environ. Rev. 15.

Bieroza, M., Baker, A., Bridgeman, J., 2009. Relating freshwater organic matter fluorescence to organic carbon removal efficiency in drinking water treatment. Sci. Total Environ. 407, 1765–1774. https://doi.org/10.1016/j.scitotenv.2008.11.013

Binding, C., Jerome, J., Bukata, R., Booty, W., 2008. Spectral absorption properties of dissolved and particulate matter in Lake Erie. Remote Sens. Environ. 112, 1702–1711. https://doi.org/10.1016/j.rse.2007.08.017

Binding, C.E., Bowers, D.G., 2003. Measuring the Salinity of the Clyde Sea from Remotely Sensed Ocean Colour. Estuar. Coast. Shelf Sci. 57, 605–611.

Bolin, B., 1981. Carbon cycle modelling (No. 16). New York: Wiley.

Bowers, D.G., Harker, G.E.L., Smith, P.S.D., Tett, P., 2000. Optical Properties of a Region of Freshwater Influence (The Clyde Sea). Estuar. Coast. Shelf Sci. 50, 717–726.

Bracchini, L., Tognazzi, A., Dattilo, A.M., Decembrini, F., Rossi, C., Loiselle, S.A., 2010. Sensitivity analysis of CDOM spectral slope in artificial and natural samples: an application in the central eastern Mediterranean Basin. Aquat. Sci. 72, 485–498. https://doi.org/10.1007/s00027-010-0150-y

Brezonik, P.L., Olmanson, L.G., Finlay, J.C., Bauer, M.E., 2015. Factors affecting the measurement of CDOM by remote sensing of optically complex inland waters. Remote Sens. Environ. 157, 199–215. https://doi.org/10.1016/j.rse.2014.04.033

Bricaud, A., Morel, A., Prieur, L., 1981. Absorption by dissolved organic matter of the sea (yellow substance) in the UV and visible domains. Limnol Ocean. 26, 43–53.

Brook, A.J., 1965. PLANKTONIC ALGAE AS INDICATORS OF LAKE TYPES, WITH SPECIAL REFERENCE TO THE DESMIDIACEAE. Limnol. Oceanogr. 10, 403–411. https://doi.org/10.4319/lo.1965.10.3.0403

Buchan, A., LeCleir, G.R., Gulvik, C.A., Gonzalez, J.M., 2014. Master recyclers: features and functions of bacteria associated with phytoplankton blooms. Nat. Rev. Microbiol. 12, 686–698. https://doi.org/10.1038/nrmicro3326

Campbell, G., Phinn, S.R., 2010. An assessment of the accuracy and precision of water quality parameters retrieved with the Matrix Inversion Method.: Accuracy and precision of the MIM. Limnol. Oceanogr. Methods 8, 16–29. https://doi.org/10.4319/lom.2010.8.16

Carder, K.L., Chen, F.R., Lee, Z.P., Hawes, S.K., Kamykowski, D., 1999. Semianalytic Moderate-Resolution Imaging Spectrometer algorithms for chlorophyll *a* and absorption with bio-optical domains based on nitrate-depletion temperatures. J. Geophys. Res. Oceans 104, 5403–5421. https://doi.org/10.1029/1998JC900082

Carder, K.L., Steward, R.G., Harvey, G.R., Ortner, P.B., 1989. Marine humic and fulvic acids: Their effects on remote sensing of ocean chlorophyll. Limnol. Oceanogr. 34, 68–81. https://doi.org/10.4319/lo.1989.34.1.0068

Carpenter, S., Benson, B., Biggs, R., Chipman, J., Foley, J., Golding, S., Hammer, R., Hanson, P., Johnson, P., Kamarainen, A., Kratz, T., Lathrop, R., Mahon, K., Provencher, B., Rusak, J., Solomon, C., Stanley, E., Turner, M., Vander Zanden, M., Whu, CH., Yuan, H., 2007. Understanding Regional Change : A Comparison of Two Lake Districts. Bioscience 57, 323–335.

Carpenter, S.R., Cole, J.J., Kitchell, J.F., Pace, M.L., 1998. Impact of dissolved organic carbon, phosphorus, and grazing on phytoplankton biomass and production in experimental lakesCarpernter et al. 1998.pdf. Limnol. Oceanogr. 43, 73–80.

Carvalho, L., Miller, C., Spears, B.M., Gunn, I.D.M., Bennion, H., Kirika, A., May, L., 2012. Water quality of Loch Leven: responses to enrichment, restoration and climate change. Hydrobiologia 681, 35–47. https://doi.org/10.1007/s10750-011-0923-x

Castillo, C.E. Del, Coble, P.G., 2000. Seasonal variability of the colored dissolved organic matter during the 1994- 95 NE and SW Monsoons in the Arabian Sea. Deep Sea Res. Part II Top. Stud. Oceanogr. 47, 1563–1579. https://doi.org/10.1016/S0967-0645(99)00154-X

Chen, C.-T.A., Borges, A.V., 2009. Reconciling opposing views on carbon cycling in the coastal ocean: Continental shelves as sinks and near-shore ecosystems as sources of atmospheric CO2. Deep Sea Res. Part II Top. Stud. Oceanogr. 56, 578–590. https://doi.org/10.1016/j.dsr2.2009.01.001

Chen, J., Zhu, W., Zheng, Y., Tian, Y.Q., Yu, Q., 2019. Monitoring seasonal variations of colored dissolved organic matter for the Saginaw River based on Landsat-8 data. Water Supply 19, 274–281. https://doi.org/10.2166/ws.2018.077

Chen, J., Zhu, W.-N., Tian, Y.Q., Yu, Q., 2017. Estimation of Colored Dissolved Organic Matter From Landsat-8 Imagery for Complex Inland Water: Case Study of Lake Huron. IEEE Trans. Geosci. Remote Sens. 55, 2201–2212. https://doi.org/10.1109/TGRS.2016.2638828

Cheng Feng Le, Yun Mei Li, Yong Zha, Deyong Sun, Bin Yin, 2009. Validation of a Quasi-Analytical Algorithm for Highly Turbid Eutrophic Water of Meiliang Bay in Taihu Lake, China. IEEE Trans. Geosci. Remote Sens. 47, 2492–2500. https://doi.org/10.1109/TGRS.2009.2015658

Clark, J.M., Bottrell, S.H., Evans, C.D., Monteith, D.T., Bartlett, R., Rose, R.J., Newton, R.J., Chapman, P.J., 2010. The importance of the relationship between scale and process in understanding long-term DOC dynamics. Sci. Total Environ. 408, 2768–2775.

Coble, P.G., Del Castillo, C.E., Avril, B., 1998. Distribution and optical properties of CDOM in the Arabian Sea during the 1995 Southwest Monsoon. Deep Sea Res. Part II Top. Stud. Oceanogr. 45, 2195–2223. https://doi.org/10.1016/S0967-0645(98)00068-X

Cole, J.J., Prairie, Y.T., Caraco, N.F., McDowell, W.H., Tranvik, L.J., Striegl, R.G., Duarte, C.M., Kortelainen, P., Downing, J. a., Middelburg, J.J., Melack, J., 2007a. Plumbing the Global Carbon Cycle: Integrating Inland Waters into the Terrestrial Carbon Budget. Ecosystems 10, 172–185. https://doi.org/10.1007/s10021-006-9013-8

Corin, N., Backhand, P., Kulovaara, M., 1996. Degradation products formed during UV-irradiation of humic waters. Chemosphere 33, 245–255. https://doi.org/10.1016/0045-6535(96)00167-1

Cory, R.M., Harrold, K.H., Neilson, B.T., Kling, G.W., 2015. Controls on dissolved organic matter (DOM) degradation in a headwater stream: The influence of photochemical and hydrological conditions in determining light-limitation or substrate-limitation of photo-degradation. Biogeosciences 12, 6669–6685. https://doi.org/10.5194/bg-12-6669-2015

Curtis, P.J., 1998. Climatic and hydrologic control of DOM concentration and quality in lakes, in: Aquatic Humic Substances. pp. 93–105.

Cuthbert, L.D., Del Giorgio, P., 1992. Toward a standard method of measuring color in freshwater. Limnol. Oceanogr. 37, 1319–1326.

De Haan, H., De Boer, T., 1987. Applicability of light absorbance and fluorescence as measures of concentration and molecular size of dissolved organic carbon in humic Lake Tjeukemeer. Water Res. 21, 731–734.

Del Castillo, C.E., Coble, P.G., 2000. Seasonal variability of the colored dissolved organic matter during the 1994–95 NE and SW Monsoons in the Arabian Sea. Deep Sea Res. Part II Top. Stud. Oceanogr. 47, 1563–1579. https://doi.org/10.1016/S0967-0645(99)00154-X

Del Castillo, C.E., Miller, R.L., 2008. On the use of ocean color remote sensing to measure the transport of dissolved organic carbon by the Mississippi River Plume. Remote Sens. Environ. 112, 836–844. https://doi.org/10.1016/j.rse.2007.06.015

Del Vecchio, R., 2004. Influence of the Amazon River on the surface optical properties of the western tropical North Atlantic Ocean. J. Geophys. Res. 109, C11001. https://doi.org/10.1029/2004JC002503

Del Vecchio, R., Blough, N. V., 2002. Photobleaching of chromophoric dissolved organic matter in natural waters: kinetics and modeling. Mar. Chem. 78, 231–253.

D'Sa, E.J., Goes, J.I., Gomes, H., Mouw, C., 2014. Absorption and fluorescence properties of chromophoric dissolved organic matter of the eastern Bering Sea in the summer with special reference to the influence of a cold pool. Biogeosciences 11, 3225–3244. https://doi.org/10.5194/bg-11-3225-2014

D'Sa, E.J., Miller, R.L., 2003. Bio-optical properties in waters influenced by the Mississippi River during low flow conditions. Remote Sens. Environ. 84, 538–549. https://doi.org/10.1016/S0034-4257(02)00163-3

Fee, E.J., Hecky, R.E., Kasian, S.E.M., Cruikshank, D.R., 1996. Effects of lake size, water clarity, and climatic variability on mixing depths in Canadian Shield lakes. Limnol. Oceanogr. 41, 912–920. https://doi.org/10.4319/lo.1996.41.5.0912

Ferrari, Giovanni M., Dowell, M.D., Grossi, S., Targa, C., 1996. Relationship between the optical properties of chromophoric dissolved organic matter and total concentration of dissolved organic carbon in the southern Baltic Sea region. Mar. Chem. 55, 299–316. https://doi.org/10.1016/S0304-4203(96)00061-8

Ficek, D., Zapadka, T., Dera, J., 2011b. Remote sensing reflectance of Pomeranian lakes and the Baltic. Oceanologia 53, 959–970. https://doi.org/10.5697/oc.53-4.959

Fichot, C., Sathyendranath, S., Miller, W., 2007. SeaUV and SeaUVC: Algorithms for the retrieval of UV/Visible diffuse attenuation coefficients from ocean color. Remote Sens. Environ. https://doi.org/10.1016/j.rse.2007.08.009

Fichot, Cédric G., Benner, R., 2012. The spectral slope coefficient of chromophoric dissolved organic matter (S275-295) as a tracer of terrigenous dissolved organic carbon in river-influenced ocean margins. Limnol. Oceanogr. 57, 1453–1466. https://doi.org/10.4319/lo.2012.57.5.1453

Fichot, C.G., Benner, R., 2011. A novel method to estimate DOC concentrations from CDOM absorption coefficients in coastal waters. Geophys. Res. Lett. 38.

Fichot, C.G., Downing, B.D., Bergamaschi, B.A., Windham-Myers, L., Marvin-DiPasquale, M., Thompson, D.R., Gierach, M.M., 2016. High-Resolution Remote Sensing of Water Quality in the San Francisco Bay–Delta Estuary. Environ. Sci. Technol. 50, 573–583. https://doi.org/10.1021/acs.est.5b03518

Fichot, C.G., Kaiser, K., Hooker, S.B., Amon, R.M.W., Babin, M., Belanger, S., Walker, S.A., Benner, R., 2013. Pan-Arctic distributions of continental runoff in the Arctic Ocean. Sci. Rep. 3, 1053.

Freeman, C., Fenner, N., Ostle, N.J., Kang, H., Dowrick, D.J., Reynolds, B., Lock, M. a, Sleep, D., Hughes, S., Hudson, J., 2004. Export of dissolved organic carbon from peatlands under elevated carbon dioxide levels. Nature 430, 195–8. https://doi.org/10.1038/nature02707

Gareis, J.A.L., Lesack, L.F.W., Bothwell, M.L., 2010. Attenuation of in situ UV radiation in Mackenzie Delta lakes with varying dissolved organic matter compositions: UVR ATTENUATION IN MACKENZIE DELTA LAKES. Water Resour. Res. 46. https://doi.org/10.1029/2009WR008747

Geller, A., 1986. Comparison of mechanisms enhancing biodegradability refractory lake water constituents ' Annette Geller. Limnol. Oceanol. 755–764.

Gordon, H.R., Brown, O.B., Evans, R.H., Brown, J.W., Smith, R.C., Baker, K.S., Clark, D.K., 1988. A semianalytic radiance model of ocean color. J. Geophys. Res. 93, 10909. https://doi.org/10.1029/JD093iD09p10909

Grasshoff, K., Kremling, K., Ehrhardt, M., 2009. Methods of Seawater Analysis. John Wiley & Sons, Ltd.

Griffin, Claire G., Finlay, J.C., Brezonik, P.L., Olmanson, L., Hozalski, R.M., 2018. Limitations on using CDOM as a proxy for DOC in temperate lakes. Water Res. 144, 719–727. https://doi.org/10.1016/j.watres.2018.08.007

Griffin, C.G., Frey, K.E., Rogan, J., Holmes, R.M., 2011. Spatial and interannual variability of dissolved organic matter in the Kolyma River, East Siberia, observed using satellite imagery. J. Geophys. Res. 116. https://doi.org/10.1029/2010JG001634

Griffin, C.G., McClelland, J.W., Frey, K.E., Fiske, G., Holmes, R.M., 2018. Quantifying CDOM and DOC in major Arctic rivers during ice-free conditions

using Landsat TM and ETM+ data. Remote Sens. Environ. 209, 395–409. https://doi.org/10.1016/j.rse.2018.02.060

Grzybowski, W., 2000. Effect of short-term sunlight irradiation on absorbance spectra of chromophoric organic matter dissolved in coastal and riverine water. Chemosphere 40, 1313–1318. https://doi.org/10.1016/S0045-6535(99)00266-0

Guéguen, C., Guo, L., Tanaka, N., 2005. Distributions and characteristics of colored dissolved organic matter in the Western Arctic Ocean. Cont. Shelf Res. 25, 1195–1207. https://doi.org/10.1016/j.csr.2005.01.005

Habib, O.A., Tippett, R., Murphy, K.J., 1997. Seasonal changes in phytoplankton community structure in relation to physico-chemical factors in Loch Lomond, Scotland 18.

Häder, D.-P., Kumar, H.D., Smith, R.C., Worrest, R.C., 2007. Effects of solar UV radiation on aquatic ecosystems and interactions with climate change. Photochem. Photobiol. Sci. Off. J. Eur. Photochem. Assoc. Eur. Soc. Photobiol. 6, 267–85. https://doi.org/10.1039/b700020k

Hajnal, É., Padisák, J., 2008. Analysis of long-term ecological status of Lake Balaton based on the ALMOBAL phytoplankton database. Hydrobiologia 599, 227–237. https://doi.org/10.1007/s10750-007-9207-x

Hancke, K., Hovland, E.K., Volent, Z., Pettersen, R., Johnsen, G., Moline, M., Sakshaug, E., 2014. Optical properties of CDOM across the Polar Front in the Barents Sea: Origin, distribution and significance. J. Mar. Syst. 130, 219–227. https://doi.org/10.1016/j.jmarsys.2012.06.006

Hanson, P.C., Pollard, A.I., Bade, D.L., Predick, K., Carpenter, S.R., Foley, J.A., 2004. A model of carbon evasion and sedimentation in temperate lakes. Glob. Change Biol. 10, 1285–1298. https://doi.org/10.1111/j.1365-2486.2004.00805.x

Harvey, E.T., Kratzer, S., Andersson, A., 2015. Relationships between colored dissolved organic matter and dissolved organic carbon in different coastal gradients of the Baltic Sea. AMBIO 44, 392–401. https://doi.org/10.1007/s13280-015-0658-4

Hedges, J.L., 2002. Why dissolved organic matter, in: Biogeochemistry of Marine Dissolved Organic Matter,. Academic.

Helms, J.R., 1998. Spectral Shape as an Indicator of Molecular Abstract Spectral Shape As an Indicator of Molecular Weight in Chromophoric Dissolved Organic Matter. Old Dominion University. https://doi.org/10.13140/2.1.3658.0645

Helms, J.R., Stubbins, A., Perdue, E.M., Green, N.W., Chen, H., Mopper, K., 2013. Photochemical bleaching of oceanic dissolved organic matter and its effect on absorption spectral slope and fluorescence. Mar. Chem. 155, 81–91. https://doi.org/10.1016/j.marchem.2013.05.015

Helms, John R., Stubbins, A., Ritchie, J.D., Minor, E.C., Kieber, D.J., Mopper, K., 2008. Absorption spectral slopes and slope ratios as indicators of molecular weight, source, and photobleaching of chromophoric dissolved organic matter. Limnol. Oceanogr. 53, 955–969. https://doi.org/10.4319/lo.2008.53.3.0955

Herndl, G.J., Muller-Niklas, G., Frick, J., 1993. Major role of ultraviolet-B in controlling bacterioplankton growth in the surface layer of the ocean. Nature 361, 717–719.

Hestir, E.L., Brando, V., Campbell, G., Dekker, A., Malthus, T., 2015. The relationship between dissolved organic matter absorption and dissolved organic carbon in reservoirs along a temperate to tropical gradient. Remote Sens. Environ. 156, 395–402. https://doi.org/10.1016/j.rse.2014.09.022

Hieronymi, M., Müller, D., Doerffer, R., 2017. The OLCI Neural Network Swarm (ONNS): A Bio-Geo-Optical Algorithm for Open Ocean and Coastal Waters. Front. Mar. Sci. 4, 140. https://doi.org/10.3389/fmars.2017.00140

Hoge, F.E., Vodacek, A., Blough, N.V., 1993. Inherent optical properties of the ocean: Retrieval of the absorption coefficient of chromophoric dissolved organic matter from fluorescence measurements. Limnol. Oceanogr. 38, 1394–1402. https://doi.org/10.4319/lo.1993.38.7.1394

Holmes, R.M., McClelland, J.W., Peterson, B.J., Tank, S.E., Bulygina, E., Eglinton, T.I., Gordeev, V.V., Gurtovaya, T.Y., Raymond, P.A., Repeta, D.J., Staples, R., Striegl, R.G., Zhulidov, A.V., Zimov, S.A., 2012. Seasonal and Annual Fluxes of Nutrients and Organic Matter from Large Rivers to the Arctic Ocean and Surrounding Seas. Estuaries Coasts 35, 369–382. https://doi.org/10.1007/s12237-011-9386-6

Hoogenboom, H.J., Dekker, A.G., De Haan, J.F., 1998. Retrieval of Chlorophyll and Suspended Matter from Imaging Spectrometry Data by Matrix Inversion. Can. J. Remote Sens. 24, 144–152.

Hooker, S.B., Van Heukelem, L., Thomas, C.S., Claustre, H., Ras, J., Barlow, R., Sessions, H., Schluter, L., Perl, J., Trees, C., Stuart, V., Head, E., 2005. The second SeaWiFS HPLC analysis round-robin experiment (SeaHARRE-2).

IOCCG, 2006. Remote sensing of inherent optical properties: fundamentals, tests of algorithms, and applications., Reports of the International Ocean-Colour Coordinating Group, No. 5, IOCCG, Dartmouth, Canada.

IPCC, 2001. The Carbon Cycle and Atmospheric Carbon Dioxide, in: Climate Change 2001. Cambridge University Press, Cambridge, pp. 183–237.

IPCC, 2007, 2007. Climate Change 2007 : An Assessment of the Intergovernmental Panel on Climate Change.

Istvánovics, V., Osztoics, A., Honti, M., 2004. Dynamics and ecological significance of daily internal load of phosphorus in shallow Lake Balaton, Hungary. Freshw. Biol. 49, 232–252. https://doi.org/10.1111/j.1365-2427.2004.01180.x

Johannessen, S.C., 2003. Calculation of UV attenuation and colored dissolved organic matter absorption spectra from measurements of ocean color. J. Geophys. Res. 108. https://doi.org/10.1029/2000JC000514

Jones, R.I., Grey, J., Quarmby, C., Sleep, D., 2001. Sources and fluxes of inorganic carbon in a deep, oligotrophic lake (Loch Ness, Scotland). Glob. Biogeochem. Cycles 15, 863–870. https://doi.org/10.1029/2001GB001423

Jones, R.I., Laybourn-Parry, M.C.W., Young, J.M., 1997. The forms and distribution of carbon in a deep, oligotrophic lake (Loch Ness, Scotland). SIL Proc. 26, 1922–2010.

Keiber, R.J., Zhou, Xi., Mopper, K., 1990. Formation of carbonyl compounds from UV-induced photodegradation of humic substances in natural waters: Fate of riverine carbon in the sea. Limnol. Oceanogr. 35, 1503–1515. https://doi.org/10.4319/lo.1990.35.7.1503

Keith, D.J., Yoder, J.A., Freeman, S.A., 2002. Spatial and Temporal Distribution of Coloured Dissolved Organic Matter (CDOM) in Narragansett Bay, Rhode Island: Implications for Phytoplankton in Coastal Waters. Estuar. Coast. Shelf Sci. 55, 705–717. https://doi.org/10.1006/ecss.2001.0922

Kirk, J.T.O., 2010. Light and Photosynthesis in Aquatic Ecosystems, Third edit. ed. Cambridge University Press.

Kouassi, A.M., Zika, R.G., Plane, J.M.C., 1990. Light-induced alteration of the photophysical properties of dissolved organic matter in seawater. Neth. J. Sea Res. 27, 33–41. https://doi.org/10.1016/0077-7579(90)90032-C

Kowalczuk, P., Cooper, W.J., Whitehead, R.F., Durako, M.J., Sheldon, W., 2003a. Characterization of CDOM in an organic-rich river and surrounding coastal ocean in the South Atlantic Bight. Aquat. Sci. - Res. Boundaries 65, 384–401. https://doi.org/10.1007/s00027-003-0678-1

Kragh, T., Søndergaard, M., Tranvik, L., 2008. Exposure to sunlight and phosphorus-limitation on bacterial degradation of coloured dissolved organicmatter (CDOM) in freshwater. FEMS Microbiol. Ecol. 64, 230–239. https://doi.org/10.1111/j.1574-6941.2008.00449.x

Kritzberg, E.S., Ekström, S.M., 2011. Increasing iron concentrations in surface waters – a factor behind brownification? Biogeosciences Discuss. 8, 12285–12316. https://doi.org/10.5194/bgd-8-12285-2011

Kutser, T., Casal Pascual, G., Barbosa, C., Paavel, B., Ferreira, R., Carvalho, L., Toming, K., 2016a. Mapping inland water carbon content with Landsat 8 data. Int. J. Remote Sens. 37, 2950–2961. https://doi.org/10.1080/01431161.2016.1186852

Kutser, T., Paavel, B., Metsamaa, L., Vahtmäe, E., 2009a. Mapping coloured dissolved organic matter concentration in coastal waters. Int. J. Remote Sens. 30, 5843–5849. https://doi.org/10.1080/01431160902744837

Kutser, T., Paavel, B., Verpoorter, C., Ligi, M., Soomets, T., Toming, K., Casal, G., 2016b. Remote Sensing of Black Lakes and Using 810 nm Reflectance Peak for Retrieving Water Quality Parameters of Optically Complex Waters. Remote Sens. 8, 497. https://doi.org/10.3390/rs8060497

Kutser, T., Pierson, D.C., Kallio, K.Y., Reinart, A., Sobek, S., 2005. Mapping lake CDOM by satellite remote sensing. Remote Sens. Environ. 94, 535–540. https://doi.org/10.1016/j.rse.2004.11.009

Kutser, T., Tranvik, L.J., Pierson, D.C., 2009b. Variations in colored dissolved organic matter between boreal lakes studied by satellite remote sensing. J. Appl. Remote Sens. 3, 033538. https://doi.org/10.1117/1.3184437

Lajtha, K., Michener, R.H., 1994. Stable Isotopes in Ecology and Environmental Science.

Laurion, I., Ventura, M., Catalan, J., Psenner, R., Sommaruga, R., 2000. Attenuation of ultraviolet radiation in mountain lakes: Factors controlling the among- and within-lake variability. Limnol. Oceanogr. 45, 1274–1288. https://doi.org/10.4319/lo.2000.45.6.1274

Laurion, I., Vincent, W.F., Lean, D.R.S., 1997. of Spectral Models for Underwater Ultraviolet Radiation : Development Northern High Latitude Lakes. Photochem. Photobiol. 65, 107–114.

Lee, E.-J., Yoo, G.-Y., Jeong, Y., Kim, K.-U., Park, J.-H., Oh, N.-H., 2015. Comparison of UV–VIS and FDOM sensors for in situ monitoring of stream DOC concentrations. Biogeosciences 12, 3109–3118. https://doi.org/10.5194/bg-12-3109-2015

Lee, Z., Carder, K.L., Arnone, R.A., 2002b. Deriving inherent optical properties from water color: a multiband quasi-analytical algorithm for optically deep waters. Appl. Opt. 41, 5755. https://doi.org/10.1364/AO.41.005755

Lee, Z., Lubac, B., Werdell, J., Arnone, R., 2009. An Update of the Quasi-Analytical Algorithm (QAA_v5) 9.

Lepane, V., Persson, T., Wedborg, M., 2003. Effects of UV-B radiation on molecular weight distribution and fluorescence from humic substances in riverine and low salinity water. Estuar. Coast. Shelf Sci. 56, 161–173. https://doi.org/10.1016/S0272-7714(02)00154-3

Levine, S.N., Borchardt, M.A., Braner, M., Shambaugh, A.D., 1999. The impact of zooplankton grazing on phytoplankton species composition and biomass in Lake Champlain (USA-Canada). J. Gt. Lakes Res. 25, 61–77. https://doi.org/10.1016/S0380-1330(99)70717-3

Li, J., Yu, Q., Tian, Y.Q., Boutt, D.F., 2018. Effects of Landcover, Soil Property, and Temperature on Covariations of DOC and CDOM in Inland Waters. J. Geophys. Res. Biogeosciences 123, 1352–1365. https://doi.org/10.1002/2017JG004179

Lindell, M.J., Granéli, H.W., Bertilsson, S., 2000. Seasonal photoreactivity of dissolved organic matter from lakes with contrasting humic content 57, 11.

Lindell, M.J., Wilhelm, G., Tranvik, L.J., 1995. Enhanced bacterial growth in response to photochetiical transformation of dissolved organic matter. Limnol. Oceanogr.

Maberly, S.C., Ainsworth, G., Carse, F., Fletcher, J.M., Groben, R., Hodgson, P., James, J.B., Kelly, J.L., Vincent, C.D., Wilson, D.R., 2006. A survey of the lakes of the English Lake District: The Lakes Tour 2005 88.

Mannino, A., Russ, M.E., Hooker, S.B., 2008. Algorithm development and validation for satellite-derived distributions of DOC and CDOM in the U.S. Middle Atlantic Bight. J. Geophys. Res. 113. https://doi.org/10.1029/2007JC004493

Maritorena, S., Siegel, D.A., Peterson, A.R., 2002. Optimization of a semianalytical ocean color model for global-scale applications. Appl. Opt. 41, 2705. https://doi.org/10.1364/AO.41.002705

Martínez–Pérez, A.M., Catalá, T.S., Nieto–Cid, M., Otero, J., Álvarez, M., Emelianov, M., Reche, I., Álvarez–Salgado, X.A., Arístegui, J., 2019. Dissolved organic

matter (DOM) in the open Mediterranean Sea. II: Basin–wide distribution and drivers of fluorescent DOM. Prog. Oceanogr. 170, 93–106. https://doi.org/10.1016/j.pocean.2018.10.019

Massi, L., Frittitta, L., Melillo, C., Polonelli, F., Bianchi, V., De Biasi, A.M., Nuccio, C., 2020. Seasonal Dynamic of CDOM in a Shelf Site of the South-Eastern Ligurian Sea (Western Mediterranean). J. Mar. Sci. Eng. 8, 703. https://doi.org/10.3390/jmse8090703

Massicotte, P., Asmala, E., Stedmon, C., Markager, S., 2017. Global distribution of dissolved organic matter along the aquatic continuum: Across rivers, lakes and oceans. Sci. Total Environ. 609, 180–191. https://doi.org/10.1016/j.scitotenv.2017.07.076

Matsuoka, a., Babin, M., Doxaran, D., Hooker, S.B., Mitchell, B.G., Bélanger, S., Bricaud, a., 2014. A synthesis of light absorption properties of the Arctic Ocean: application to semianalytical estimates of dissolved organic carbon concentrations from space. Biogeosciences 11, 3131–3147. https://doi.org/10.5194/bg-11-3131-2014

Matsuoka, A., Bricaud, A., Benner, R., Para, J., Sempéré, R., Prieur, L., Bélanger, S., Babin, M., 2012. Tracing the transport of colored dissolved organic matter in water masses of the Southern Beaufort Sea: relationship with hydrographic characteristics. Biogeosciences 9, 925–940. https://doi.org/10.5194/bg-9-925-2012

McCarthy, J.J., 2001. Climate change 2001: impacts, adaptation, and vulnerability: contribution of Working Group II to the third assessment report of the Intergovernmental Panel on Climate Change.

Millennium Ecosystem Assessment, 2005. Millennium Ecosystem Assessment, Ecosystems and Human Well-being: Synthesis. Washington, DC. https://doi.org/10.1196/annals.1439.003

Mishra, S., Mishra, D.R., Lee, Z., Tucker, C.S., 2013. Quantifying cyanobacterial phycocyanin concentration in turbid productive waters: A quasi-analytical approach. Remote Sens. Environ. 133, 141–151. https://doi.org/10.1016/j.rse.2013.02.004

Mobley, C.D., Stramski, D., Bissett, W.P., Boss, E., 2004. Optical modeling of ocean waters: Is the Case 1-Case 2 classification still useful? Oceanogr.-Wash. DC-Oceanogr. Soc.- 17, 60–67.

Moore, T.S., Dowell, M.D., Bradt, S., Ruiz Verdu, A., 2014. An optical water type framework for selecting and blending retrievals from bio-optical algorithms in lakes and coastal waters. Remote Sens. Environ. 143, 97–111. https://doi.org/10.1016/j.rse.2013.11.021

Moran, M.A., Sheldon, W.M., Zepp, R.G., 2000. Carbon loss and optical property changes during long-term photochemical and biological degradation of estuarine dissolved organic matter. Limnol. Oceanogr. 45, 1254–1264. https://doi.org/10.4319/lo.2000.45.6.1254

Morel, A., Prieur, L., 1977. Analysis of variations in ocean color. Limnol. Oceanogr. 22, 709–722. https://doi.org/10.4319/lo.1977.22.4.0709

Morel, A.Y., 2001. Bio-optical models, Academic Press. ed. Villefranche-sur-mer, France.

Morel, A.Y., Gordon, 1980. Report of the working group on water color 18, 343–355.

Morris, D.P., Zagarese, H., Williamson, C.E., Balseiro, E.G., Hargreaves, B.R., Modenutti, B., Moeller, R., Queimalinos, C., 1995. The attenuation of solar UV radiation in lakes and the role of dissolved organic carbon. Limnol. Oceanogr. 40, 1381–1391. https://doi.org/10.4319/lo.1995.40.8.1381

Mózes, A., Présing, M., Vörös, L., 2006. Seasonal dynamics of picocyanobacteria and picoeukaryotes in a large shallow lake (Lake Balaton, Hungary). Int. Rev. Hydrobiol. 91, 38–50. https://doi.org/10.1002/iroh.200510844

Müller, R. a, Kothawala, D.N., Podgrajsek, E., Sahlée, E., Koehler, B., Tranvik, L.J., Weyhenmeyer, G. a, 2014. Hourly, daily, and seasonal variability in the absorption spectra of chromophoric dissolved organic matter in a eutrophic, humic lake. https://doi.org/10.1002/2014JG002719.Received

Neff, J.C., Finlay, J.C., Zimov, S.A., Davydov, S.P., Carrasco, J.J., Schuur, E.A.G., Davydova, A.I., 2006. Seasonal changes in the age and structure of dissolved organic carbon in Siberian rivers and streams. Geophys. Res. Lett. 33. https://doi.org/10.1029/2006GL028222

Neil, C., Spyrakos, E., Hunter, P.D., Tyler, A.N., 2019. A global approach for chlorophyll-a retrieval across optically complex inland waters based on optical water types. Remote Sens. Environ. 229, 159–178. https://doi.org/10.1016/j.rse.2019.04.027

Nelson, N.B., Carlson, C.A., Steinberg, D.K., 2004. Production of chromophoric dissolved organic matter by Sargasso Sea microbes. Mar. Chem. 89, 273–287. https://doi.org/10.1016/j.marchem.2004.02.017

Nelson, N.B., Siegel, D.A., 2013. The Global Distribution and Dynamics of Chromophoric Dissolved Organic Matter. Annu. Rev. Mar. Sci. 5, 447–476. https://doi.org/10.1146/annurev-marine-120710-100751

Nelson, N.B., Siegel, D.A., Michaels, A.F., 1998. Nelson et al. 1998.pdfSeasonal dynamics of colored dissolved material in the Sargasso Sea. Deep Sea Res. Part Oceanogr. Res. Pap.

Nouchi, V., Kutser, T., Wüest, A., Müller, B., Odermatt, D., Baracchini, T., Bouffard, D., 2019. Resolving biogeochemical processes in lakes using remote sensing. Aquat. Sci. 81. https://doi.org/10.1007/s00027-019-0626-3

Odermatt, D., Gitelson, A., Brando, V.E., Schaepman, M., 2012. Review of constituent retrieval in optically deep and complex waters from satellite imagery. Remote Sens. Environ. 118, 116–126. https://doi.org/10.1016/j.rse.2011.11.013

O'Donnell, D.M., Effler, S.W., Perkins, M., Strait, C., 2013. Optical characterization of lake champlain: Spatial heterogeneity and closure. J. Gt. Lakes Res. 39, 247–258. https://doi.org/10.1016/j.jglr.2013.03.004

O'Donnell, D.M., Effler, S.W., Strait, C.M., Leshkevich, G. a., 2010. Optical characterizations and pursuit of optical closure for the western basin of Lake Erie through in situ measurements. J. Gt. Lakes Res. 36, 736–746. https://doi.org/10.1016/j.jglr.2010.08.009

Osburn, C.L., O'Sullivan, D.W.', Boyd, T.J., 2009. Increases in the longwave photobleaching of chromophoric dissolved organic matter in coastal waters. Limnol. Oceanogr. 54, 145–159. https://doi.org/10.4319/lo.2009.54.1.0145

Osburn, C.L., Stedmon, C.A., 2011. Linking the chemical and optical properties of dissolved organic matter in the Baltic–North Sea transition zone to differentiate three allochthonous inputs. Mar. Chem. 126, 281–294. https://doi.org/10.1016/j.marchem.2011.06.007

Padisak, J., Reynolds, C.S., 1998. Selection of phytoplankton associations in Lake Balaton, Hungary, in response to eutrophication and restoration measures, with special reference to the cyanoprokaryotes. Hydrobiologia 384, 41–53. https://doi.org/10.1023/A:1003255529403

Palmer, S.C.J., Kutser, T., Hunter, P.D., 2015b. Remote sensing of inland waters: Challenges, progress and future directions. Remote Sens. Environ. 157, 1–8. https://doi.org/10.1016/j.rse.2014.09.021

Palmer, S.C.J., Pelevin, V. V., Goncharenko, I., Kovács, A.W., Zlinszky, A., Présing, M., Horváth, H., Nicolás-Perea, V., Balzter, H., Tóth, V.R., 2013. Ultraviolet fluorescence LiDAR (UFL) as a measurement tool for water quality parameters in turbid lake conditions. Remote Sens. 5, 4405–4422. https://doi.org/10.3390/rs5094405

Para, J., Charrière, B., Matsuoka, a., Miller, W.L., Rontani, J.F., Sempéré, R., 2013. UV/PAR radiation and DOM properties in surface coastal waters of the Canadian shelf of the Beaufort Sea during summer 2009. Biogeosciences 10, 2761–2774. https://doi.org/10.5194/bg-10-2761-2013

Peel, M.C., Finlayson, B.L., McMahon, T. a., 2006. Updated world map of the Köppen-Geiger climate classification. Meteorol. Z. 15, 259–263. https://doi.org/10.1127/0941-2948/2006/0130

Pegau, W.S., 2002. Inherent optical properties of the central Arctic surface waters. J. Geophys. Res. 107, 8035. https://doi.org/10.1029/2000JC000382

Pegau, W.S., Gray, D., Zaneveld, J.R., 1997. Absorption and attenuation of visible and near-infrared light in water: dependence on temperature and salinity. Appl. Opt. 36, 6035–6046. https://doi.org/10.1364/AO.36.006035

Peuravuori, J., Pihlaja, K., 1997. Molecular size distribution and spectroscopic properties of aquatic humic substances. Anal. Chim. Acta 337, 33–149.

Pham, S. V., Leavitt, P.R., Mcgowan, S., Peres-neto, P., 2008. Spatial variability of climate and land-use effects on lakes of the northern Great Plains 53, 728–742.

Philipson, P., Kratzer, S., Ben Mustapha, S., Strömbeck, N., Stelzer, K., 2016. Satellite-based water quality monitoring in Lake Vänern, Sweden. Int. J. Remote Sens. 37, 3938–3960. https://doi.org/10.1080/01431161.2016.1204480

Pinney, M.L., Westerhoff, P.K., Baker, L., 2000. Transformations in dissolved organic carbon through constructed wetlands. Water Res. 34, 1897–1911. https://doi.org/10.1016/S0043-1354(99)00330-9

Présing, M., Herodek, S., Vörös, L., Kóbor, I., 1996. Nitrogen fixation, ammonium and nitrate uptake during a bloom of Cylindrospermopsis raciborskii in Lake Balaton. Arch. Für Hydrobiol. 136.4, 553–562.

Présing, M., Preston, T., Takátsy, A., Sprober, P., Kovács, A.W., Vörös, L., Kenesi, G., Kóbor, I., 2008. Phytoplankton nitrogen demand and the significance of internal and external nitrogen sources in a large shallow lake (Lake Balaton, Hungary). Hydrobiologia 599, 87–95. https://doi.org/10.1007/s10750-007-9191-1

Prieur, L., Sathyendranath, S., 1981. An optical classification of coastal and oceanic waters based on the specific spectral absorption curves of phytoplankton pigments, dissolved organic matter, and other particulate materials1: Optical classification. Limnol. Oceanogr. 26, 671–689. https://doi.org/10.4319/lo.1981.26.4.0671

R Core Team (2017), n.d. R: A language and environment for statistical computing. R Foundation for Statistical Computing, Vienna, Austria.

Read, Jordan S., Rose, K.C., 2013. Physical responses of small temperate lakes to variation in dissolved organic carbon concentrations. Limnol. Oceanogr. 58, 921–931. https://doi.org/10.4319/lo.2013.58.3.0921

Reche, I., Pace, M., Cole, J., 1998. Interactions of Photobleaching and Inorganic Nutrients in Determining Bacterial Growth on Colored Dissolved Organic Carbon. Microb. Ecol. 36, 270–280.

Reche, I., Pace, M.L., Cole, J.J., 1999. Relationship of trophic and chemical conditions to photobleaching of dissolved organic matter in lake ecosystems. Biogeochemistry 44, 259–280. https://doi.org/10.1007/BF00996993

Reinart, A., Paavel, B., Pierson, D., Strömbeck, N., 2004. Inherent and apparent optical properties of Lake Peipsi, Estonia. Boreal Environ. Res. 9, 429–445.

Riddick, Caitlin A. L., Hunter, P.D., Tyler, A.N., Martinez-Vicente, V., Horváth, H., Kovács, A.W., Vörös, L., Preston, T., Présing, M., 2015. Spatial variability of absorption coefficients over a biogeochemical gradient in a large and optically complex shallow lake. J. Geophys. Res. Oceans 120, 7040–7066.

Ritchie, J.C., Zimba, P.V., Everitt, J.H., 2003. Remote Sensing Techniques to Assess Water Quality. Photogramm. Eng. Remote Sens. 69, 695–704. https://doi.org/10.14358/PERS.69.6.695

Rochelle-Newall, E., Delille, B., Frankignoulle, M., Gattuso, J.P., Jacquet, S., Riebesell, U., Terbruggen, A., Zondervan, I., 2004. Chromophoric dissolved organic matter in experimental mesocosms maintained under different pCO2 levels. Mar. Ecol. Prog. Ser. 272, 25–31. https://doi.org/10.3354/meps272025

Rosenzweig, C., Karoly, D., Vicarelli, M., Neofotis, P., Wu, Q., Casassa, G., Menzel, A., Root, T.L., Estrella, N., Seguin, B., Tryjanowski, P., Liu, C., Rawlins, S., Imeson, A., 2008. Attributing physical and biological impacts to anthropogenic climate change. Nature 453, 353–7. https://doi.org/10.1038/nature06937

Roulet, N., Moore, T.R., 2006. Environmental chemistry: browning the waters. Nature 444, 283.

Santos, L., Santos, E.B.H., Dias, J.M., Cunha, a, Almeida, a, 2014. Photochemical and microbial alterations of DOM spectroscopic properties in the estuarine system Ria de Aveiro. Photochem. Photobiol. Sci. Off. J. Eur. Photochem. Assoc. Eur. Soc. Photobiol. 1146–1159. https://doi.org/10.1039/c4pp00005f

Schindler, D.W., 2009. Lakes as sentinels and integrators for the effects of climate change on watersheds, airsheds, and landscapes. Limnol. Oceanogr. 54, 2349–2358. https://doi.org/10.4319/lo.2009.54.6_part_2.2349

Schindler, D.W., Curtis, P.J., 1997. The role of DOC in protecting freshwaters subjected to climatic warming and acidification from UV exposure 1–8.

Schwarz, J.N., Kowalczuk, P., Chavez, F.P., 2002. Two models for absorption by coloured dissolved organic matter. Oceanologia 44, 209–241.

Sempéré, R., Cauwet, G., 1995. Occurrence of organic colloids in the stratified estuary of the Krka River (Croatia). Estuar. Coast. Shelf Sci. 40, 105–114. https://doi.org/10.1016/0272-7714(95)90016-0

Shao, T., Wang, T., Liang, X., Xu, H., Li, L., 2019. Characterization of DOC and CDOM and their relationship in turbid waters of a high-altitude area on the western Loess Plateau, China. Water Sci. Technol. 80, 1796–1806. https://doi.org/10.2166/wst.2020.004

Siegel, D.A., Maritorena, S., Nelson, N.B., Hansell, D.A., Lorenzi-Kayser, M., 2002. Global distribution and dynamics of colored dissolved and detrital organic materials: COLORED DISSOLVED AND DETRITAL ORGANIC MATERIALS. J. Geophys. Res. Oceans 107, 21-1-21–14. https://doi.org/10.1029/2001JC000965

Smith, R.C., Prezelin, B.B., Baker, K.S., Bidigare, R.R., Boucher, N.P., Coley, T., Karentz, D., MacIntyre, S., Matlick, H.A., Menzies, D., Ondrusek, M., Wan, Z., Water, K.J., 1992. Ozone depletion: ultraviolet radiation and phytoplankton biology in Antarctic waters. Science 255, 952–959.

Somlyódy, L., & van Straten, G., 2012. Modeling and managing shallow lake eutrophication: with application to Lake Balaton. Springer Science & Business Media.

Song, K., Zhao, Y., Wen, Z., Fang, C., Shang, Y., 2017. A systematic examination of the relationships between CDOM and DOC in inland waters in China. Hydrol Earth Syst Sci 21, 5127–5141. https://doi.org/10.5194/hess-21-5127-2017

Song, K.S., Zang, S.Y., Zhao, Y., Li, L., Du, J., Zhang, N.N., Wang, X.D., Shao, T.T., Guan, Y., Liu, L., 2013. Spatiotemporal characterization of dissolved carbon for inland waters in semi-humid/semi-arid region, China. Hydrol. Earth Syst. Sci. 17, 4269–4281. https://doi.org/10.5194/hess-17-4269-2013

Soppa, M.A., Pefanis, V., Hellmann, S., Losa, S.N., Hölemann, J., Martynov, F., Heim, B., Janout, M.A., Dinter, T., Rozanov, V., Bracher, A., 2019. Assessing the Influence of Water Constituents on the Radiative Heating of Laptev Sea Shelf Waters. Front. Mar. Sci. 6. https://doi.org/10.3389/fmars.2019.00221

Specchiulli, A., Cilenti, L., D'Adamo, R., Fabbrocini, A., Guo, W., Huang, L., Lugliè, A., Padedda, B.M., Scirocco, T., Magni, P., 2018. Dissolved organic matter dynamics in Mediterranean lagoons: The relationship between DOC and CDOM. Mar. Chem. 202, 37–48. https://doi.org/10.1016/j.marchem.2018.02.003

Spencer, R.G.M., Butler, K.D., Aiken, G.R., 2012. Dissolved organic carbon and chromophoric dissolved organic matter properties of rivers in the USA:

DISSOLVED ORGANIC MATTER IN U.S. RIVERS. J. Geophys. Res. Biogeosciences 117, n/a-n/a. https://doi.org/10.1029/2011JG001928

Spencer, R.G.M., Hernes, P.J., Ruf, R., Baker, A., Dyda, R.Y., Stubbins, A., Six, J., 2010. Temporal controls on dissolved organic matter and lignin biogeochemistry in a pristine tropical river, Democratic Republic of Congo. J. Geophys. Res. 115, G03013. https://doi.org/10.1029/2009JG001180

Spencer, R.G.M., Stubbins, A., Hernes, P.J., Baker, A., Mopper, K., Aufdenkampe, A.K., Dyda, R.Y., Mwamba, V.L., Mangangu, A.M., Wabakanghanzi, J.N., Six, J., 2009. Photochemical degradation of dissolved organic matter and dissolved lignin phenols from the Congo River. J. Geophys. Res. 114. https://doi.org/10.1029/2009JG000968

Spyrakos, E., O'Donnell, R., Hunter, P.D., Miller, C., Scott, M., Simis, S.G.H., Neil, C., Barbosa, C.C.F., Binding, C.E., Bradt, S., Bresciani, M., Dall'Olmo, G., Giardino, C., Gitelson, A.A., Kutser, T., Li, L., Matsushita, B., Martinez-Vicente, V., Matthews, M.W., Ogashawara, I., Ruiz-Verdú, A., Schalles, J.F., Tebbs, E., Zhang, Y., Tyler, A.N., 2018a. Optical types of inland and coastal waters: Optical types of inland and coastal waters. Limnol. Oceanogr. 63, 846–870. https://doi.org/10.1002/lno.10674

Stedmon, C. a., Markager, S., Kaas, H., 2000. Optical Properties and Signatures of Chromophoric Dissolved Organic Matter (CDOM) in Danish Coastal Waters. Estuar. Coast. Shelf Sci. 51, 267–278. https://doi.org/10.1006/ecss.2000.0645

Stedmon, C.A., Amon, R.M.W., Rinehart, A.J., Walker, S.A., 2011. The supply and characteristics of colored dissolved organic matter (CDOM) in the Arctic Ocean: Pan Arctic trends and differences. Mar. Chem. 124, 108–118.

Stedmon, C.A., Markager, S., 2001. The optics of chromophoric dissolved organic matter (CDOM) in the Greenland Sea: An algorithm for differentiation between marine and terrestrially derived organic matter. Limnol. Oceanogr. 46, 2087–2093. https://doi.org/10.4319/lo.2001.46.8.2087

Stedmon, C.A., Markager, S., Kaas, H., 2000. Optical Properties and Signatures of Chromophoric Dissolved Organic Matter (CDOM) in Danish Coastal Waters. Estuar. Coast. Shelf Sci. 51, 267–278. https://doi.org/10.1006/ecss.2000.0645

Suttle, C.A., Chan, A.M., Cottrell, M.T., 1990. Infection of phytoplankton by viruses and reduction of primary productivity. Nature 347, 467–469. https://doi.org/10.1038/347467a0

Swan, C.M., Nelson, N.B., Siegel, D. a., Kostadinov, T.S., 2012. The effect of surface irradiance on the absorption spectrum of chromophoric dissolved organic matter in the global ocean. Deep Sea Res. Part Oceanogr. Res. Pap. 63, 52–64. https://doi.org/10.1016/j.dsr.2012.01.008

Szilágyi, F., Somlyódy, L., Koncsos, L., 1990. Operation of the Kis-Balaton reservoir: evaluation of nutrient removal rates. Hydrobiologia 191, 297–306. https://doi.org/10.1007/BF00026065

Tanaka, A., Kishino, M., Oishi, T., Doerffer, R., Schiller, H., 2000. Application of neural network method to case II water. Remote Sens. Ocean Sea Ice 2000 4172, 144–152.

Tátrai, I., Mátyás, K., Korponai, J., Paulovits, G., Pomogyi, P., 2000. The role of the Kis-Balaton Water Protection System in the control of water quality of Lake Balaton. Ecol. Eng. 16, 73–78. https://doi.org/10.1016/S0925-8574(00)00091-4

Tehrani, N., D'Sa, E., Osburn, C., Bianchi, T., Schaeffer, B., 2013. Chromophoric Dissolved Organic Matter and Dissolved Organic Carbon from Sea-Viewing Wide Field-of-View Sensor (SeaWiFS), Moderate Resolution Imaging Spectroradiometer (MODIS) and MERIS Sensors: Case Study for the Northern Gulf of Mexico. Remote Sens. 5, 1439–1464. https://doi.org/10.3390/rs5031439

Tilstone, G., Moore, G., Sorensen, K., Doerffer, R., Rottgers, R., Ruddick, K., Pasterkamp, R., Jorgensen, P., 2002. REVAMP regional validation of MERIS chlorophyll products in North Sea coastal waters: Protocols document, Proceedings of the "Working meeting on MERIS and AATSR Calibration and Geophysical Validation (ENVISAT MAVT-2003).

Toming, Kaire, Kutser, T., Laas, A., Sepp, M., Paavel, B., Nõges, T., 2016. First Experiences in Mapping Lake Water Quality Parameters with Sentinel-2 MSI Imagery. Remote Sens. 8, 640. https://doi.org/10.3390/rs8080640

Toming, K., Kutser, T., Tuvikene, L., Viik, M., Nõges, T., 2016. Dissolved organic carbon and its potential predictors in eutrophic lakes. Water Res. 102, 32–40.

Townsend, S.A., Boland, K.T., Wrigley, T.J., 1992. Factors contributing to a fish kill in the Australian wet/dry tropics. Water Res. 26, 1039–1044.

Tranvik, Lars J, Downing, J.A., Cotner, J.B., Loiselle, S.A., Striegl, R.G., Ballatore, T.J., Dillon, P., Finlay, K., Fortino, K., Knoll, L.B., Kortelainen, P.L., Kutser, T., Larsen, S., Laurion, I., Leech, D.M., Mccallister, S.L., Mcknight, D.M., Melack, J.M., Overholt, E., Porter, J.A., Prairie, Y., Renwick, W.H., Roland, F., Sherman, B.S., Schindler, D.W., Sobek, S., Tremblay, A., Vanni, M.J., Verschoor, A.M., Wachenfeldt, E. Von, Weyhenmeyer, G.A., 2009. Lakes and reservoirs as regulators of carbon cycling and climate 54, 2298–2314.

Tsui, M.T.K., Finlay, J.C., 2011. Influence of dissolved organic carbon on methylmercury bioavailability across Minnesota stream ecosystems. Environ. Sci. Technol. 45, 5981–5987.

Twardowski, M.S., Boss, E., Sullivan, J.M., Donaghay, P.L., 2004. Modeling the spectral shape of absorption by chromophoric dissolved organic matter. Mar. Chem. 89, 69–88. https://doi.org/10.1016/j.marchem.2004.02.008

Twardowski, M.S., Donaghay, P.L., 2001. Separating in situ and terrigenous sources of absorption by dissolved materials in coastal waters. J. Geophys. Res. Oceans 106, 2545–2560. https://doi.org/10.1029/1999JC000039

UNFCC, 2009, 1992. UNITED NATIONS FRAMEWORK CONVENTION ON CLIMATE CHANGE UNITED NATIONS 1–33.

Vähätalo, A. V., Wetzel, R.G., Paerl, H.W., 2005. Light absorption by phytoplankton and chromophoric dissolved organic matter in the drainage basin and estuary of the Neuse River, North Carolina (U.S.A.). Freshw. Biol. 50, 477–493. https://doi.org/10.1111/j.1365-2427.2004.01335.x

Vantrepotte, V., Brunet, C., Mériaux, X., Lécuyer, E., Vellucci, V., Santer, R., 2007. Bio-optical properties of coastal waters in the Eastern English Channel. Estuar. Coast. Shelf Sci. 72, 201–212. https://doi.org/10.1016/j.ecss.2006.10.016

Vantrepotte, V., Danhiez, F.-P., Loisel, H., Ouillon, S., Mériaux, X., Cauvin, A., Dessailly, D., 2015. CDOM-DOC relationship in contrasted coastal waters: implication for DOC retrieval from ocean color remote sensing observation. Opt. Express 23, 33. https://doi.org/10.1364/OE.23.000033

Verpoorter, C., Kutser, T., Seekell, D.A., Tranvik, L.J., 2014. A Global Inventory of Lakes Based on High-Resolution Satellite Imagery. Geophys. Res. Lett. 41, 6396–6402. https://doi.org/10.1002/2014GL060641

Vignudelli, S., Santinelli, C., Murru, E., Nannicini, L., Seritti, a., 2004. Distributions of dissolved organic carbon (DOC) and chromophoric dissolved organic matter (CDOM) in coastal waters of the northern Tyrrhenian Sea (Italy). Estuar. Coast. Shelf Sci. 60, 133–149. https://doi.org/10.1016/j.ecss.2003.11.023

Vincent, A., Warwick, F., Laurion, I., Pienitz, R., 1998. Artic and Antartic lakes as optical indicators of global change. Ann. Glaciol. 27, 691–696.

Vodacek, A., Blough, N. V, Degrandpre, M.D., Peltzer, E.T., Nelson, R.K., Bloughl, N. V, Bruce, L., 1997. Seasonal variation of CDOM and DOC in the Middle Atlantic Bight : Terrestrial inputs and photooxidation. Limnol. Oceanogr. 42, 674–686.

Ward, N.D., Keil, R.G., Medeiros, P.M., Brito, D.C., Cunha, A.C., Dittmar, T., Yager, P.L., Krusche, A.V., Richey, J.E., 2013. Degradation of terrestrially derived macromolecules in the Amazon River. Nat. Geosci. 6, 530–533. https://doi.org/10.1038/ngeo1817

Weishaar, J.L., Aiken, G.R., Bergamaschi, B.A., Fram, M.S., Fujii, R., Mopper, K., 2003b. Evaluation of Specific Ultraviolet Absorbance as an Indicator of the Chemical Composition and Reactivity of Dissolved Organic Carbon. Environ. Sci. Technol. 37, 4702–4708. https://doi.org/10.1021/es030360x

Wetzel, R.G., 2001. Limnology. Lake and river ecosystems. ELSEVIER. Academic Press.

Wetzel, R.G., Hatcher, P.G., Bianchi, T.S., 1995. Natural photolysis by ultraviolet irradiance of recalcitrant dissolved organic matter to simple substrates for rapid bacterial metabolism 40, 1369–1380.

Wickham, H., 2016. ggplot2: Elegant Graphics for Data Analysis. Springer-Verlag New York.

Wilkinson, G.M., Pace, M.L., Cole, J.J., 2013. Terrestrial dominance of organic matter in north temperate lakes. Glob. Biogeochem. Cycles 27, 43–51. https://doi.org/10.1029/2012GB004453

Willén, E., 2001. Phytoplankton and Water Quality Characterization: Experiences from the Swedish Large Lakes Mälaren, Hjälmaren, Vättern and Vänern 30, 9.

Willen, E., 1984. The large lakes of Sweden: Vänern, Vättern, Mälaren and Hjälmaren. Ecosyst. World 23, 107–134.

Williamson, C.E., Brentrup, J. a., Zhang, J., Renwick, W.H., Hargreaves, B.R., Knoll, L.B., Overholt, E.P., Rose, K.C., 2014. Lakes as sensors in the landscape: Optical metrics as scalable sentinel responses to climate change. Limnol. Oceanogr. 59, 840–850. https://doi.org/10.4319/lo.2014.59.3.0840

Williamson, C.E., Dodds, W., Kratz, T.K., Palmer, M. a, 2008. Lakes and streams as sentinels of environmental change in terrestrial and atmospheric processes. Front. Ecol. Environ. 6, 247–254. https://doi.org/10.1890/070140

Williamson, Craig E., Morris, D.P., Pace, M.L., Olson, O.G., 1999. Dissolved organic carbon and nutrients as regulators of lake ecosystems: Resurrection of a more integrated paradigm. Limnol. Oceanogr. 44, 795–803. https://doi.org/10.4319/lo.1999.44.3_part_2.0795

Williamson, Craig E, Neale, P.J., Gard, G., De Lange, H.J., Hargreaves, B.R., 2001. Beneficial and deterimental effects of UV on aquatic organsisms: Implications of spectral variation. Ecol. Appl. 11, 1843–1857. https://doi.org/Doi 10.2307/3061100

Williamson, C.E., Overholt, E.P., Pilla, R.M., Leach, T.H., Brentrup, J.A., Knoll, L.B., Mette, E.M., Moeller, R.E., 2016. Ecological consequences of long-term browning in lakes. Sci. Rep. 5. https://doi.org/10.1038/srep18666

Williamson, C. E., Saros, J.E., Schindler, D.W., 2009. CLIMATE CHANGE: Sentinels of Change. Science 323, 887–888. https://doi.org/10.1126/science.1169443

Williamson, Craig E., Saros, J.E., Vincent, W.F., Smol, J.P., 2009a. Lakes and reservoirs as sentinels, integrators, and regulators of climate change. Limnol. Oceanogr. 54, 2273–2282. https://doi.org/10.4319/lo.2009.54.6_part_2.2273

Williamson, C.E., Stemberger, R.S., Morris, D.P., Frost, T.M., Paulsen, S.G., 1996. Ultraviolet radiation in North American lakes: Attenuation estimates from DOC measurements and implications for plankton communities. Limnol. Oceanogr. 41, 1024–1034. https://doi.org/10.4319/lo.1996.41.5.1024

Wipple, G., 1914. The microscopy of drinking water.

Yacobi, Y.Z., Alberts, J.J., Takács, M., McELVAINE, M., 2003a. Absorption spectroscopy of colored dissolved organic carbon in Georgia (USA) rivers: the impact of molecular size distribution. J. Limnol. 62, 41. https://doi.org/10.4081/jlimnol.2003.41

Yamashita, Y., Kloeppel, B.D., Knoepp, J., Zausen, G.L., Jaffé, R., 2011. Effects of Watershed History on Dissolved Organic Matter Characteristics in Headwater Streams. Ecosystems 14, 1110–1122. https://doi.org/10.1007/s10021-011-9469-z

Yamashita, Y., Nosaka, Y., Suzuki, K., Ogawa, H., Takahashi, K., Saito, H., 2013. Photobleaching as a factor controlling spectral characteristics of chromophoric dissolved organic matter in open ocean. Biogeosciences 10, 7207–7217. https://doi.org/10.5194/bg-10-7207-2013

Yamashita, Y., Tanoue, E., 2004. In situ production of chromophoric dissolved organic matter in coastal environments. Geophys. Res. Lett. 31, 2–5. https://doi.org/10.1029/2004GL019734

Yang, H., Andersen, T., Dörsch, P., Tominaga, K., Thrane, J.-E., Hessen, D.O., 2015. Greenhouse gas metabolism in Nordic boreal lakes. Biogeochemistry 126, 211–225. https://doi.org/10.1007/s10533-015-0154-8

Ylöstalo, P., Kallio, K., Seppälä, J., 2014. Absorption properties of in-water constituents and their variation among various lake types in the boreal region. Remote Sens. Environ. 148, 190–205. https://doi.org/10.1016/j.rse.2014.03.023

Zhang, Yunlin, Liu, M., Qin, B., Feng, S., 2009a. Photochemical degradation of chromophoric-dissolved organic matter exposed to simulated UV-B and natural solar radiation. Hydrobiologia 627, 159–168. https://doi.org/10.1007/s10750-009-9722-z

Zhang, Yunlin, Qin, B., Zhu, G., Zhang, L., Yang, L., 2007b. Chromophoric dissolved organic matter (CDOM) absorption characteristics in relation to fluorescence in Lake Taihu, China, a large shallow subtropical lake. Hydrobiologia 581, 43–52. https://doi.org/10.1007/s10750-006-0520-6

Zhang, Yunlin, van Dijk, M. a, Liu, M., Zhu, G., Qin, B., 2009b. The contribution of phytoplankton degradation to chromophoric dissolved organic matter (CDOM) in eutrophic shallow lakes: field and experimental evidence. Water Res. 43, 4685–97. https://doi.org/10.1016/j.watres.2009.07.024

Zhang, Y., Yin, Y., Liu, X., Shi, Z., Feng, L., Liu, M., Zhu, G., Gong, Z., Qin, B., 2011. Spatial-seasonal dynamics of chromophoric dissolved organic matter in Lake Taihu, a large eutrophic, shallow lake in China. Org. Geochem. 42, 510–519. https://doi.org/10.1016/j.orggeochem.2011.03.007

Zhang, Y., Zhang, E., Liu, M., Wang, X., Qin, B., 2007b. Variation of chromophoric dissolved organic matter and possible attenuation depth of ultraviolet radiation in Yunnan Plateau lakes. Limnology 8, 311–319. https://doi.org/10.1007/s10201-007-0219-z

Zhao, Y., Song, K., 2018. Relationships Between DOC and CDOM Based on the Total Carbon-Specific Fluorescence Intensities for River Waters Across China. J. Geophys. Res. Biogeosciences 123, 2353–2361.

Zhao, Y., Song, K., Shang, Y., Shao, T., Wen, Z., Lv, L., 2017. Characterization of CDOM of river waters in China using fluorescence excitation-emission matrix and regional integration techniques: DOC and CDOM in Rivers in China. J. Geophys. Res. Biogeosciences 122, 1940–1953. https://doi.org/10.1002/2017JG003820

Zhu, W., Yu, Q., 2013. Inversion of Chromophoric Dissolved Organic Matter From EO-1 Hyperion Imagery for Turbid Estuarine and Coastal Waters. Geosci. Remote Sens. IEEE Trans. On 51, 3286–3298. https://doi.org/10.1109/TGRS.2012.2224117

Zhu, W., Yu, Q., Tian, Y.Q., Becker, B.L., Zheng, T., Carrick, H.J., 2014a. An assessment of remote sensing algorithms for colored dissolved organic matter in complex freshwater environments. Remote Sens. Environ. 140, 766–778. https://doi.org/10.1016/j.rse.2013.10.015

Zhu, W., Yu, Q., Tian, Y.Q., Chen, R.F., Gardner, G.B., 2011. Estimation of chromophoric dissolved organic matter in the Mississippi and Atchafalaya river plume regions using above-surface hyperspectral remote sensing. J. Geophys. Res. 116. https://doi.org/10.1029/2010JC006523

Zhu, W.-Z., Zhang, H.-H., Zhang, J., Yang, G.-P., 2018. Seasonal variation in chromophoric dissolved organic matter and relationships among fluorescent

components, absorption coefficients and dissolved organic carbon in the Bohai Sea, the Yellow Sea and the East China Sea. J. Mar. Syst. 180, 9–23. https://doi.org/10.1016/j.jmarsys.2017.12.003